

The Maximum Effect of Wind on Wave Overtopping at Rubble Mound Breakwaters with the Influence of the Slope and a Crest Element

MSc. Hydraulic Engineering - Thesis Report

L.F. (Lars) van Vliet

The Maximum Effect of Wind on Wave Overtopping at Rubble Mound Breakwaters with the Influence of the Slope and a Crest Element

MSc. Hydraulic Engineering - Thesis Report

by

L.F. (Lars) van Vliet

in partial fulfillment of the requirements for the degree of

Master of Science
in Civil Engineering

at the Delft University of Technology
Faculty of Civil Engineering and Geosciences
Department of Hydraulic Engineering
Section of Coastal Engineering
Commissioned by Deltares

To be defended publicly on December 5th, 2023

Studentnumber: 4387503
Thesis Committee: Prof.dr.ir M.R.A. (Marcel) van Gent TU Delft, Deltares, Chair
Dr.dipl.-ing. G. (Guido) Wolters Deltares
Dr.ir. D. (Davide) Wüthrich TU Delft
Date: Monday 27th November, 2023

Preface

This thesis marks the end of my master programme of Hydraulic Engineering at the Delft University of Technology. It has been a pleasant time where I obtained valuable lessons, which was made possible with the help and support of many people.

First of all, I would like to express my gratitude to Marcel van Gent, who was not only the chair of my committee but also my daily supervisor, guiding me through the many stages of the process. His approachability, initiative, experience, and interest in the subject greatly enhanced the progress I was able to make. Moreover, Marcel provided me with the opportunity of graduating at the company Deltares, which was a valuable experience and a place where I met a lot of interesting people.

Furthermore, I want to thank Guido Wolters, who occasionally helped and advised me throughout the progress. His valuable feedback, especially his critical look on the scientific approach of the research, was of significant help. Finally, I would like to thank Davide Wüthrich for his welcoming advice, especially concerning my writing style. Each member of the committee provided their own unique contribution, enabling me to produce a satisfying result.

This research was also made possible with the help of my predecessors on this subject: Ruben van der Bijl and Sam Dijkstra. Their work, added by their advice, helped me with making decisions during the experiments and the analysis that would otherwise be much more time consuming. Consequently, their works are often credited and cited throughout this research.

I owe a lot of thanks to the staff from the Hydrolab: Wesley Stet, Danny van Doeveren, Peter Albers, and Sytse Riedstra. With their help, I was able to conduct the experiments in a most desirable way. I would like to thank them for changing the configurations and modifying the setup. Not only their practical insights were of great importance, also their knowledge on experimental research itself was of great help during the analysis. Their work and expertise made me realize what an essential role they play for the graduation students they support and for Deltares and its employees.

I would also like to show my gratitude towards the Coastal Structures and Waves department from Deltares. It was a privilege to work at the department, where the people were very helpful, professional, and inspiring. I had a great time learning more about the company, its employees, and the work ethics. I was not the only student working at Deltares, as numerous ambitious young people with a variety of backgrounds were able to inspire me and help me develop myself.

Last but not least, I would like to grant my special thanks to my family and friends. The roles they took on were of several kinds. However, each was of great value to me!

*Lars van Vliet
Delft, December 2023*

Summary

The impact of climate change, particularly the rise in sea levels, obstructs the effectiveness of existing coastal structures. Therefore, adaptation measures are required for these structures to ensure their efficiency in protecting coastal areas from flooding and water hazards. Additionally, climate change can also have an amplifying effect on wind speeds, especially at sea and coastal areas (Takagi & Esteban, 2013). Without proper control, the accumulation of changing environmental boundary conditions could lead to disastrous events.

Presently, the common method of designing rubble mound breakwaters is based on the EurOtop (2018) guideline. While widely accepted, these guidelines may not incorporate all the influencing factors essential for structure design or adaptation to changing boundary conditions. Recent studies carried out by Van Gent et al. (2022) and Irias Mata & van Gent (2023) have contributed to new insights that address these limitations. They aimed to identify numerous influencing factors that enhance the accuracy of wave overtopping expressions for rubble mound breakwaters. However, several influencing factors still require a more thorough understanding.

Furthermore, recent insights on the influence of wind have proven to be significant. Previous studies indicate that the mean overtopping discharge has the potential to amplify its quantity several times beyond its initial value (de Waal et al., 1996; Wolters & van Gent, 2007; Van Gent et al., 2023; Dijkstra, 2023). These investigations included tests on different structure types, such as vertical sea walls and rough and smooth sloped dikes with a varying slope angle.

The objective of this research is to investigate the maximum effect of wind on wave overtopping for a rubble mound breakwater with varying slope angles and crest element designs. In line with previous studies on this topic, the key focus is on determining the maximum wind effect factor γ_w , described as a function of the non-dimensional overtopping discharge (denoted by $q^* = q / (g H_{m0}^3)$). To examine the influence of wind, a mild slope (1:6) and a steep slope (1:2) are investigated using small-scale models of rubble mound breakwaters inside a flume. To learn more about the influence of a crest wall, the initial crest wall of 5 cm is compared with an 8 cm crest wall. Finally, the influence of a recurved crest wall is studied by comparing crest walls with the same height and with a varying shape, which is defined in this study as a bull nose.

An extensive experimental programme was carried out within the Pacific Basin at Deltares. In this basin, a flume was constructed in which the breakwater model was built. Various hydraulic conditions, incorporating the water level and the wave characteristics, were systematically tested. All conditions were repeated, both with and without including the maximum wind effect.

The results of the overtopping discharges without wind demonstrated deviations from the expressions found in literature, acquiring the need for the development of a new expression that effectively defines a new maximum wind effect factor. The newly proposed expression takes the form of an exponential function, incorporating the effect of the slope, breaker parameter, wave height, freeboard, wave steepness, and influence factors of other elements denoted by γ . Note that this report provides a detailed elaboration on γ_v and γ_p , respectively corresponding to the crest element height and crest element shape, while the other factors are mentioned but not thoroughly investigated. The exponents and constant factors were obtained iteratively and were found to accurately predict the overtopping discharges that were obtained during the experiments. This expression is presented below:

$$\frac{q}{\sqrt{g H_{m0}^3}} = \sqrt{\cot(\alpha)} s_{m-1,0}^{-0.25} \exp \left[-\frac{6.4 R_c}{\gamma_f \gamma_b \gamma_\beta \gamma_v \gamma_p s_{m-1,0}^{0.5} H_{m0}} \right] \quad (4.3)$$

The relationship between the maximum wind effect and non-dimensional overtopping, as observed in previous research, was confirmed for these measurements. This observation suggests that a maximum effect of wind increases when the non-dimensional overtopping discharge decreases. While each configuration showed a similar curve, the configuration of a 1:6 slope and 8 cm crest wall stood out by showing a notable influence on

the maximum wind effect. Moreover, the wind effect is more pronounced for an increasing water level when similar amounts of overtopping discharges are taken into consideration.

Both observations are explained with the assumption that the properties of the structure change when the A_c/R_c ratio is altered. Consequently, the properties associated with a rubble mound breakwater diminish, and new properties corresponding to a vertical wall are adopted. This is supported by the discoveries of [de Waal et al. \(1996\)](#), finding larger wind effects for seawalls than were found for a dike by [Van Gent et al. \(2023\)](#).

An increased accuracy of 24 to 30 percent was observed for Equation (4.6) when the maximum wind effect factors developed by [Van der Bijl \(2022\)](#) and [Dijkstra \(2023\)](#) were implemented into γ_w . However, since the factors from previous studies also showed a negative impact on the accuracy of some elements, new expressions for the wind factor have been developed. These were derived based on the bulk of the data and are categorized per slope ($\cot \alpha$), per non-dimensional crest wall height (h_{wall}^*), and per individual configuration. Ultimately, the following generalized expression is proposed with the aim of providing a wide applicability range:

$$\gamma_w = 0.025q^{*-0.31} + 1 \quad (4.6)$$

In conclusion, this research has contributed to a deeper understanding of the influence of wind on wave overtopping for rubble mound breakwaters with varying slope angles and crest elements. The presented wind factor expressions significantly improved the accuracy of the expression for each measurement, offering broader applicability across different structure types. Moreover, the amplification factors constructed in previous studies and in this study, have proven to be applicable across various structure types. This enhances overtopping predictions initially obtained for this study.

Table of Contents

Preface	ii
Summary	iii
Preface	viii
List of Figures	ix
List of Tables	xii
I Introduction and Theoretical background	1
1 Introduction	3
1.1 Problem analysis	3
1.2 Objective	4
1.3 Approach of the research	5
1.3.1 Overview of the experiment	5
1.3.2 Experimental Plan	5
1.4 Outline	6
2 Theoretical Background	7
2.1 Wave overtopping at rubble mound breakwaters	7
2.1.1 Wave overtopping in general	7
2.1.2 Mean overtopping discharge during an overtopping event	8
2.1.3 Overtopping volumes of individual waves	10
2.2 Hydraulic boundary conditions	10
2.2.1 Wave Spectrum	10
2.2.2 Water level	11
2.2.3 Wave steepness	11
2.2.4 Breaker parameter	12
2.3 Influence factors corresponding to the wave overtopping discharge.	12
2.3.1 Influence factor for roughness	12
2.3.2 Influence factor of the obliqueness of waves.	13
2.3.3 Influence factor for the berm	14
2.3.4 Height of the crest wall	14
2.3.5 Shape of the crest wall	15
2.4 Influence of wind	16
2.4.1 Background theory	16
2.4.2 Methodologies	17
2.4.3 Concluding remarks on wind.	18
II Physical model tests and analysis	19
3 Methodology	21
3.1 Model Set-Up	21
3.2 Experiment programme	23
3.3 Model limitations	25

3.4	Method validation	25
3.5	Froude scaling	25
4	Results	27
4.1	Data Overview	27
4.2	Comparison of the measurements with previous literature	29
4.2.1	Reference Model	29
4.2.2	Comparison with the most recent guideline (Irias Mata & van Gent, 2023)..	32
4.2.3	Influence of the slope	34
4.2.4	Influence of a crest wall with an increased height	35
4.2.5	Influence of a recurved parapet.	37
4.2.6	Recap	39
4.3	Maximum influence of wind	39
4.3.1	First look at the influence of wind	40
4.3.2	Influence of the wave characteristics	40
4.3.3	Influence of the water level	41
4.3.4	Influence of the crest wall	42
4.3.5	Influence of the slope	43
4.3.6	Constructing the influence factor.	44
4.4	Implementing the influence factors	47
III	Discussion, Conclusion and Recommendations	53
5	Discussion	55
5.1	Discussion on the methodology	55
5.2	Applicability and limitations	56
5.2.1	Overtopping discharge (without wind).	56
5.2.2	Influence of the elements on the maximum wind effect.	57
6	Conclusions & Recommendations	59
6.1	Conclusion	59
6.1.1	Influence of the water level, wave period, and wave height on wave overtopping and the maximum wind effect.	60
6.1.2	Influence of the height and shape of a crest wall on wave overtopping and the maximum wind effect.	60
6.1.3	Influence of the slope angle on the mean overtopping discharge and the maximum wind effect.	61
6.1.4	Final remarks	61
6.2	Recommendations	61
	References	65
IV	Appendices	67
A	Statistical Methods	69
B	Wave conditions	70
C	Technical Drawings	72
D	Grading curves	74
D.1	Core Material	74
D.2	Filter Material	75
D.3	Armour Material.	75
D.4	Summary	76

E	Data Overview with wind	77
E.1	Influence of wind - wave steepness	78
F	Pictures of the Setup	80

List of symbols

Symbol	Unit	Description
α	°	Slope angle of the breakwater
β	°	Angle of wave attack
γ	-	Influence factor
γ_β	-	Influence factor for the angle of wave attack
γ_b	-	Influence factor for the berm
γ_f	-	Influence factor for the roughness
γ_p	-	Influence factor for a parapet
γ_v	-	Influence factor for a crest element
γ_w	-	Influence factor for wind
ϵ	-	Angle of the recurved parapet
λ	-	Height Ratio of the protruding element height over the total crest wall height
$\xi_{m-1,0}$	-	Spectral surf similarity parameter
A_c	m	Crest level of the armour at the crest
A_R	m ²	Empty area underneath the recurved parapet
B	m	Berm width
B_L	m	Berm level measured from the level of the armour at the crest to the berm level
B_R	m	Horizontal distance from the face of the protruding surface to the vertical face of the crest wall
D_{n50}	m	Nominal stone diameter
G_c	m	Width of the armour at the crest in front of the crest wall
g	m ² /s	Gravitational acceleration
H_{m0}	m	Significant wave height of the incident waves based on the wave energy spectrum
H_s	m	Significant wave height of the incident waves
Hz	s ⁻¹	Unit of frequency, equivalent to one event cycle per second
h	m	Water depth
h_b	m	Berm depth relative to the still water level (negative for emerged berm)
h_{crest}	m	Height of the armoured crest of the breakwater
h_{wall}	m	Height of the crest wall
h_{wall}^*	-	Non-dimensional crest wall
h_n	m	Height of the protruding element on a crest wall (Oh et al., 2018)
h_R	m	Height of the protruding element on a crest wall (Van Doorslaer et al., 2015)
h_{tot}	m	Total height of the breakwater including the height of the crest wall
$L_{m-1,0}$	m	Wavelength based on the spectral wave period $T_{m-1,0}$ ($L_{m-1,0} = 2\pi/gT_{m-1,0}^2$)
N	-	Amount of waves during an experiment
q	m ³ /s/m	Overtopping discharge per meter crest width
q_w	m ³ /s/m	Overtopping discharge per meter crest width, including the effect of wind
q^*	-	Non-dimensional overtopping discharge per meter crest width
q_w^*	-	Non-dimensional overtopping discharge per meter crest width, including the effect of wind
R_c	m	Freeboard (crest height relative to the still water level)
s_0	-	Wave steepness
$s_{m-1,0}$	-	Spectral wave steepness
$T_{m-1,0}$	s	Spectral mean wave period based on the ratio of the spectral moments m_{-1} and m_0 of the incident wave spectrum
T_p	s	Peak period

List of Figures

1.1	Severe wave impact during storm Babet at a seawall at the east coast of Scotland (NOS, 2023)	3
2.1	Failure modes for a rubble mound breakwater Burcharth (1994)	7
2.2	A JONSWAP spectrum plotted with a PM spectrum (Holthuijsen, 2007).	10
2.3	The trend of changes in overtopping discharge (l/s/m) in the coming years (2030–2100) for the two different design approaches; blue line is for the conventional design method and the pink is for the joint design method (Radfar et al., 2021).	11
2.4	This figure shows various methods describing the influence of oblique waves on wave overtopping for (Van Gent, 2022).	14
2.5	Dimensional parameters for a recurved parapet in line with literature; a) The definitions of the parameters related to the recurved parapet reduction factor of Equation (2.16) (Oh et al., 2018); b) A Schematization of a crown wall with parapet as demonstrated by Van Doorslaer et al. (2015)	15
3.1	Set-up of the experiment; a) Top view of the flume 1:6; b) Side view of the flume	21
3.2	Construction sequence of the 1:6 sloped breakwater; (a) Construction of the breakwater core; (b) Construction of the filter layer on top of the core; (c) Construction of the armour layer on top of the filter layer; (d) Covering the armour layer with epoxy.	22
3.3	Parameters for the parapet mounted on the crest wall; (a) Dimensions according to Oh et al. (2018); (b) Dimensions according to Van Doorslaer et al. (2015).	23
4.1	Measured overtopping discharges for all configurations; (a) Measurements without the maximum wind effect; (b) Measurements with the maximum wind effect.	28
4.2	Measured overtopping discharges for all configurations with a different wave steepness for each plot; (a) Observations with wave steepness $s_{m-1,0} = 0.013$; (b) Observations with wave steepness $s_{m-1,0} = 0.028$; (c) Observations with wave steepness $s_{m-1,0} = 0.042$.	28
4.3	Measured overtopping discharges for each configuration excluding the results with the maximum wind effect; (a) Observations from configuration 1 (25V); (b) Observations from configuration 2 (28V); (c) Observations from configuration 3 (65V); (d) Observations from configuration 4 (68V); (e) Observations from configuration 5 (65P);	29
4.4	Measurement points of the reference model with the emphasis on wave steepness and wave breaking; (a) Observations without comparison from literature; (b) Observations compared to the guideline expressed in Equation (2.3) from EurOtop (2018); (c) Observations compared to the guideline expressed in Equation (2.2) from TAW (2002).	30
4.5	Measurements of the reference tests according to the expression proposed by van Irias Mata & van Gent (2023) with a) with the roughness influence factors determined according to Equation (2.9); and b) with γ_f determined with the use of constant values.	31
4.6	Calculated values for the observations determined with Equation (4.2)	32
4.7	Measurements of the reference tests according to the expression proposed by van Van Gent et al. (2022) with a) with the roughness influence factors determined according to Equation (2.9); and b) with γ_f determined with the use of constant values	32
4.8	Calculated values for the observations determined with Equation (4.3)	33
4.9	Measurements with varying slope angles compared with various expressions; (a) Measurements calculated using Equation (2.4) (Van Gent et al., 2022); (b) Measurements calculated using Equation (4.2); (c) Measurements calculated using Equation (2.5) (Irias Mata & van Gent, 2023); (d) Measurements calculated using Equation (4.3).	34

4.10	Measurements without the influence of the crest wall height ($\gamma_v = 1$); (a) measurements obtained from the configurations with a 1:2 slope; (b) measurements obtained from the configurations with a 1:6 slope.	35
4.11	Influence of the crest wall according to Equation (2.15); (a) measurements obtained from the configurations with a 1:2 slope; (b) measurements obtained from the configurations with a 1:2 slope.	36
4.12	Influence of the crest wall according to Equation (4.4); (a) Results obtained for the 1:2 slope; (b) Results obtained for the 1:6 slope	37
4.13	Measured overtopping discharges for configurations with a 1:6 slope and a 5 cm crest wall with and without a parapet ; (a) No influence of the parapet taken into account ($\gamma_p = 1$); (b) Influence of the parapet using Equation (2.17) (Van Doorslaer et al., 2015); (c) Influence of the crest wall using Equation (2.16) (Oh et al., 2018).	37
4.14	Measured overtopping discharges for configurations with a 1:2 slope and a 5 cm crest wall with and without a parapet ; (a) No influence of the parapet taken into account ($\gamma_p = 1$); (b) Influence of the parapet using Equation (2.16); (c) Influence of the crest wall using Equation (2.17).	38
4.15	Influence of the parapet according to Equation (4.5); (a) measurements obtained from the configurations with a 1:2 slope; (b) measurements obtained from the configurations with a 1:6 slope.	38
4.16	Calculations for the bulk of the data containing each separate configuration, including the factor 10 confidence area above and below function y	39
4.17	The influence of the relative crest freeboard on the maximum wind effect; (a) influence for the 1:2 slope; (b) influence for the 1:6 slope.	40
4.18	Maximum influence of wind for the wave steepness including the median and mean line of all configurations; (a) Data points for the configurations with a 1:2 slope; (b) Data points for the configurations with a 1:6 slope	41
4.19	Maximum influence of wind within the water level ranges for; (a) 1:2 slope; (b) 1:6 slope	42
4.20	Influence of the crest wall for each water level; (a) 5 cm vs 8 cm crest wall at a breakwater with a 1:2 slope; (b) 5 cm vs 8 cm crest wall at a breakwater with a 1:6 slope.	43
4.21	Comparison of each configuration for the maximum wind effect for water level $h = 0.80$ m and $s_{m-1,0} = 0.013$ with; (a) The effect of the non-dimensional freeboard; (b) The effect of the non dimensional overtopping discharge.	44
4.22	Generalized fit describing the maximum wind effect, including all measurement points; (a) Maximum wind effect on a linear scale; (b) Maximum wind effect on a logarithmic scale.	45
4.23	Fitted curves describing the maximum wind effect that distinguish between the influence of the 1:2 slope and the 1:6; (a) Fitted curve for the 1:2 slope; (b) Fitted curve for the 1:6 curve.	45
4.24	Fitted curves describing the maximum wind effect that makes a distinction of the non-dimensional crest height; (a) Fitted curve on linear scale; (b) Fitted curve on logarithmic scale.	46
4.25	Fitted curves describing the maximum wind effect that distinguishes each configuration; (a) Fitted curve on linear scale; (b) Fitted curve on logarithmic scale.	47
4.26	Measurements obtained from the experiments with wind predicted with Equation (4.6) where $\gamma_w = 1$	48
4.27	Predicted data with the influence of wind determined by parameters obtained from prior research; (a) General equation for the influence of wind constructed by Van Gent et al. (2023); (b) General equation for the influence of wind constructed by Dijkstra (2023); (c) General equation for the influence of wind with a dependency on the relative crest wall constructed by Dijkstra (2023).	49
4.28	Predicted data with the influence of wind determined by parameters obtained from prior research; (a) General equation for the influence of wind constructed by Van Gent et al. (2023); (b) General equation for the influence of wind constructed by Dijkstra (2023); (c) General equation for the influence of wind with a dependency on the relative crest wall constructed by Dijkstra (2023).	50
5.1	Schematics on the trajectory of a water droplet emerging from the nod at the slope	58

5.2	Schematization of wave overtopping at the crest wall for different shapes; (a) : Crest wall with vertical shape; (b) Crest wall with a recurved shape.	58
C.1	Side view and front view of the installation, showing the breakwater, paddle wheel, splash board, transportation chute and overtopping box	72
C.2	Technical drawing including the cross-sections of the different breakwater models and crest walls	73
D.1	Weight distribution of the core material ($d_{n15} = 0.5$ cm; $d_{n50} = 0.65$ cm; $d_{n85} = 0.82$ cm). . .	74
D.2	Weight distribution of the core material ($d_{n15} = 1.23$ cm; $d_{n50} = 1.68$ cm; $d_{n85} = 2.54$ cm). . .	75
D.3	Weight distribution of the core material ($d_{n15} = 3.28$ cm; $d_{n50} = 3.85$ cm; $d_{n85} = 4.49$ cm). . .	75
E.1	Measured overtopping discharges for all configurations; (a) Measurements with the maximum wind effect; (b) Measurements with the maximum wind effect.	77
E.2	Measured overtopping discharges for each configuration including the results with the maximum wind effect; (a) Observations from configuration 1 (25V); (b) Observations from configuration 2 (28V); (c) Observations from configuration 3 (65V); (d) Observations from configuration 4 (68V); (e) Observations from configuration 5 (65P);	78
E.3	Maximum influence of wind for the wave steepness including the median and mean line for different water levels; (a) Data points for the 1:2 slope with $A_c = 30$; (b) Data points for the 1:6 slope with $A_c = 25$; (c) Data points for the 1:2 slope with $A_c = 20$; (d) Data points for the 1:6 slope with $A_c = 20$; (e) Data points for the 1:2 slope with $A_c = 15$; (f) Data points for the 1:2 slope with $A_c = 10$	79
F.1	Side picture of the setup including the paddle wheel.	80
F.2	Picture of the front of the setup, showing the measurement devices and the flume	80
F.3	Picture of the back of the setup.	81
F.4	Isometric view of the model.	81
F.5	Picture of the chute and the overtopping box at the back of the model setup.	82
F.6	Picture of wave overtopping at the crest wall.	82
F.7	Picture of a breaking wave on the slope of the breakwater with $\cot \alpha = 6$	83
F.8	Picture of the bull nose that was attached to the 5 cm crest wall	83

List of Tables

2.1	Conducted research on the Influence of wind on wave overtopping for different water retaining structures	18
3.1	Dimensional parameters of the first rubble mound breakwater (based on previous research by Van Gent et al. (2022))	24
3.2	Non-Dimensional parameters of the first rubble mound breakwater (based on previous research by Van Gent et al. (2022))	24
3.3	Accuracy tests for a water level of 90 cm, a 1:6 slope, and a 5 cm bull nose crest wall (Configuration 65P).	25
4.1	Error values obtained for different values for the wave steepness	32
4.2	Root mean squared log error values for expression	33
4.3	Root mean squared log errors between calculations with Equation (4.3) and the measurements without the maximum wind effect.	39
4.4	Influence ranges of the maximum wind effect γ_w for each configuration with various wave characteristics including the wave steepness and the spectral wave height.	41
4.5	Influence ranges of the maximum wind effect γ_w for each configuration with various water levels.	42
4.6	The R_c/h_{crest} ratios with the corresponding values for the crest height h_{crest} and water levels h	43
4.7	Root mean squared log error values.	48
4.8	Summary of the RMSLE for all relevant configurations and conditions	51
B.1	Hydrodynamic conditions as input variables for the various breakwater scale models.	70
D.1	Gradings of the materials applied for the core, filter layer and armour layer.	76

I

Introduction and Theoretical background

Introduction

The aim of the introduction is to briefly state the problem, to explain the importance of increasing our knowledge of wave overtopping at rubble mound breakwaters, and to highlight the current state of knowledge on this subject. After stating the problem, the objective is clarified by listing the research question and sub-questions. Subsequently, an elaboration of the research approach is provided. In this part the methodology is presented, consisting of a brief explanation of the research plan, programme and analysis. Finally, the outline of the thesis is shown, which provides an overview of the report to help the reader navigate through the document efficiently.

1.1. Problem analysis

To safeguard coastal areas from water-related hazards, numerous types of coastal structures have been developed including dikes, dams, artificial dunes and breakwaters. The vertical dimension of such a structure is typically determined by factors as the water level and the characteristics of the waves leading to wave overtopping. If wave overtopping is not properly managed, it can lead to disastrous events as the stability of the structure is likely to be compromised. The [EurOtop \(2018\)](#) manual provides various allowable discharge limits for these structures.

According to the guidelines in [EurOtop \(2018\)](#) manual, the factors contributing to wave overtopping can be summarized into wave height, freeboard, roughness and angle of wave attack. However, recent research conducted by [Van Gent et al. \(2022\)](#) demonstrated that the wave steepness, the presence of a berm and the configuration of the crest wall also have an influence on the overtopping discharge. In the report it is also mentioned that wind has an increasing effect on the overtopping volume, but is not included in the report since the experiments are conducted without simulating the maximum wind effect. Nevertheless, with climate change in mind and conducting SWANone experiments, research performed by [Takagi & Esteban \(2013\)](#) demonstrated that wind speeds potentially increase with 10%. This will primarily increase the wave height, and also increase the effect of wind on wave overtopping, explained by the fact that vertical spray will be subjected to these increased future wind speeds. Additionally, through field measurements empirical evidence was found that the highest overtopping discharges occur during the highest astronomical tide in combination with strong onshore winds ([Marsman et al., 2007](#)). Considering the predicted sea level rise as a result from climate change in the next decades ([IPCC, 2022](#)), the relevance of re-evaluating the existing design methods is signified.



Figure 1.1: Severe wave impact during storm Babet at a seawall at the east coast of Scotland ([NOS, 2023](#))

As a consequence, current guidelines are outdated, leading to inaccurate and inefficient designs of structures that require to be adapted to the effects of climate change. New design expressions need to be developed that incorporate the numerous extra factors of which some have been overlooked or have been inadequately addressed in the current guidelines. Notably, the impact of wind on this phenomenon remains poorly understood, since it has been considered influential in the past. Nevertheless, research has been conducted in this direction with earlier studies focusing on vertical structures (de Waal et al., 1996), and more recently on dikes with varying crest walls, berms, and wave directions (Wolters & van Gent, 2007; Chowdhury et al., 2020; Van Gent et al., 2023). These three studies suggest that the maximum effect of wind can potentially lead to a substantial increase, sometimes up to 6.3 times the overtopping discharge when wind is not considered. It is important to note that high onshore wind speeds are likely to occur during big storm events, of which the boundary conditions generally govern the design parameters of a rubble mound breakwater. This raises the question why the effect of wind is overlooked during the design phase of a rubble mound breakwater. In addition, in Figure 1.1 a water volume is in the position of being transported over the breakwater when subjected to strong wind forces, hence pointing out the relevance of this study.

Wolters & van Gent (2007) carried out experiments to investigate the influence of wind on rough sloped structures (e.g. breakwaters) and smooth sloped structures (e.g. dikes). However, the experiments were exclusively conducted on steep slopes (1:2 and 1:1.5) with a sharp crest using vertical crest walls of varying height on wave overtopping. There are numerous effects of the dimensions of a crest element. The main dimensions treated in this research are the height and shape. The crest wall shape influence has been investigated during research carried out by Oh et al. (2018). The influence of the slope is examined by Dijkstra (2023) for dikes. The main difference between a breakwater and a dike are the permeability and the roughness of the slope. Consequently, the maximum effect of wind on dikes may deviate from the maximum effect of wind on rubble mound breakwaters.

Previous research demonstrated an increase in overtopping volume due to the maximum effect of wind on wave overtopping. Therefore, it is reasonable to think that this also occurs for permeable breakwaters with mild slopes, establishing the objective of this research. Experiments on the maximum effect of wind on wave overtopping, including tests on scale models, have already been conducted and are proven to provide valuable information. Therefore it can be assumed that performing experiments on rubble mound breakwaters can be conducted to obtain similar results for rubble mound breakwaters.

1.2. Objective

The primary objective of this research is to quantify the maximum effect of wind on wave overtopping at a rubble mound breakwater. This analysis focuses on situations where the maximum effect of wind is simulated and where it is excluded. The study also includes an examination of various additional factors that might affect the maximum wind effect. The factors that will be investigated include the influence of the breakwater slope angle, crest element size, and crest element shape. Variations of the hydraulic boundary conditions such as the wave height, wave steepness, and water level are also considered. The research question follows:

”What is the maximum effect of onshore wind on the mean overtopping discharge at rubble mound breakwaters with a crest element?”

Which is supported by the following sub-questions:

1. “How do various hydrodynamic conditions such as water level, wave period, and wave height influence the maximum onshore directed wind effect on wave overtopping at a rubble mound breakwater?”
2. ”How is the maximum effect of onshore directed wind on the mean overtopping discharge affected by the height and shape of the crest wall located on top of a rubble mound breakwater?”
3. ”How is the maximum effect of onshore directed wind on the mean overtopping discharge affected by the angle of the seaward slope of a rubble mound breakwater?”

The first sub-question contributes to the understanding of different hydrodynamic interactions between the waves and the structure. It is evident that larger waves will lead to an increase of the overtopping discharge.

However, a fundamental question arises: does this also lead to a larger maximum wind effect? Similar considerations can be applied for the wave steepness and water level. Addressing the second sub-question will provide clarity on how different crest wall heights and crest wall shapes affect the influence of wind, which is tested by generating the different hydrodynamic conditions on the structure. As prior research demonstrated an increased wind influence for higher crest walls on dikes, it is currently unknown whether this also applies for rubble mound breakwaters. Once this is better understood, financially attractive design decisions can be made since the construction of a crest wall is significantly more cost effective than increasing the crest height. The final sub-question provides insight into the influence of the breakwater slope. The different crest wall shapes and different hydrodynamic conditions will be applied on two slope types in order to obtain thorough representations of its effect.

1.3. Approach of the research

This study aims to answer the research questions supported by the results obtained from physical experiments. This section provides a brief overview of the experimental approach, covering the objectives of the experiments, the main components of the setup and the experimental plan.

1.3.1. Overview of the experiment

In order to address the research question and its associated sub-questions, a series of physical experiments are carried out at the Pacific Basin at Deltares in Delft, the Netherlands. In this setup, a paddle wheel has been applied to obtain the maximum effect of wind on wave overtopping, as was also done in prior research covering the maximum influence of wind on coastal structures (de Waal et al., 1996; Wolters & van Gent, 2007; Van der Bijl, 2022). Within the basin, a flume with a width of 1 meter and a length of approximately 10 meters is constructed, being the test environment for the breakwater. The setup is illustrated in Figure 3.1. The paddle wheel is positioned close above the crest wall with sufficient space for the paddle wheel to rotate accordingly. The wheel rotates with a frequency of 29 Hz, which was determined to be the optimal rotational speed (as demonstrated by de Waal et al., 1996). When water passes over the crest wall, it is transported through the chute into the overtopping box. The structure is constructed to facilitate easy modifications to the crest wall, i.e. attaching the recurved parapet or increasing the crest wall height. The literature study provides further information about the current state of knowledge of these elements. Furthermore, changes of the slope of the structure can only be made without additional modifications of the crest. The reconstruction of the slope is a labor-intensive process and, for this reason, can only be executed once.

The data is obtained from various measuring instruments situated within the setup. In order to measure the wave height accurately, three wave gauges are positioned about 8 m from the crest wall within the flume. These are essential for calibrating the waves, ensuring a reliable and reproducible JONSWAP spectrum comprising of circa a thousand waves.

To monitor water levels, one wave gauge is installed in each water reservoir. The wave gauge in the largest reservoir is connected to a pump. When the reservoir reaches its maximum capacity, the pump receives a signal to drain the reservoir which is required for the experiment to proceed properly. Eventually, each experiment will return a mean overtopping discharge value from which a value is obtained for the ration of the situation including the maximum effect of wind over a situation excluding the effect of wind.

1.3.2. Experimental Plan

The experiments have been conducted on 5 different configurations, varying in slope, crest wall height and crest wall shape. Each configuration was subjected to a set of hydraulic boundary conditions with various water levels, wave heights and wave periods. In total, 288 experiments were conducted, which consisted of 144 experiments including the maximum effect of wind on wave overtopping and 144 excluding the maximum effect of wind on wave overtopping.

After finishing the experiments, the data is analysed within various scientific programming tools that are either open source or are provided by the TU Delft or Deltares.

1.4. Outline

In the first part of this study the basis of the report is provided, incorporating the introduction and the background theory. The context of the research is covered highlighting the significance, objective, and state of the art. Once Part I is finished, enough context is provided to understand the steps taken in the remainder of the report.

In the second part of the thesis, context is provided that resolves around the methodology and the data analysis. First, the steps taken during the test programme are covered providing a complete guide enabling the reader to reproduce experiments and obtain similar results. This is followed by a full data analysis. In this analysis, the results are presented and simultaneously discussed. At the end of Part II, sufficient evidence must be provided to discuss the findings and eventually draw conclusions.

The third part of the thesis begins with a discussion that describes the theoretical meaning of the results obtained. This is followed by the conclusions that highlight the main findings resulting from the research, after which the recommendations provide additional insights for future researchers to take into account when continuing on this subject. In this final phase, the obtained findings are listed and presented as the concluding chapter of the thesis.

The last part of the thesis contains the Appendices, aiming to provide supplementary or additional information for the main content of the report.

Theoretical Background

In this chapter the background theory is presented. This is done by reviewing literature that considers the relevant characteristics of a rubble mound breakwater such as the overtopping discharge caused by waves, and how different design elements and physical processes contribute to or limit the overtopping quantity. This is approached by first explaining wave overtopping in broad terms, where it is treated in literature, and what consequences are linked to wave overtopping. Subsequently, the hydraulic boundary conditions that correspond to the expressions describing the wave overtopping discharge are discussed in more detail. Next, the effects of the dimensional parameters are considered, which include the slope angle and the crest height. This is followed by the influence of several design elements that are described as influence factors, considering roughness of the slope, a berm, obliqueness of waves, and the characteristics of a crest wall. Finally, the effect of wind on wave overtopping is looked into, with the focus on the methodology, findings, and proposed expressions from previous literature.

2.1. Wave overtopping at rubble mound breakwaters

In this section, various methods are proposed that treat the quantification of wave overtopping. The aim is to show how these methods can be applied and to explain when such a method is valid. First, the relevance of wave overtopping is presented, providing various failure modes and limit states. Subsequently, four different expressions are proposed that are either roughly applicable for a mild sloped breakwater, or fall under the necessary criteria for a breakwater with a steep slope.

2.1.1. Wave overtopping in general

A rubble mound breakwater is a type of coastal structure that is built to shelter areas from wave and current action that could otherwise lead to shoreline erosion or unnavigable waters. The structure is constructed of piles of stones with layers that vary in thickness and unit weight. The smaller stones are located at the core, and the larger stones are found at the armour layer with the aim to increase wave dissipation on the slope. A rubble mound breakwater can experience various modes of failure, with the most important mechanisms depicted in Figure 2.1. As a result of the increasing sea level, these mentioned failure modes are more likely to occur. Therefore, various adaptation methods have been developed to prevent disasters from happening as a consequence of structural failure induced by climate change. This literature study will focus primarily on wave overtopping, which is a process where a quantity of water per meter unit width is discharged over the structure, due to its significant potential for wind induced overtopping occurrences.

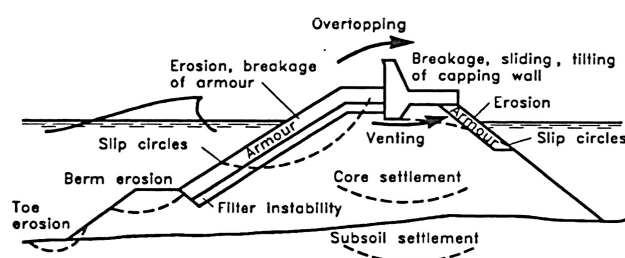


Figure 2.1: Failure modes for a rubble mound breakwater Burcharth (1994)

Allowable limits have been established for rubble mound breakwaters. These are both determined for the ultimate limit state (ULS), concerning the structural strength and resistance, and for the protection of serviceability limit state (SLS). The limit for the structural design is based on the displacements of the armour layer, leading to failure of the structural strength of the breakwater. The [EurOtop \(2018\)](#) guidelines state that this happens when the overtopping discharge exceeds 5 l/s/m. However, this value is largely dependent on the structural strength of the breakwater and is not identical for all circumstances. The serviceability limit state is achieved for large overtopping discharges while the structure remains intact, but the serviceability of the area behind the structure is affected. In other words; the limit is met when property is damaged behind the breakwater such as vessels, buildings, or natural habitats without compromising the structural properties of the structure itself.

The characterization of wave overtopping at coastal structures can be approached in three ways. The first method involves determining the mean overtopping discharge during a peak storm. The second approach focuses on calculating the overtopping volume of an individual wave. The third technique involves analyzing flow velocities and the flow depth during an overtopping event. However, this literature study exclusively focuses on the mean overtopping discharge during a peak storm and the overtopping volume of an individual wave.

2.1.2. Mean overtopping discharge during an overtopping event

Several studies have been conducted to determine the mean overtopping discharge during a peak storm. Pioneering research was conducted by [Goda \(1971\)](#); [Battjes \(1974\)](#); [Owen \(1980\)](#). Each study aimed to obtain a non-dimensional parameter for the overtopping discharge q^* obtained from the normal overtopping discharge q , gravitational acceleration g , and the spectral significant wave height H_{m0} . Equation (2.1) describes the fundamental equation of the expressions that are proposed throughout the literature study.

$$q^* = \frac{q}{\sqrt{gH_{m0}^3}} = a \exp \left[-\frac{b}{\gamma} \left(\frac{R_c}{H_{m0}} \right)^c \right] \quad (2.1)$$

Where γ denotes the comprehensive form of the influence factors including effects such as roughness (γ_f) and the crest wall height (γ_v). The coefficients a , b and c vary per guideline considering different types of structures whose values were eventually calibrated on. They are generally rewritten in the form of an expression and are directly implemented in Equation (2.1).

The first expression that will be discussed is obtained from the [TAW \(2002\)](#) guideline, which is used as guideline for safety assessment for dikes; being a seawall with an impermeable slope. Nonetheless, this expression is included in this study as it accounts for the influence of the seaward slope angle, which is scarcely considered when dealing with mildly sloped rubble mound breakwaters. Moreover, the expression makes a distinction between non-breaking waves, and breaking waves (for more information on wave breaking, see Section 2.2.4). Equation (2.2) is presented as follows:

$$\frac{q}{\sqrt{gH_{m0}^3}} = \begin{cases} \frac{0.067}{\sqrt{\tan \alpha}} \gamma_b \xi_0 \exp \left(-4.3 \frac{R_c}{H_{m0}} \frac{1}{\xi_0 \gamma_b \gamma_f \gamma_\beta \gamma_v} \right) & \text{(For non-breaking waves)} \\ \frac{0.067}{\sqrt{\tan \alpha}} \gamma_b \xi_0 \exp \left(-4.75 \frac{R_c}{H_{m0}} \frac{1}{\xi_0 \gamma_b \gamma_f \gamma_\beta \gamma_v} \right) & \text{(For breaking waves)} \end{cases} \quad (2.2)$$

A common guideline for the design of coastal structures is the Overtopping Manual ([EurOtop, 2018](#)), which is primarily based on physical experiments. The manual includes several expressions for the dimensionless overtopping discharge, neglecting some parameters in order to simplify the equation. From these equations it is concluded that the influence of the wave steepness, a berm and the crest wall, are negligible. However, occasionally these factors are included in an influence factor expressed with γ . The expression they provide is presented in Equation (2.3). Note that this expression is only valid for structures with a slope ratio ranging from 1:2 to 1:4/3, where the latter is the maximum physical limit under which the structure does not collapse. Moreover, the expression is originally developed for non-breaking. While the guideline also proposes an expression for breaking waves, it is stated that it can not be used for rubble mound breakwaters.

$$\frac{q}{\sqrt{gH_{m0}^3}} = 0.09 \exp \left[- \left(\frac{1.5R_c}{\gamma_f \gamma_b \gamma_\beta \gamma_v \gamma_p H_{m0}} \right)^{1.3} \right] \quad (2.3)$$

However, research conducted by [Van Gent et al. \(2022\)](#) has indicated that the wave steepness, the presence of a berm and the presence of a crest wall, affect the overtopping discharge (Equation (2.4)). It is important to note that the applicability of the expression is limited to numerous boundary conditions. When considering the angle of the slope α , the expression is only valid within the range of 1:1.5 to 1:3. The tests were performed on crest walls without a recurved parapet, which has the potential to reduce the overtopping discharge considerably (for normally incident waves). Furthermore, a minimum value of $\gamma_f > 0.33$ is advised as values below this threshold were not validated in the research. The ratio of the protruding part of the crest wall and the freeboard $(R_c - A_c)/R_c$ was smaller than 0.35 in the present test programme, leading to a maximum influence of the crest wall of $\gamma_v = 1.16$. Finally, the expression is only validated for an influence factor that represents the berm within the range $0.5 \leq \gamma_b \leq 1$.

$$\frac{q}{\sqrt{gH_{m0}^3}} = 0.016s_{m-1,0}^{-1} \exp \left[- \frac{2.4R_c}{\gamma_f \gamma_b \gamma_\beta \gamma_v \gamma_p H_{m0}} \right] \quad (2.4)$$

Recent findings obtained by [Irias Mata & van Gent \(2023\)](#) have indicated that slope angle also affects the mean overtopping discharge, either as a separate parameter or via the surf-similarity parameter (with the slope angle and the wave steepness). These findings were validated using numerical methods, resulting in the formulation presented in Equation (2.5). However, the expression has not been validated on physical experiments over a wide range of structure configurations. Moreover, the influence of a recurved parapet is demonstrated to be small to negligible for the model, which means earlier developed expressions for reduction factor γ_p are not applicable. [Irias Mata & van Gent \(2023\)](#) proposed the following expression, in which for simplicity γ_p can be taken 1.

$$\frac{q}{\sqrt{gH_{m0}^3}} = 0.03s_{m-1,0}^{-0.5} \cot \alpha \exp \left[- \frac{4R_c}{\gamma_f \gamma_b \gamma_\beta \gamma_v \gamma_p \xi_{m-1,0}^{0.5} H_{m0}} \right] \quad (2.5)$$

The equations include five influence factors (γ -factors):

1. The first factor (γ_f) is determined by the roughness of the slope varying for various armour types and sizes. For smooth slopes the effect of this parameter is negligible and increases when the slope profile increases in roughness.
2. The second factor (γ_b) is influenced by the berm, which is not included within the research scope of this thesis. This value is simply taken as $\gamma_b = 1$ when no berm is present.
3. The third factor (γ_v) characterizes the influence of the crest wall. When no crest wall is present this value equals $\gamma_v = 1$.
4. The fourth factor (γ_β) represents the influence of the obliqueness of waves. For normally incident waves this value is also simply taken as $\gamma_\beta = 1$;
5. The last influence factor (γ_p) represents the presence of the parapet and is governed by the shape.

The expressions also sometimes include the parameter $s_{m-1,0}$, described as the wave steepness based on the spectral wave height and period. The surf similarity parameter or breaker parameter ξ_0 is also included for some of the expressions and describes the way waves break. The parameter R_c is the free crest height above the water level and H_{m0} , which is the spectral wave height. The last two parameters are included in each expression from the literature, as also shown in Equation (2.1).

It is worth noting that [Van Gent et al. \(2022\)](#) also mentions the influence of wind, but provided no guideline to account for the effects of wind for rubble mound breakwaters. Experimental results will be compared with this equation to find a relation with the contribution of wind.

2.1.3. Overtopping volumes of individual waves

It is also suggested in literature that overtopping hazards should directly be related to individual wave overtopping events (Franco et al., 1994). As the maximum volume of an individual wave is likely to be much larger in comparison with the flattened mean volume over a storm event, some research suggests that overtopping risks should be directly related to the maximum overtopping volume of a single wave. This can be done by identifying the wave that causes increased overtopping volumes. In terms of the methodology, Koosheh et al. (2021) concluded that a continuous drainage system at the crest leading to a reservoir is the least complex method of measuring individual overtopping volumes.

2.2. Hydraulic boundary conditions

The primary objective of this section is to investigate the influence of the various hydraulic boundary conditions that influence wave overtopping. The relevant hydraulic processes considered and discussed include the wave spectrum, water level, wave steepness, wave breaking, and the angle of wave incidence.

2.2.1. Wave Spectrum

Instead of approaching the coast in a perfect sinusoidal motion, waves typically approach the shore in a manner that is characterized by a wave spectrum, providing wide information on wave energy considering different directions and frequencies. In a spectral analysis the wave energy is summed up for each frequency that corresponds to an investigated sea-state. The wave height H is defined as the spectral mean wave height H_{m0} , which equals the normal significant wave height H_s for deep water, but differs in shallow water. The governing period the spectral mean wave period $T_{m-1,0}$. For deep water the spectral mean period can be derived from the peak wave period using the following expression:

$$T_{m-1,0} = T_p/1, 1 \quad (2.6)$$

The use of the spectral period $T_{m-1,0}$ is typically recommended in shallow water to accommodate for spectral shape changes. In such conditions, at both higher and lower frequencies the peak becomes less pronounced and more energy is distributed across the spectrum. As severe wave breaking also flattens the spectrum, identifying the peak of the spectrum becomes increasingly difficult (CETMEF, 2007).

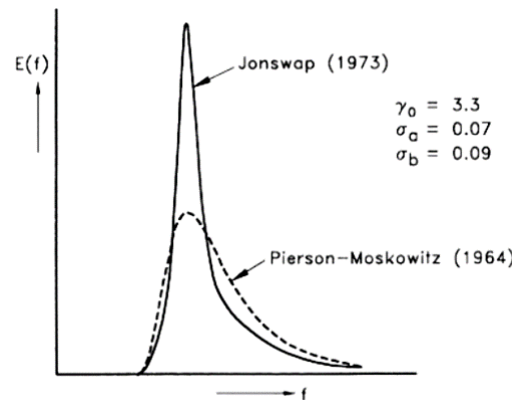


Figure 2.2: A JONSWAP spectrum plotted with a PM spectrum (Holthuijsen, 2007).

There are two types of spectra that are widely used: the Pierson-Moskowitz (PM) spectrum, introduced by Pierson & Moskowitz (1963) and the JONSWAP spectrum (Joint North Sea Wave Project), introduced by Hasselmann et al. (1973). The PM spectrum represents a spectrum for a fully developed sea state in deep water, while the JONSWAP spectrum represents fetch-limited sea states (i.e. growing sea). It incorporates an additional term in comparison with the original PM spectrum and also depends on the (limited) fetch length. Therefore, the JONSWAP spectrum has a sharper peak in comparison with the PM spectrum which can be observed in Figure 2.2. It is worth noting that more variations of wave spectra have been developed. However,

but for the purpose of this thesis, the decision is made to focus simply on the JONSWAP spectrum because the influence of the spectral shape is accounted for by using the spectral mean wave period.

2.2.2. Water level

The water level has an influence on the overtopping discharge at dikes and breakwaters as the freeboard R_c increases or decreases (Equation (2.1)). As the water level is certain to increase in the future as a result from climate change, coastal structures require to be upgraded. In addition, Radfar et al. (2021) investigated the joint effect of wave heights and water levels in the design of rubble mound breakwaters using Copula functions, including a comparison with the conventional method. Both methods lead to a more or less linear increase of the mean overtopping discharge over time (see Figure 2.3). The difference in the water level is inversely proportional to the difference of the total crest elevation. This is a dominant factor in various guidelines (EurOtop, 2018; TAW, 2002), which also emphasizes the relevance of acquiring knowledge about this phenomenon.

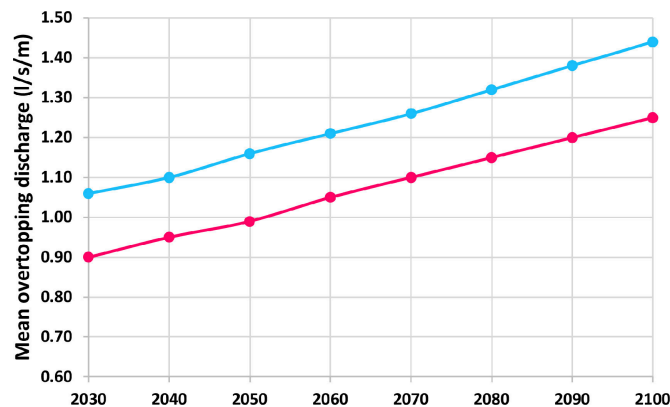


Figure 2.3: The trend of changes in overtopping discharge (l/s/m) in the coming years (2030–2100) for the two different design approaches; blue line is for the conventional design method and the pink is for the joint design method (Radfar et al., 2021).

In addition, Hogeveen (2021) investigated adaption measures for a rising sea level by using climate adaption pathways considering the berm, crest wall, foreshore and adding a low crested structure. He emphasizes that no single solution exists and that all options should be included throughout an adapted design process. As they are well understood for situations without wind, research still needs to be conducted on situations with wind.

2.2.3. Wave steepness

The wave steepness is a dimensionless ratio of wave height H to wave length L and is represented by symbol s_0 . While the concept is straightforward for periodic waves, for random waves the waves steepness s_0 is defined by the significant wave height H_s divided by the wave length L_0 in deep water. Considering the latter, waves tend to break, in the absence of wave dissipation, when the steepness of waves exceeds the threshold of 1:7.

Furthermore, when describing the wave steepness $s_{m-1,0}$ in shallow waters approaching coastal structures, the spectral wave period $T_{m-1,0}$ is generally accepted to define the wavelength and is used to define numerous processes like wave run-up, overtopping, reflection, and armour layer stability (see Van Gent, 1999 for wave run-up and wave overtopping).

$$s = \begin{cases} s = H/L & \text{for periodical waves in deep water.} \\ s_0 = H_s/L_0 = 2\pi H_s/(gT_p^2) & \text{for random waves in deep water.} \\ s_{m-1,0} = H_s/L_0 = 2\pi H_s/(gT_{m-1,0}^2) & \text{for random waves in shallow water.} \end{cases} \quad (2.7)$$

EurOtop (2018) and TAW (2002) predict no influence of wave steepness for rubble mound breakwaters. However, Lioutas et al. (2012) and Koosheh et al. (2022) showed that for rock armoured revetments with an impermeable core, wave steepness does affect the mean overtopping discharge. Additionally, these results were further confirmed by Van Gent et al. (2022), who investigated the influence of several factors on wave overtopping. However, the methods describing this reduction have various outcomes.

2.2.4. Breaker parameter

To distinguish the types of wave breaking, the breaker parameter ξ is used (i.e. Surf similarity parameter or Iribarren number), which is described with a function of the wave steepness and the bottom slope angle. Schiereck & Verhagen (2019) mentions four different types of wave breaking, using the Iribarren number ξ , and are described as follows: spilling waves ($\xi < 0.3$), plunging waves ($0.5 < \xi < 3$), collapsing waves ($\xi \approx 3$), and finally, surging waves ($\xi > 3$). Generally, waves are considered to be of breaking type when parameter ξ is smaller than 2.5, and considered to be of the non-breaking type when ξ exceeds 2.5.

$$\xi_{m-1,0} = \frac{\tan(\alpha)}{\sqrt{s_{m-1,0}}} \quad (2.8)$$

As the breakwater is located in shallow water and is subjected to a random wave spectrum. The spectral breaker parameter $\xi_{m-1,0}$ must be applied instead of the general breaker parameter ξ_0 for deep water.

The slope of a seaward structure is characterized by $\cot(\alpha)$, where α is the degree of the slope angle. Generally, the slope ranges from $\cot(\alpha) = 6$ to $\cot(\alpha) = 1$. For a slope that holds $\cot(\alpha) \geq 6$, the slope is mild. For the situation where $\cot(\alpha) \leq 1$ the value of the slope is considered too steep and is treated as a (near) vertical wall. The decision of $\cot(\alpha)$ commonly depends on the cost efficiency of the structure, but also influences the wave breaking process which is expressed with the dimensionless Iribarren number given in Section 2.2.4, where the spectral time period is expressed by $s_{m-1,0} = 2\pi/(gT_{m-1,0}^2)$. With data obtained from experiments conducted by Van Gent et al. (2022), the research was continued by developing a numerical model of which the results of the simulations showed a strong dependency on the effect of the slope angle for wave overtopping at rubble mound breakwaters (Irias Mata & van Gent, 2023). As mentioned in Section 2.1, not every method incorporates the effect of the slope. While some expressions do incorporate its effect, it is not done by including a new factor representing the slope (as a function of γ), but add α in the expression. The effect of the slope is also incorporated in the breaker parameter $\xi_{m-1,0}$, which is both presented in the expressions for breaking waves as for instance proposed by TAW (2002) and in expression for non-breaking waves as proposed by Irias Mata & van Gent (2023).

2.3. Influence factors corresponding to the wave overtopping discharge

The Equations 2.2-2.5 as introduced in Section 2.1 depend on various influence factors γ_f , γ_β , γ_b , γ_v , and γ_p and are treated in this Section respectively. This Section of the literature review takes a closer look at these parameters with the aim of providing information on how they are calculated and under what conditions they are validated. Numerous expressions exist for obtaining the appropriate values for these factors, each corresponding to different boundary conditions that are derived from physical experiments or data obtained from numerical models.

2.3.1. Influence factor for roughness

The seaward slope of a rubble mound structure is defined by several key parameters, the slope angle (α), its roughness (represented by the roughness factor γ_f), and permeability P . These factors play a crucial role in determining the structures stability and performance.

The roughness factor, denoted as γ_f , characterizes the irregularity or roughness of the seaward slope of a rubble mound structure. It quantifies how effectively the structure dissipates the energy from wave action. For structures with smooth slopes like dikes, γ_f approaches 1, indicating minimal energy dissipation. In contrast, rougher slopes have lower γ_f values, signifying greater energy dissipation. This energy dissipation is a key factor influencing overtopping discharge and can result in reduced overtopping for rougher slopes.

The design of the armour layer of a rubble mound breakwater is primarily governed by dynamic wave loading. The size and shape of the armour stones are designed to allow for a certain degree of stone displacements over the structures design lifetime (CETMEF, 2007). Several factors impact the extent of stone displacement, including the weight of the stones (which is determined by the material used) and the degree of interlocking between the stones, which depends on their placement and shape. For an increase of roughness the reduction factor decreases leading to lower overtopping volumes (Van Gent, 2020). According to some literature, this parameter for roughness has been found to deviate in the range between $\gamma_f = 0.4$ to 0.5 when an armour layer with a thickness of twice the stone diameter d_{n50} is present (Bruce et al., 2009; Molines & Medina, 2016).

$$\gamma_f = 1 - 0.7 \left(\frac{D_{n50}}{H_{m0}} \right)^{0.1} \quad (2.9)$$

An alternative approach that determines the value for the roughness factor is presented with the simple expression presented with Equation (2.9), which is a function of the non-dimensional stone diameter. This equation is validated for Equation (2.4) and Equation (2.5). In the TAW (2002) manual, a constant value for a permeable rock revetment with value $\gamma_f = 0.55$ is suggested when the Iribarren parameter falls below $\xi_0 < 1.8$. As the breaker parameter ranges from $1.8 < \xi_{m-1,0} < 10$ the value increases linearly towards $\gamma_f = 1.0$, leading to:

$$\gamma_f = \begin{cases} 0.55 & \xi_{m-1,0} < 1.8 \\ 0.55 + \frac{0.45}{8.2}(\xi_{m-1,0} - 1.8) & 1.8 < \xi_{m-1,0} < 10 \end{cases} \quad (2.10)$$

Moreover, the EurOtop (2018) proposes a modification of Equation (2.10). In this version, the roughness factor increases linearly from $\gamma_f = 0.40$ within in the range $5 < \xi_{m-1,0} < 10$, as depicted in the expression from Equation (2.11). It's important to note that for rubble mound breakwaters with a permeable core, there is an upper limit set for the roughness factor, which is $\gamma_f = 0.60$. This means that even if the linear trend in γ_f would suggest a higher value, it must not exceed $\gamma_f = 0.60$, in accordance with the EurOtop (2018) guidelines.

$$\gamma_f = \begin{cases} 0.40 & \xi_{m-1,0} < 5 \\ 0.40 + 0.12(\xi_{m-1,0} - 5) & 5 < \xi_{m-1,0} < 10 \end{cases} \quad (2.11)$$

While the equation under consideration is applicable to breakwaters with a permeable core, more comprehensive expressions have been formulated to account for the influences of various factors on impermeable slopes. These factors include the volume of overtopping, freeboard, wave steepness, the surf-similarity parameter, and the presence of protruding blocks. These expressions can provide a more detailed understanding of how roughness is affected. However, throughout this research it is adopted that Equation (2.9) suffices for the analysis conducted in Chapter 4, as outlined in the research by Van Gent et al. (2022).

2.3.2. Influence factor of the obliqueness of waves

In natural settings, waves don't always approach coastal structures at a normal angle ($\beta = 0^\circ$), but often approach obliquely. Studies investigating the impact of obliquely incident waves are of additional value to the existing guidelines on wave overtopping. It is important to note that obliquely incident waves generally lead to a reduced amount of wave overtopping, compared to waves that arrive at the structure under a normal angle. This reduction effect is characterized by the reduction coefficient γ_β , which has been defined in various studies (see Figure 2.4). It is worth mentioning that all methods depicted in the figure are developed for different wave loading, overtopping parameters, and different structures Van Gent (2014). Additionally, recent research has also investigated the effect of obliquely incident waves for caisson breakwaters (Van Gent, 2021), and on smooth and rough sloped dikes with a berm (Van Gent, 2020).

Additional research has been carried out by Van Gent & van der Werf (2019) to investigate the influence of a crest wall, enabling more advanced designs possibilities. In conclusion, this paper provides a sufficient expression (Equation (2.12)) for the reduction factor for wave overtopping of a rubble mound breakwater with a crest wall, depending only on the angle of wave incidence β . The presence of a crest wall would obviously lead to a reduction of the overtopping discharge, but has no direct influence on the influence factor representing the obliqueness of waves.

$$\gamma_\beta = 0.65 \cos^2(\beta) + 0.35 \quad (2.12)$$

It is mentioned by Van Gent (2014) that this equation can be used as a first estimate for other rubble mound breakwaters with crest elements. However, it is recommended to analyse its validity outside the range of the present test programme. Especially when other armour layer types or shapes are used, such as concrete blocks with a specific shape, or different variants of crest wall configurations.

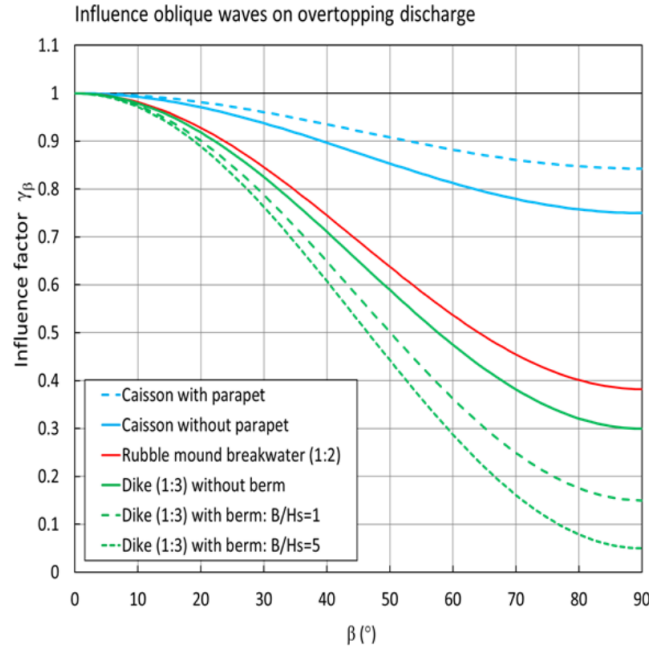


Figure 2.4: This figure shows various methods describing the influence of oblique waves on wave overtopping for (Van Gent, 2022).

2.3.3. Influence factor for the berm

A berm in a rubble mound breakwater can be described as a horizontal platform constructed along the seaward slope of the structure. The function of this element is to redistribute wave energy and to provoke wave breaking further off-shore. This leads to a dissipation of wave forces reducing the risk of erosion and wave overtopping at the crest of the structure. For an increasing width of the berm, the overtopping volume will be reduced (Besley, 1998). In the absence of a berm, the value of the reduction factor is evidently $\gamma_b = 1$, and decreases for an increasingly present berm. The expression by Van Gent et al. (2022) used to determine the value of the berm influence factor γ_b is presented below:

$$\gamma_b = 1 - 18 \left(\frac{s_{m-1,0} B}{H_{m0}} \right)^{1.3} \left(1 - 0.34 \left(\frac{B_L}{s_{m-1,0} A_c} \right)^{0.2} \right) \quad (2.13)$$

Where B is the width of the berm, B_L is the berm level measured from the level of the armour in front of the crest wall to the berm level, $s_{m-1,0}$ the wave steepness calculated with the spectral time period $T_{m-1,0}$, H_{m0} the spectral wave height and A_c the distance between the still water level and the level of the armour at the crest. For some breakwater designs the armour width in front of the crest is greater than the common amount of four times the stone diameter. This leads to an increase of wave dissipation leading to a reduction in discharge. For these circumstances the armour width in front of the crest wall can be taken as the berm ($B = G_c - 4D_{n50}$), where $B_L = A_c + h_b$ equals zero (Van Gent et al., 2022). This leads to a simplification of Equation (2.14), as described below:

$$\gamma_b = 1 - 18 \left(\frac{s_{m-1,0} B}{H_{m0}} \right)^{1.3} \quad (2.14)$$

2.3.4. Height of the crest wall

Increasing the height of a crest wall can be beneficial as an adaptation method for dealing with the rising sea level. Research on crest modification for seawalls was conducted by Van Doorslaer et al. (2015) as an addition to the commonly applied guidelines by the TAW (2002) and EurOtop (2018). However, as van Van Doorslaer et al. (2015) studied the effect on smooth slopes, the proposed expression might not be applicable for a rubble mound breakwater. Therefore, the height of a crest wall is accounted for in the reduction factor γ_v as demonstrated by Van Gent et al. (2022):

$$\gamma_v = 1 + 0.45 \left(\frac{R_c - A_c}{R_c} \right) \quad (2.15)$$

The equation presents a simple relation that incorporates the impact of the crest wall by introducing a linear relationship between the ratio of the protruding part of the crest wall ($R_c - A_c$) and the crest elevation (R_c).

Another method that includes the influence factor for the crest wall height is proposed in the [TAW \(2002\)](#) guideline. This factor is validated for configurations where the crest wall forms an essential part of the slope. This is to be considered when the following criteria is met:

- The average slope from the toe to a height of $1.5H_{m0}$ below the still water line must lie between 1:2.5 and 1:3.5;
- The sum of all berm widths (if more than one) may not exceed $3H_{m0}$;
- The foot of the wall must be located at a maximum of $1.2H_{m0}$ above the still water line;
- The height of the wall itself must range be in the range of $0.5H_{m0} \leq h_{crest} \leq 3H_{m0}$.

A constant value of $\gamma_v = 0.65$ is obtained when the criteria is met and a vertical wall is present. The influence factor for the crest wall height $\gamma_v = 1$ if the criteria is not met.

The [EurOtop \(2018\)](#) manual does not include the effect of a crest wall and is therefore treated as $\gamma_v = 1$. Meaning, according to the guideline, a crown wall does not affect the overtopping discharge on a rubble mound breakwater.

2.3.5. Shape of the crest wall

In some cases a protruding element, for example a bull nose, is attached to a crest wall with the goal reduce overtopping discharges. However, the available amount of information and conducted research on this topic is limited and specific for different situations. Experiments on the shape of a crest wall were conducted by [Oh et al. \(2018\)](#) for various protruding crests and proposed the following expression:

$$\gamma_p = 1 - 0.1 \frac{B_r}{h_r} \quad (2.16)$$

In Figure 2.5a the parameters of Equation (2.16) are visualized in order to provide an explanation of this formula. [Oh et al. \(2018\)](#) conducted experiments on a limited amount of shapes, but did conclude that wave loading almost proportionally increases with the degree of the curvature, although the tendency showed some discrepancy depending on the crest height.

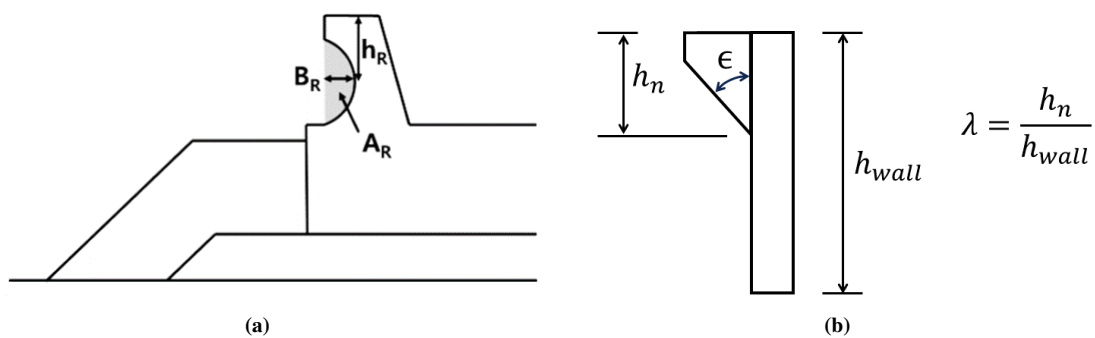


Figure 2.5: Dimensional parameters for a recurved parapet in line with literature; **a)** The definitions of the parameters related to the recurved parapet reduction factor of Equation (2.16) ([Oh et al., 2018](#)); **b)** A Schematization of a crown wall with parapet as demonstrated by [Van Doorslaer et al. \(2015\)](#)

[Irias Mata & van Gent \(2023\)](#) concluded using a numerical model that the shape of a crest wall only has influence on very low overtopping volumes and is therefore neglected in the equation. However, past research concluded that the influence of wind on wave overtopping is found to be largest for the lower overtopping regime, which makes it relevant to analyse the influence on the wind effect in the presence of a recurved parapet or bull nose.

Another expression to determine the reduction caused by a recurved parapet (bull nose) was developed by [Van Doorslaer et al. \(2015\)](#). However, this expression was exclusively validated for the measurements obtained after the experiments corresponding to impermeable smooth sloped structures. The expression proposed by [Van Doorslaer et al. \(2015\)](#) is as follows:

$$\gamma_p = \begin{cases} 1.80 (1.53 \cdot 10^{-4} \cdot \epsilon^2 - 1.63 \cdot 10^{-2} \cdot \epsilon + 1) \cdot (0.75 - 0.20\lambda) & \frac{h_{wall}}{R_c} \geq 0.25 \\ 1.80 (1 - 0.003\epsilon) \cdot (1 - 0.14\lambda) - 0.53 & \frac{h_{wall}}{R_c} < 0.25 \end{cases} \quad (2.17)$$

These equations assume that ϵ and λ are within the ranges set by [Van Doorslaer et al. \(2015\)](#). In this form they applicable for the relevant setup examined in this research. The definitions of ϵ and λ are described in [Figure 2.5b](#).

Additionally, [Molines et al. \(2019\)](#) demonstrated after carrying out extensive research including physical experiments and creating a numerical model that the influence of a recurved parapet is negligible for large overtopping discharges ($q > 10^{-3}$). For lower overtopping discharges, the reduction of the overtopping discharge was primarily dependent on the angle of the parapet ϵ . Eventually, it is recommended to apply a parapet with $\epsilon \approx 30^\circ$ and $w_p/h_p \approx 1$ to optimize the reduction of the overtopping discharge, whilst considering the technical feasibility of the parapet. Despite the recommendation of an optimum, an expression as a function of these two parameters has not been proposed.

2.4. Influence of wind

In general, the influence of wind is not taken into consideration for the design of a rubble mound breakwater. Therefore, this section aims to provide an overview of the state of knowledge on this subject. First, this section looks into the background theory on what is currently known and what requires to be investigated. Afterwards, known experimental methods are shown that focuses on the potential influence of wind. Eventually, a concluding remark is made to obtain an overview of what needs to be researched and what methods there are already available to implement.

2.4.1. Background theory

So far, numerous influencing factors have been treated. However, at present the influence of wind is still overlooked. The question that arises is whether it is valid to neglect its effect, as the magnitude of this influence will likely increase during the coming decades as there is a general consensus among climate scientists that hurricane intensity will, at least in the US, increase in the future ([Mayo & Lin, 2022](#)). This is one of many reasons to look further into the maximum effect of wind on wave overtopping. Pioneering research carried out by [de Waal et al. \(1996\)](#) demonstrated that the effect of wind could increase overtopping volumes with a factor of 3.0 for vertical seawalls. Still, as this is pioneering research, in the end of the study it is recommended to perform further research to quantify overtopping volumes accurately.

In a subsequent study, [Wolters & van Gent \(2007\)](#) carried out similar experiments involving rough and smooth sloped structures with slopes 1:2 and 1:1.5. The results showed that the mean overtopping discharge with wind 1.3-6.3 times larger than the mean overtopping discharge without the maximum effect of wind. Meaning, the increase is in the same range as was concluded by [de Waal et al. \(1996\)](#).

More recent research including physical experiments was carried out by [Chowdhury et al. \(2020\)](#). Rather than quantifying overtopping discharges, the research aimed to develop a CFD tool to gain further understanding of the processes concerning the effect of wind on wave overtopping. While it is mentioned that wind has an impact on increasing the mean overtopping discharge, the study does not provide specific quantitative values to support this conclusion.

Recently, research was carried out by [Van der Bijl \(2022\)](#) on smooth sloped dikes, including the effect of a crest wall and a promenade, which was later published by [Van Gent et al. \(2023\)](#). The results of this research show an increase of the mean overtopping discharge that amounts to a factor 4 in comparison with the situation without wind, coinciding with the finding from prior research. The location and the height of the crest wall were varied, and found for an increasing crest wall an increasing wind effect, which was motivated with the decreasing overtopping discharge, which evidently leads to an increasing maximum wind effect. A promenade only led to an observable effect for a higher crest wall. It is argued that for a lower crest wall, water easily fills

the triangular area above the promenade, which can be treated as an extension of the slope. As a consequence, the waves can flow over the crest without being obstructed by the crest wall.

Eventually, a contributing factor for wind described as γ_w is proposed. This factor is determined with Equation (2.18), simply being the ratio of the overtopping discharge of the experiment with paddle wheel (with wind) over the experiment without using the paddle wheel (without wind). In Equation (2.18) the non-dimensional overtopping discharge q^* is used, which is a valid choice as the application of the normal overtopping discharge q would result in the same value.

$$\gamma_w = \frac{q_w^*}{q^*} \quad (2.18)$$

At the end of the researches conducted by Van Gent et al. (2023), an expression is proposed to determine the value for the influence factor of wind:

$$\gamma_w = 0.011q^{*-0.43} + 1 \quad (2.19)$$

Most recently, Dijkstra (2023) also studied the maximum wind effect with the influence of a smooth sloped dyke, focusing on the slope angle. No dependency was found for a different slope angle while an effect of the slope itself could be identified. This is explained with the breaker parameter, as he also demonstrated that an increase of wave breaking increases the maximum wind effect. Additionally, he investigated the influence of the crest wall height and found a dependency on the dimensionless crest wall height h_{wall}^* , stating that a larger value results in larger wind influence. A theory regarding the promenade in front of a crest wall was also proposed. The theory describes the process of overshooting when a virtual continuation of the slope line passes over the crest wall, indicating that no waves crash against the element. This results in less vertically directed spray, that would either falls down or would be transported over the crest wall by wind, or in this case the paddle wheel. As a result, he provides an improved version of the equation that was proposed by Van Gent et al. (2023).

With the extended data set provided by the research carried out by Dijkstra (2023), an improvement of the expression in Equation (2.19) was found, including the discovery of the observable dependency of the crest wall height. This equation is shown in the expression below:

$$\gamma_w = 0.051q^{*-0.281} + 1 \quad (2.20)$$

$$\gamma_w = \begin{cases} 0.0665q^{*-0.217} + 1, & \text{if: } 0.25 \leq h_w^* \leq 0.40 \\ 0.0102q^{*-0.231} + 1, & \text{if: } 0.40 \leq h_w^* \leq 0.80 \end{cases} \quad (2.21)$$

These equations involve the non-dimensional crest height ($h_{wall}^* = h_{wall} / H_{m0}$), from which it is clear that an increasing value of h_{wall}^* leads to an increasing maximum wind effect.

A significant amount of research remains to be conducted to sufficiently understand the influence of wind. One can think of elements and relations such as slope dependencies, crest wall shapes, armour stone dimensions, foreshore changes, and numerous other dimensional characteristics.

2.4.2. Methodologies

Currently, physical experiments have been conducted with two different methods. de Waal et al. (1996) applied a paddle wheel to mechanically transport water over the water retaining structure, while Chowdhury et al. (2020) chose to use two rows of fans and implement the results to develop new CFD tools.

The idea of the paddle wheel is to maximize the influence of wind. That is to say, all water above the crest is transported to the lee side of the structure. An optimal rotational speed is acquired to maximize the transport. The estimated water transport efficiency of the wheel with a rotational speed of 22 revolutions per minute leads to >90% Van Gent et al. (2023). Chowdhury et al. (2020) applied fans to generate wind as they wanted to make adjustments to the wind speeds and were not investigating the maximum influence on wave overtopping specifically.

2.4.3. Concluding remarks on wind

As a concluding remark, Table 2.1 shows the literature of the mentioned studies in which experiments were carried out to improve our understanding of the influence of wind on wave overtopping. These studies provide the fundamentals for the present study, operating as a guideline through the methodology, the analysis and to the conclusion. Adding to that, a significant amount of research remains to be done to create a reliable expression that accurately describes the effect on wind to determine proper dimensions for various seawalls.

Table 2.1: Conducted research on the Influence of wind on wave overtopping for different water retaining structures

Source	Structure	Elements	Schematization of wind
de Waal et al. (1996)	Vertical structure	Water depth, relative crest height, wave steepness	Paddle Wheel
Wolters & van Gent (2007)	Rubble mound Breakwater and smooth sloped dike	roughness and slope	Paddle wheel
Chowdhury et al. (2020)	Vertical Seawall	Wind speeds	Fans
Van Gent et al. (2023)	Smooth sloped dyke	Crest Element, promenade, Wave steepness, water level, wave height	Paddle Wheel
Dijkstra (2023)	Smooth sloped dyke	Mild slope, crest wall height, and promenade	Paddle wheel

II

Physical model tests and analysis

Methodology

In this chapter a clear record on how the data was obtained is provided, with the aim to show the methodology is reliable and repeatable. First, an elaboration of the model-setup is given where it is clarified what design decisions were made, and how the hydrodynamics were chosen. Afterwards, an explanation is provided on how data was collected and analyzed. Subsequently, it is covered how biases are being mitigated, concerning the credibility of data when data is correct or why it can be disposed. Finally, an analysis is made to highlight processes that met the expectations and those that did not.

3.1. Model Set-Up

The experimental set-up is shown in Figure 3.1, showing a detailed presentation of the flume, breakwater, paddle wheel and water reservoirs. The flume is situated inside the Pacific Basin at Deltares, which is a large water basin with dimensions of $28 \times 14 \times 1.25$ m. The wave spectrum is generated by two large wave generators with each a width of 7 m to occupy the total width of the basin. The flume itself has a length of 12 m, a width of 1.0 m, and a height of 1.25 m, and contains a breakwater, paddle wheel, and a transportation chute with an overtopping box (see Appendix F for pictures of the model setup). The installation of the paddle wheel is identical to installation used by [Van Gent et al. \(2023\)](#) and [Dijkstra \(2023\)](#), having a width of 0.98 m, a diameter of 1.4 m and 12 paddles. The function of the paddle wheel is to transport the water that exceeds the height of the crest wall into the chute with a width of 90 cm. The rotational speed of the paddle wheel is motorized and optimized (29 Hz) to transport at least 90% of the water.

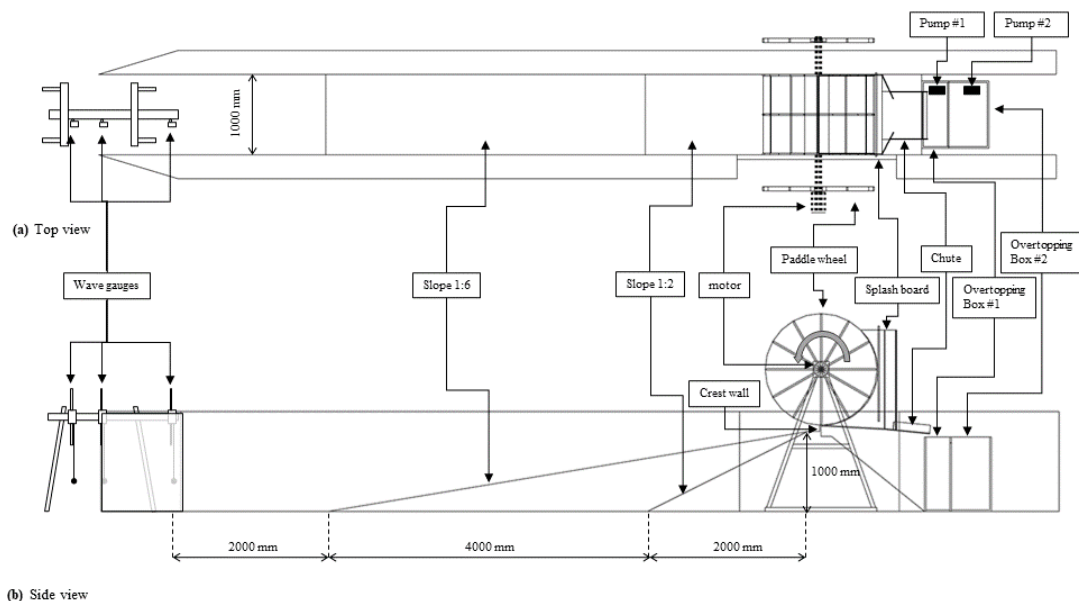


Figure 3.1: Set-up of the experiment; **a)** Top view of the flume 1:6; **b)** Side view of the flume

The first breakwater configuration had a 1:2 slope with two different crest walls on top of the structure: a vertical crest wall with a height of 5 cm, and a vertical crest wall with a height of 8 cm (see Figure C.2 for more details). After completing the experiments on this configuration, a new 1:6 sloped breakwater was constructed inside the flume. The previous breakwater first needed to be demolished to extend the core four meters "offshore". After completing the core by hand, the filter layer was put into position. Subsequently, the armour layer was constructed which had to be reinforced with an epoxy layer. This epoxy layer is a plastic glue that prevents movement of the stones, aiming to guarantee identical slope properties for each test.

Directly after an overtopping event, the water is transported into the small compartment of the overtopping box with a capacity of 75 liters. When this capacity is exceeded, the water overflows into the second compartment, which has a capacity of 180 liters. When the maximum volume of the latter is reached, a pump will be activated to drain the water out of the reservoir.

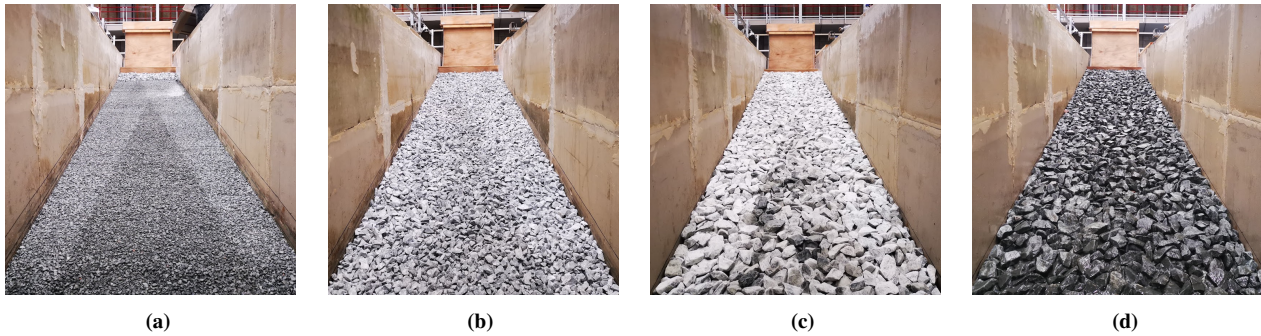


Figure 3.2: Construction sequence of the 1:6 sloped breakwater; (a) Construction of the breakwater core; (b) Construction of the filter layer on top of the core; (c) Construction of the armour layer on top of the filter layer; (d) Covering the armour layer with epoxy.

The breakwater cross-sections are provided in Figure C.2, including the dimensions of the breakwater, the stone-types that were used for each component of the breakwater, and the thickness of each layer. The figure also includes a detailed design of the crest wall, presenting different modifications with the associated dimensions. It is important to note that the 1:6 sloped breakwater only differs from the 1:2 sloped breakwater with the slope and an additional crest wall configuration where a bull nose is attached on the 5 cm crest wall. The bull nose has a protruding part of $B_r = 8$ mm, a height of $h_r = 16$ mm, and an exit angle of $\epsilon = 45^\circ$. The height ratio will then be $\lambda = 0.32$. All designs have a permeable core with a nominal stone diameter d_{n50} of 0.038 m at the armour layer, 16 mm at the filter layer and of 7 mm at the core of the structure. The layer thickness of the armour layer is about two times the nominal stone diameter ($2d_{n50}$), which amounts to 75 mm. The grading curve of each stone layer can be observed within Appendix D. The width of the armour layer in front of the crest wall ($G_c = 15$ cm) is identical for each configuration. The initial crest wall was 5 cm and could be conveniently heightened up to 8 cm with an attachment of 3 cm. The height of the paddle wheel on top of the crest wall could just as convenient be adapted to the proper height. Eventually, the bull nose could be mounted quickly on the crest wall with the use of screws.

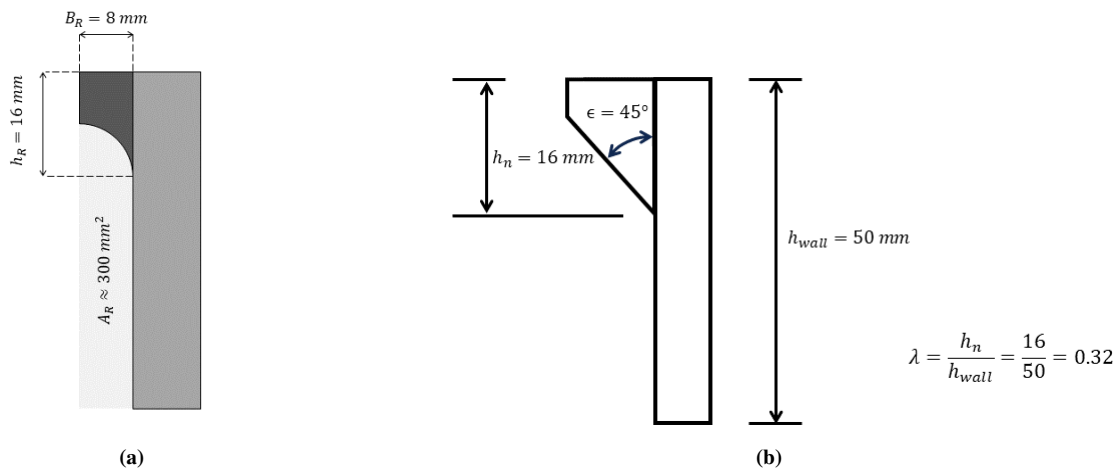


Figure 3.3: Parameters for the parapet mounted on the crest wall; (a) Dimensions according to Oh et al. (2018); (b) Dimensions according to Van Doorslaer et al. (2015).

Three wave gauges were installed in the opening of the flume to measure the wave height. The distance between the first wave gauge and the crest wall is around 8 meters. These wave gauges were used to predict the incident wave height at the breakwater. The wave height was predetermined with the wavelength to obtain the desired wave steepness and breaking behaviour and were generated with the wave generators present in the basin. This technique is derived from the method explained and performed by Zelt & Skjelbreia (1992), who used the linear wave theory to predict the incident wave height at the crest wall. The mean wave overtopping discharges were measured using an overtopping chute transporting the water into the overtopping box. The inside of the box consisted of two compartments: a small compartment and a large compartment. The first is used to measure small mean overtopping discharges more accurately. When the small compartment exceeds its capacity, the water inside overflows into the large box where a larger water volume can be stored. The water volume is measured with a wave gauge installed in each storage compartment, which is capable of measuring its water content. When the large reservoir has reached its capacity, a pump connected to the wave gauge automatically drains the box, which enables the continuation of the test.

3.2. Experiment programme

Five different rubble mound breakwater configurations with different combinations of the slope angle and crest walls were tested. These designs are shown in Section 3.2 where each configuration corresponds to an abbreviation that is used throughout the remainder of this report. The first character describes the value of $\cot \alpha$ (either 2 or 6), the second the height of the crest wall in centimeters (differs between 5 or 8), and the last character represents the shape of the crest wall (V for vertical shape and P for parapet).

Configuration	Design	Abbreviation
1	Breakwater with a 1:2 slope and a 5 cm crest wall	25V
2	Breakwater with a 1:2 slope and an 8 cm crest wall	28V
2.5	Breakwater with a 1:2 slope and an 8 cm recurved crest wall (bull nose)	25P
3	Breakwater with a 1:6 slope and a 5 cm crest wall	65V
4	Breakwater with a 1:6 slope and an 8 cm crest wall	68V
5	Breakwater with a 1:6 slope and a 5 cm recurved crest wall (bull nose)	65P

Each set-up had initially 36 varying hydraulic conditions. However, some of the predetermined conditions led to insufficient overtopping discharges where either its non-dimensional quantity was too small (below 10^{-7}) or zero. For very small discharges the scaling effects have become dominant, resulting in an unreliable result. The experiments that were carried out on the 1:2 slope, including a recurved crest wall, exclude the tests with a paddle wheel. Nevertheless, these tests are included to contribute to the development of the influence parameter representing the parapet in Equation (4.5). Nonetheless, the results obtained from Configuration 5 (65P) are judged to be sufficient to determine the influence of a recurved crest wall on the maximum wind effect.

After the test program, a limited amount of experiments had to be removed as the amount of overtopping for the situation without onshore wind exceeded the amount for the situation with wind, which is unrealistic. This primarily occurred during the tests with the 1:2 slope and recurved crest wall shape. Consequently, leading to the removal the results obtained for this configuration (at least when wind is included). This is motivated by the fact that onshore blowing wind can only have an increased influence on the effect of wind as the paddle wheel does not exert forces in the offshore (negative) direction.

Eventually, the idea to combine four different wave heights with three different wave steepness values was still abided. This did not lead to complications during the experiments on the 1:2 slope, but for the 1:6 slope waves broke too early for steeper waves at lower water levels, leading to the decision to only generate mild waves for the lowest water level (80 cm), mild and medium steepness waves for the intermediate water level (85 cm), and mild to steep waves for the deepest water level (90 cm). It would have been favourable to apply all steepness waves for deeper water depths, but that would exceed the physical limit of the basin leading to overflowing the height of the boundary walls. A summary of the parameters used for all configurations is found in Table 3.1.

Table 3.1: Dimensional parameters of the first rubble mound breakwater (based on previous research by Van Gent et al. (2022))

Parameter	Symbol	Values/Ranges	
		Slope 1:2	Slope 1:6
Armour stone Diameter (m)	D_{n50}	0.038	0.038
Water depth (m)	h	0.70-0.80	0.80-0.90
Incident significant wave height at toe (m)	H_{m0}	0.120-0.220	0.12-0.22
Wave steepness: $s_{m-1,0} = 2\pi H_{m0}/gT_{m-1,0}^2$ (-)	$s_{m-1,0}$	0.013-0.042	0.013-0.42
Surf similarity parameter: $\xi_{m-1,0}$ (-)	$\tan \alpha/s_{m-1,0}^{0.5}$	2.44-4.39	0.81-1.46
Amount of waves (-)	N	~1000	~1000
Freeboard (m)	R_c	0.25-0.38	0.15-0.38
Level of armour in front of crestwall (m)	A_c	0.20-0.30	0.10-0.20
Width of armour in front of crest wall (m)	G_c	0.15	0.15

A total of 48-72 experiments were conducted for each breakwater configuration (See also Appendix B, Table B.1), considering various hydrodynamic conditions that act on the structure. Each experiment was extended to a duration of approximately one thousand waves. Table B.1 shows the different hydrodynamic conditions tested. Initially, the basin was filled to a water level of 0.70 meters. It is also observed that for each water level one to three wave steepness values $s_{m-1,0}$ (0.013, 0.028, 0.042) were applied with each four different wave heights H_{m0} with 2 cm steps in between each wave height. After completing these 4-12 experiments per water level, the water level was raised with 5 cm. For the 1:2 slope the water level was varied from 0.70 m to 0.80 m, and for the 1:6 slope the water level was varied from 0.80 m to 0.90 m. This decision was made during the progress as overtopping did not occur for water levels lower than 80 cm at the 1:6 slope.

Some parameters are made dimensionless for the purpose of scaling and comparing different hydraulic properties. These parameters can be observed in Table 3.2.

Table 3.2: Non-Dimensional parameters of the first rubble mound breakwater (based on previous research by Van Gent et al. (2022))

Parameter	Symbol	Values/Ranges
Non dimensional freeboard	R_c / H_{m0}	0.83-3.17
Non-dimensional level of armour at crest	A_c / H_{m0}	0.56-2.50
Non-dimensional protruding part of the crest wall (h_{wall}^*)	$(R_c - A_c) / H_{m0}$	0.23-0.80
Ratio of protruding part of crest wall and the crest freeboard	$(R_c - A_c) / R_c$	0.14-0.44
Non-dimensional width of armour in front of crest wall	G_c / H_{m0}	0.68-1.50
Non-dimensional stone diameter	D_{n50} / H_{m0}	0.17-0.38

3.3. Model limitations

When considering a physical model, it should be taken into account that when wave conditions are generated twice, they do not necessarily generate identical wave trains and consequently do not lead to identical wave overtopping discharge values. This is also shown in Section 3.4, where two spectra were generated four times to investigate the accuracy of the resulting overtopping discharge. Nonetheless, it is demonstrated that the influence of different wave trains from the same wave spectrum appears to be limited.

When water drops exceeded the height of the top of the crest wall, the paddle wheel transported it into the overtopping box behind the breakwater model. It was observed that a very small portion of the water already descended on the slope before it could be transported to the other side of the crest wall. However, this volume is assumed to be negligible.

Additionally, during the time span of a pumping event, the overtopping discharge was not measured, which means that experiments with numerous pumping events are likely to be less accurate in terms of the wave overtopping discharge than experiments without any pumping events. As there was no emphasis on investigating this error, the phenomenon is not studied throughout this report.

3.4. Method validation

To demonstrate the accuracy of the setup, several accuracy tests were carried out. This was executed for two wave conditions and the configuration with a 1:6 slope and a bull nose attached to the crest wall (65P). The results of the accuracy tests can be observed in Table 3.3. For the first hydraulic conditions mean discharge of $\bar{q} = 2.229\text{E-}5$ [m³/s/m] is obtained with a standard deviation of $q_\sigma = 1.720\text{E-}6$, and for the second hydraulic conditions the mean discharge is $\bar{q} = 2.416\text{E-}6$ with a standard deviation of $q_\sigma = 3.036\text{E-}7$. The standard deviations are approximately 10% of the mean value, which is relatively small on a logarithmic scale. However, an explanation for the slightly larger deviation of the second condition is the increasing effect of scale effects for lower overtopping volumes. In addition, the overtopping was mainly caused by one wave event, which obviously is more sensitive to inaccuracies. Nonetheless, this inaccuracy seems to be sufficiently small to arrive at an adequate accurate result.

Table 3.3: Accuracy tests for a water level of 90 cm, a 1:6 slope, and a 5 cm bull nose crest wall (Configuration 65P).

Test #	H_{m0} [m]	$T_{m-1,0}$ [s]	$s_{m-1,0}$ [-]	q [m ³ /s/m]
1.1	0.139	2.596	0.01321	2.445E-5
1.2	0.139	2.598	0.01319	2.228E-5
1.3	0.139	2.598	0.01319	2.220E-5
1.4	0.139	2.598	0.01339	2.204E-5
2.1	0.180	1.684	0.04065	2.656E-6
2.2	0.180	1.689	0.04041	1.974E-6
2.3	0.180	1.691	0.04032	2.477E-6
2.4	0.180	1.691	0.04032	2.557E-6

3.5. Froude scaling

When scale models are used for experimental tests, various scale factors should be taken into account. While viscosity and surface tensions are generally significant parameters in the presence of water, they are not dominant in this case. When dealing with monophasic physical model tests in hydraulic engineering, while considering large gradients in surface elevations, Froude scaling laws will be applied (Schierreck & Verhagen, 2019). The first factor that is considered is the Froude number, which is an inertia term divided by a gravitational term (Equation (3.1)).

$$\frac{u_m}{\sqrt{g_m L_m}} = \frac{u_p}{\sqrt{g_p L_p}} \quad (3.1)$$

The variables u , g , and L are a characteristic velocity, gravitational term, and a characteristic length parameter. The subscript m describes the model, and the subscript p the prototype.

When scaling armour units, the differences in stone and water density must be considered for both the prototype and the model. In the circumstances where the slope is subjected to wave-attack, the stability number must be equal for both the model and the prototype (See Equation (3.2)). Where H is the wave height, Δ is the relative submerged density ($\Delta = \rho_s/\rho_w - 1$), and d is the armour diameter.

$$\frac{H_m}{\Delta_m d_m} = \frac{H_p}{\Delta_p d_p} \quad (3.2)$$

The main principle is that the Froude number for the model and prototype should be equal. The size reduction of the model is defined by the scale factor n_L which is described as the ratio of the length parameter of the prototype over the length parameter of the model (Equation (3.3)).

$$n_L = \frac{L_p}{L_m} \quad (3.3)$$

When no scale differences are assumed to be present for the gravitational term (i.e. $g_m = g_p$) and combining Eq. Equation (3.1) and Equation (3.3), the Froude law can be simplified to the following expression:

$$\frac{u_p}{u_m} = \sqrt{n_L} \quad (3.4)$$

The scales according to the Froude scaling rules are applied for the model set-up. These correspond to a scale factor range of $n_L = 10$ to 20. With this information, the time and discharge scale factors are respectively $n_L^{0.5}$ and $n_L^{2.5}$.

The data analysis consists of a complete presentation and thorough analysis of the results. The objective is to provide evidence in order to answer the research questions, concerning the effect of the various hydraulic conditions and the shape and dimensions of the breakwater and its elements. First, a reference frame is developed comprised of a modified version of expressions from literature that calculates the values of the measurements. This reference model is configuration 1 (25V), which has a straight 5 cm crest wall and a 1:2 slope. A new expression is proposed associated with some parameters that are validated with the experiments. The development of such an expression is required to construct the factor representing the maximum wind effect. First, it is demonstrated how the maximum wind effect is influenced by the relevant elements of the breakwater and the hydraulic conditions. These influences are then taken into account during the development of the multiple wind factors. Finally, the wind effect parameters γ_w developed by [Van Gent et al. \(2023\)](#) and [Dijkstra \(2023\)](#) are tested for validity for this rubble mound breakwater, and are then compared with the factors from this report.

4.1. Data Overview

Primarily, an overview of the measurements is presented. Some correlations and conclusions can already be drawn that clarify the effect of the hydraulic boundary conditions and the breakwater configurations. [Figure 4.1](#) shows a complete presentation of the data, consisting of the measurements excluding the maximum wind effect (see [Figure 4.3](#)) and including the maximum wind effect (see [Figure E.2](#)). On the y -axis, the non-dimensional overtopping discharge q^* is depicted on a logarithmic scale. On the x -axis, the relative crest freeboard R_c/H_{m0} , representing a physical parameter of the breakwater, is depicted on a linear scale. It can directly be observed that the measurements with the maximum effect of wind strongly correspond to those without wind. However, this section exclusively focuses on the experiments without wind, as the first part of this chapter mainly focuses on the development of a valid expression governed by the influential parameters without wind. An analysis that includes the maximum wind effect is found in [Appendix E](#).

The dependence of the overtopping discharge on the varying elements corresponding to the different configurations is shown in [Figure 4.2](#) and [4.3](#). While wind does not appear to greatly influence the patterns in the results during this analysis (for a detailed analysis on wind, see [Section 4.3](#)), it can be seen that the slope has a discernible effect on the overtopping discharge outcomes.

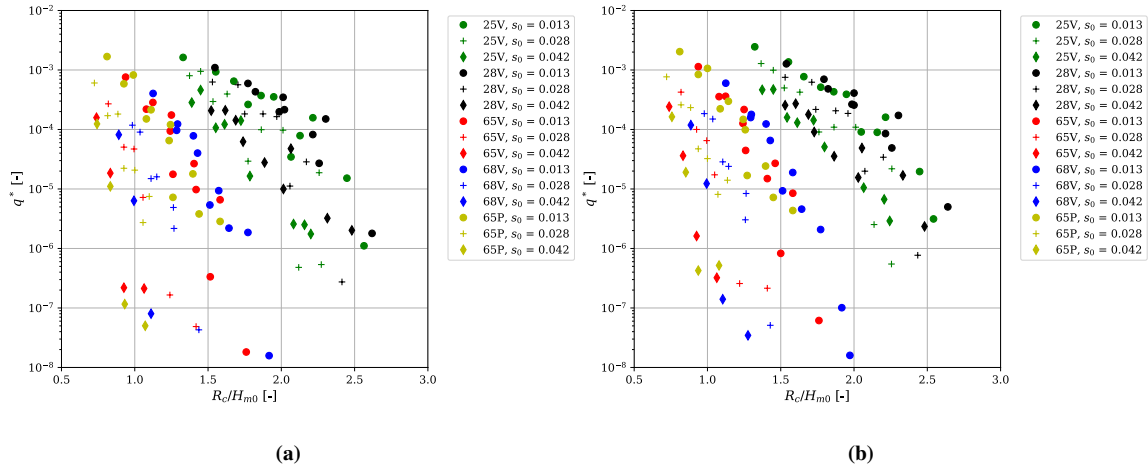


Figure 4.1: Measured overtopping discharges for all configurations; (a) Measurements without the maximum wind effect; (b) Measurements with the maximum wind effect.

In Figure 4.2, it is observed that the overtopping discharge is significantly lower for a mild slope, once again emphasizing the importance of the breaker parameter $\xi_{m-1,0}$. Additionally, it is evident that an exponential relation exists between the non-dimensional overtopping discharge q^* and the relative crest freeboard R_c/H_{m0} , which aligns with the guidelines and literature. This is also supported by the observation that a near-linear negative correlation can be observed for each configuration. Furthermore, the gradient of the data cluster containing the measurements of the mild slope appears to have a steeper gradient, meaning that the overtopping discharge increases more dominantly as the wave height increases.

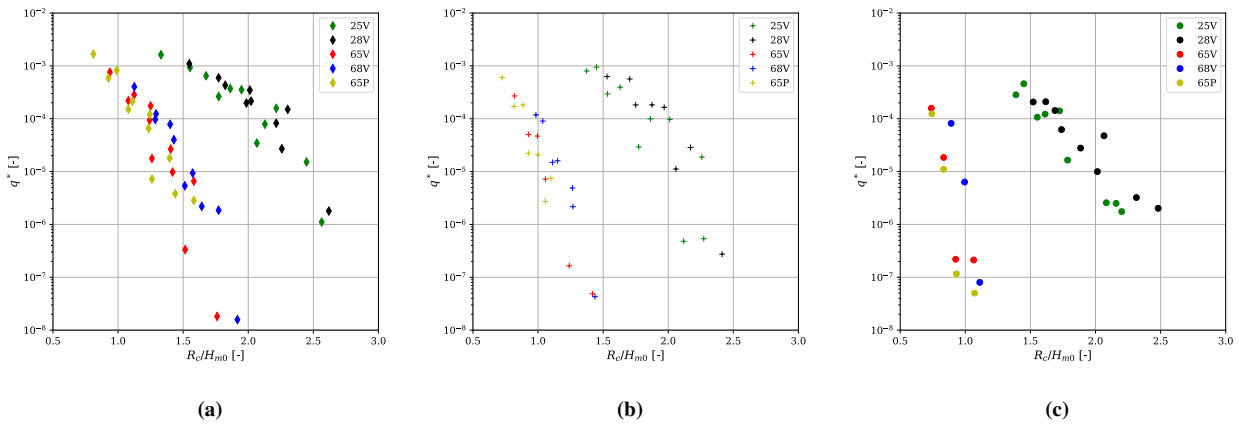


Figure 4.2: Measured overtopping discharges for all configurations with a different wave steepness for each plot; (a) Observations with wave steepness $s_{m-1,0} = 0.013$; (b) Observations with wave steepness $s_{m-1,0} = 0.028$; (c) Observations with wave steepness $s_{m-1,0} = 0.042$.

Subsequently, each configuration is presented in a separate graph in Figure 4.3 to provide a clear overview of the individual behaviour of the varying parameters. In this figure, it is visualized how the influence of a larger crest wall results in different overtopping outcomes, which mainly leads to lower quantities. This is covered in detail in Section 4.2.4.

Another direct observation is the influence of the presence of the parapet. It is seen that the measurement points slightly shift downwards when compared to the configuration where a parapet is absent. This indicates a small decrease of the mean overtopping discharge. The influence of the parapet is highlighted in Section 4.2.5. The last noteworthy observation that can be drawn from these figures is related to the slope, which is further treated in Section 4.2.3.

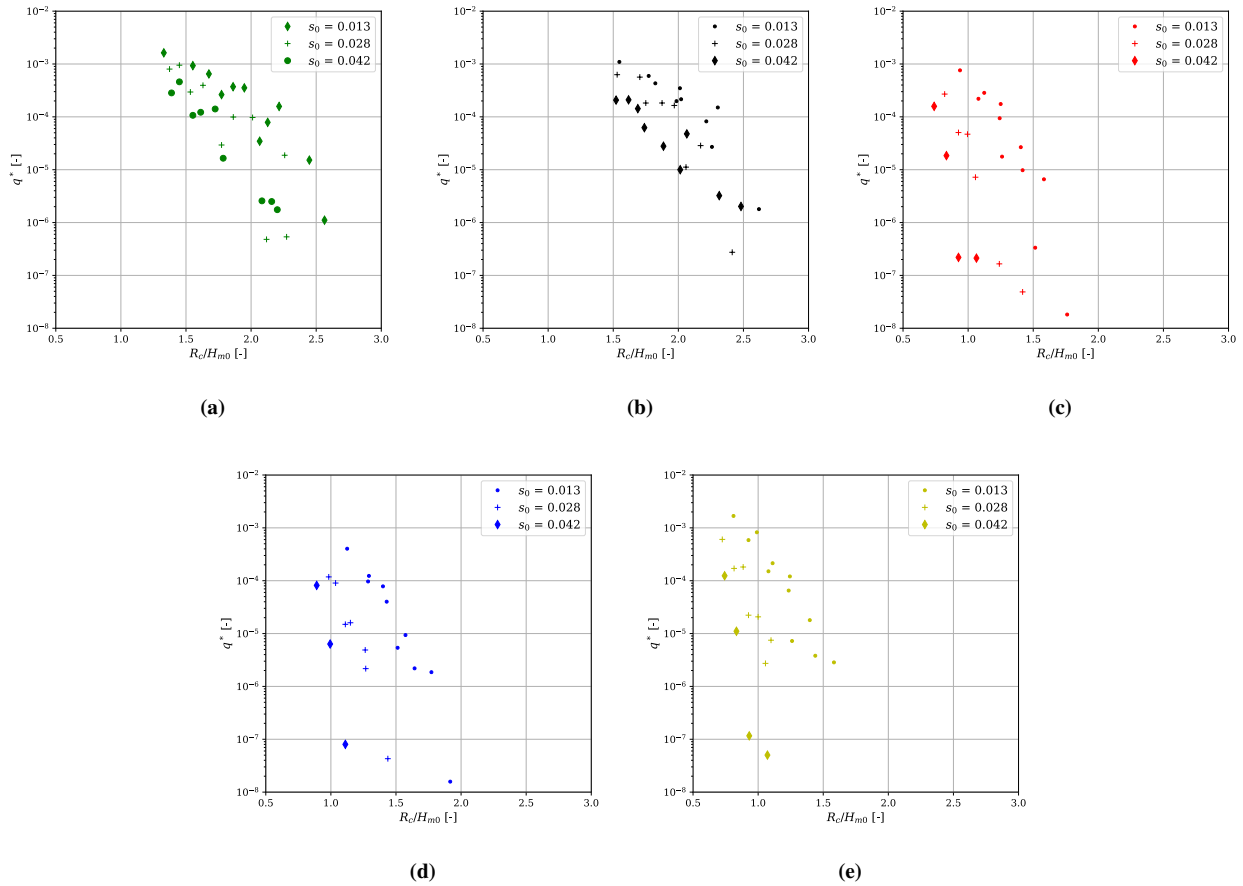


Figure 4.3: Measured overtopping discharges for each configuration excluding the results with the maximum wind effect; (a) Observations from configuration 1 (25V); (b) Observations from configuration 2 (28V); (c) Observations from configuration 3 (65V); (d) Observations from configuration 4 (68V); (e) Observations from configuration 5 (65P);

4.2. Comparison of the measurements with previous literature

As mentioned in the literature study, [Van Gent et al. \(2023\)](#) and [Irias Mata & van Gent \(2023\)](#) have proposed expressions that are validated for rubble mound breakwaters with a 1:2 slope. While [Irias Mata & van Gent \(2023\)](#) used numerical models to predict overtopping discharges for various slopes, the models did not include a 1:6 slope. Consequently, no validated expressions for mildly sloped rubble mound breakwaters have been developed yet. An alternative approach to compare the results of the measurements with the corresponding configurations, is to use the expression provided by the overtopping manual ([TAW, 2002](#)) as it is validated for mildly sloped dikes. In the following pages, the data obtained during the experimental program will be used to validate and adapt the relevant expressions from the literature if (it is required).

4.2.1. Reference Model

To assess whether the measurements align with existing expressions in the literature, a direct comparison of the first configuration (1:2 slope and $h_{wall} = 5$ cm) with the equations proposed by [Van Gent et al. \(2022\)](#) and [Irias Mata & van Gent \(2023\)](#) is made. A graph containing measurement values is depicted in [Figure 4.4a](#). On the y-axis the value for the non-dimensional discharge q^* is presented, while the x-axis shows the relative crest freeboard. As demonstrated by [Van Gent et al. \(2023\)](#), the results seem to be significantly influenced by wave steepness $s_{m-1,0}$, which implies a present influence of wave breaking. It is observed that the overtopping discharge is lower for the same relative crest freeboard and has an increased gradient as the relative crest freeboard increases. [Figure 4.4b](#) compares the method proposed by the [EurOtop \(2018\)](#) manual with the measurements, clearly showing how the results from the experiment are greatly underestimated ($10 - 10^4$ times). While [Van Gent et al. \(2022\)](#) already demonstrated that the [EurOtop \(2018\)](#) underestimates overtopping discharges, these

quantities are extraordinarily far off. Consequently, it is assumed that the method proposed by the overtopping manual (EurOtop, 2018) is not applicable to this specific experimental programme.

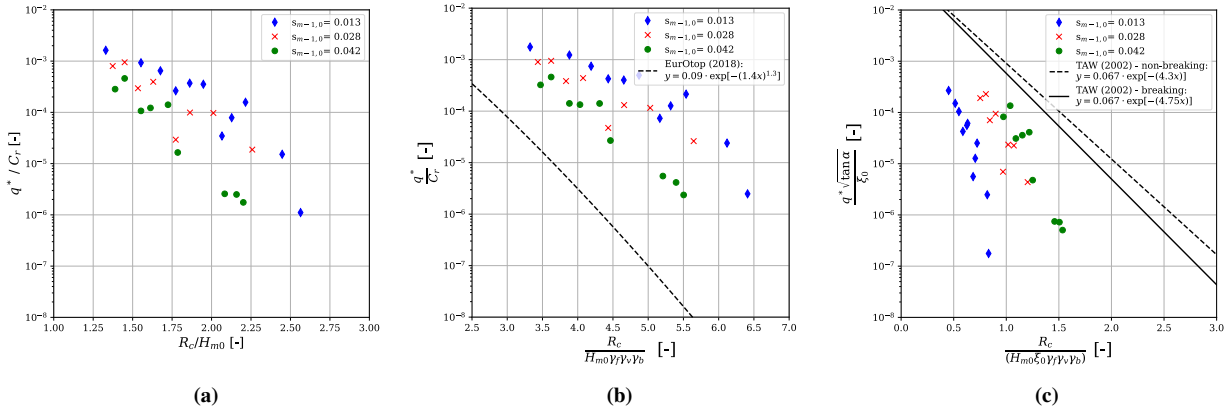


Figure 4.4: Measurement points of the reference model with the emphasis on wave steepness and wave breaking; (a) Observations without comparison from literature; (b) Observations compared to the guideline expressed in Equation (2.3) from EurOtop (2018); (c) Observations compared to the guideline expressed in Equation (2.2) from TAW (2002).

As mentioned in Chapter 2, the influence factors can vary significantly for different boundary conditions and should therefore always be carefully considered. The influence factor can be determined using Equation (2.9), or treated as a constant (Section 2.3.1).

The influence of the berm, denoted as γ_b is set to 1 for both methods, as the width of the armour layer in front of the berm can only be considered as a berm when it exceeds four times the nominal stone diameter. With nominal stone diameter of $d_{n50} = 3.8$ cm, the criterion requires an armour width greater than 15.2 cm, which is not satisfied for the concerned configurations in this research report. Consequently, each configuration is treated as a breakwater without a berm.

All waves were generated at a normally incident angle ($\beta = 0^\circ$), leading to $\gamma_\beta = 1$. The influence of the crest wall is considered through the implementation of Equation (2.15) and is applied to all measurement points. The last influence parameter, representing the effect of a parapet, is not applicable for this configuration, as the seaward shape of the wall is flat, leading to $\gamma_p = 1$.

First the roughness coefficient is evaluated for the generated data. In Figure 4.5a the data is compared to the expression presented by Van Gent et al. (2022) with the roughness influence taken as a variable (calculated with Equation (2.9)). Overall, it can be observed that the method still underestimates the overtopping discharge. However, the results for breaking waves are calculated accurately. A reasonable explanation is the pronounced turbulent behaviour of steeper waves, which might be amplified due to the roughness of the slope, leading to more energy dissipation and eventually to lower overtopping values. Consequently, leading to a more accurate calculation of the results of this method.

In Figure 4.5b, where the influence is considered as constant γ_f in the range of 0.40 to 0.55. Consequently, a lower value of the influence factor for roughness leads to a decrease of the predicted overtopping discharge, as it indicates the presence of a rougher slope leading to more wave dissipation. For this configuration, the most accurate region appears to be in the constant range between $0.40 \leq \gamma_f \leq 0.45$.

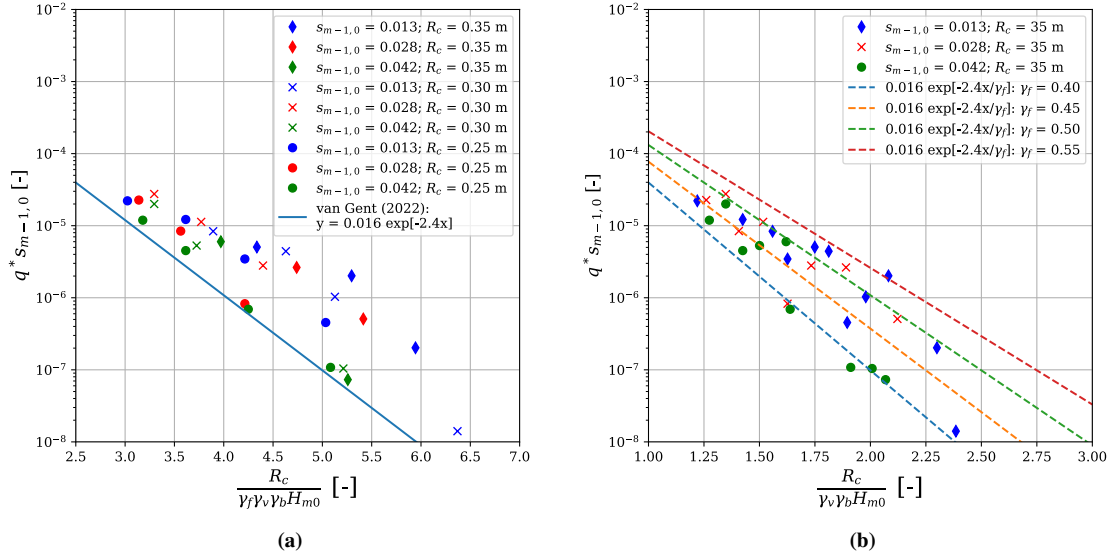


Figure 4.5: Measurements of the reference tests according to the expression proposed by van Irias Mata & van Gent (2023) with **a)** with the roughness influence factors determined according to Equation (2.9); and **b)** with γ_f determined with the use of constant values.

Another observation from Figure 4.5a is the influence of the water level. For similar x -axis values, an increasing water level appears to significantly affect the mean overtopping discharge. This effect is likely related to the crest freeboard and the characterization of the structure. In other words, as the water level increases, the presence of the breakwater diminishes, while the structure becomes increasingly characterized by a wall (represented by the A_c/R_c ratio). Therefore, a factor $(1.55 - A_c / R_c)$ is introduced in the expression for the crest wall height, leading to:

$$\gamma_v = \frac{1 + 0.45 \left(\frac{R_c - A_c}{R_c} \right)}{1.55 - A_c / R_c} \quad (4.1)$$

Eventually, a new expression is proposed in Equation (4.2), providing a more accurate calculation while making a distinction between breaking waves and non-breaking waves.

$$\frac{q}{\sqrt{g H_{m0}^3}} = \begin{cases} 0.01 s_{m-1,0}^{-1} \exp \left[-\frac{2.6 R_c}{\gamma_f \gamma_b \gamma_\beta \gamma_v \gamma_\rho H_{m0}} \right] & \text{if } \xi_{m-1,0} < 2.5 \quad (\text{Breaking waves}) \\ 0.12 s_{m-1,0}^{-1} \exp \left[-\frac{3.8 R_c}{\gamma_f \gamma_b \gamma_\beta \gamma_v \gamma_\rho H_{m0}} \right] & \text{if } \xi_{m-1,0} \geq 2.5 \quad (\text{Non-breaking waves}) \end{cases} \quad (4.2)$$

These equations are incorporated in Figure 4.6, where it can be observed that the error around these solutions is optimized for this specific setup. For breaking waves ($s_{m-1,0} = 0.042$) an RMSLE of 0.507 is obtained. The non-breaking waves are divided into two components, including the intermediate wave steepness $s_{m-1,0} = 0.028$ with the lowest RMSLE of 0.436 and the mildest wave steepness $s_{m-1,0} = 0.013$ with an RMSLE of 0.612. These are acceptable error values and represent a great improvement of the expression on the currently developed guidelines.

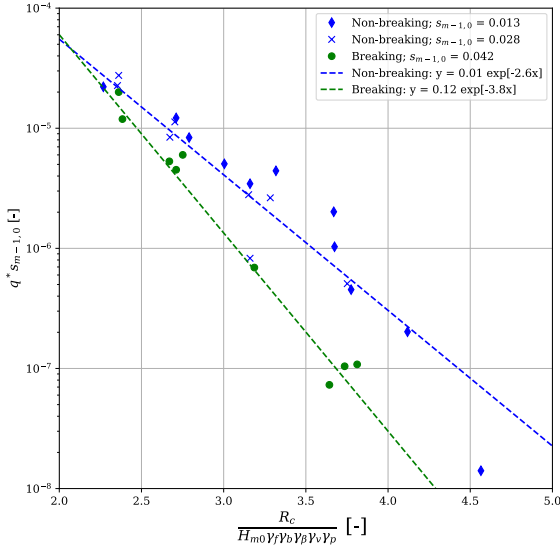


Figure 4.6: Calculated values for the observations determined with Equation (4.2)

Table 4.1: Error values obtained for different values for the wave steepness

Type of waves	$S_{m-1,0}$	RMSLE
Non-Breaking	0.013	0.670
Non-breaking	0.028	0.453
Breaking	0.042	0.338

4.2.2. Comparison with the most recent guideline (Irias Mata & van Gent, 2023).

In Equation (2.5) (Irias Mata & van Gent, 2023) a more comprehensive version of Equation (2.4) (Van Gent et al., 2022) is presented. While this expression is also applicable to a rubble mound breakwater with a steep slope and a crest wall, the expression incorporates the surf similarity parameter $\xi_{m-1,0}$ and the slope angle α as well. Since this research aims to understand the influence of the slope angle and the influence of the wave characteristics, this expression is also compared with the observations obtained from the measurement programme. In Figure 4.7a a clear dependency on $\xi_{m-1,0}$ is depicted as the measurements show less distinction for different types of waves, including wave breaking, resulting in a more dense cluster of the observations. Nonetheless, it is still observed that the method underestimates the overtopping discharges.

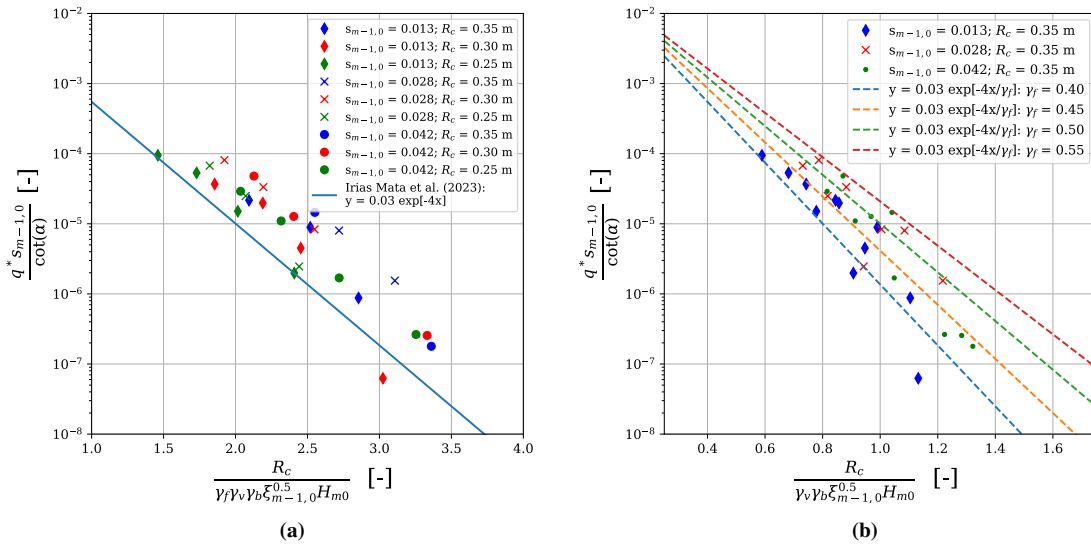


Figure 4.7: Measurements of the reference tests according to the expression proposed by van Van Gent et al. (2022) with a) with the roughness influence factors determined according to Equation (2.9); and b) with γ_f determined with the use of constant values

Similar to Equation (2.4), the method used to determine the roughness factor significantly influences the outcomes of the calculated values. While the spread generally becomes increasingly scattered, applying a constant value as a roughness factor, it can still be a satisfying approach to take a constant value. Especially, as the roughness factors determined with Equation (2.9) are on the low side, leading to an underestimation of the overtopping discharges. Additionally, as noted in Section 2.3.1 it is a common approach to choose a constant value for the roughness factor.

The results of these considerations are presented in Figure 4.7b, where is shown that for increasing values within the acceptable range, the roughness factor tends to provide a more accurate calculation of the overtopping discharge values. However, implementing a variable value for the roughness factor in the wave overtopping discharge equation likely increases its applicability range, as it also incorporates the effect of various stone dimensions. Consequently, this can be advantageous in the case of developing a comprehensive expression incorporating a wide range of conditions.

Therefore, the decision is made to construct a modified version of the expression that includes the concept of a variable roughness factor, presented in Equation (4.3). It is also evident that the water level influences the overtopping discharge and gives a larger error as the water level increases. This influence has been expressed as a factor depending on the (A_c / R_c) ratio in the previous sub-section. When this ratio is incorporated in the equation, it is observed that the influence of the water level is mitigated, and it no longer leads to significant deviations that would otherwise result in a less accurate calculations.

$$\frac{q}{\sqrt{gH_{m0}^3}} = s_{m-1,0}^{-0.25} \sqrt{\cot(\alpha)} \exp \left[-\frac{6.4R_c}{\gamma_f \gamma_b \gamma_\beta \gamma_v \gamma_p s_{m-1,0}^{0.5} H_{m0}} \right] \quad (4.3)$$

In Figure 4.8, the values for the calculations determined with Equation (4.3) are shown. The RMSLE values that align with these calculations are shown in Table 4.2, which indicates that the error is similar for all wave steepness values. Although the errors tend to be slightly larger for this method than the method proposed in Equation (4.2), this expression will be validated for the other configurations throughout this chapter. This is argued with the fact that the effect of wave breaking and the slope are incorporated within this expression.

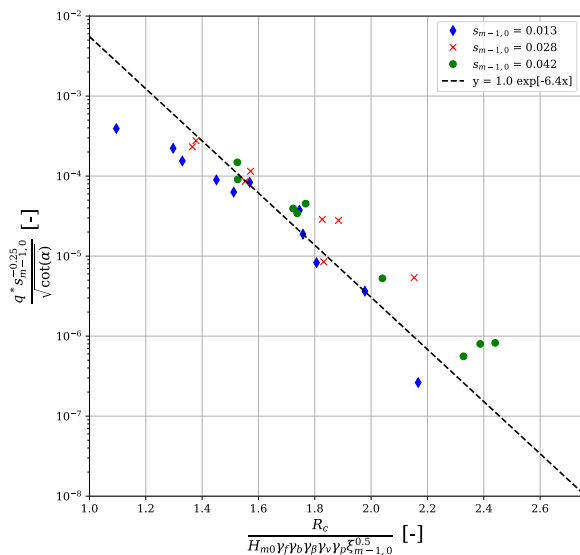


Table 4.2: Root mean squared log error values for expression

Type of waves	$s_{m-1,0}$	RMSLE
Non-Breaking	0.013	0.601
Non-breaking	0.028	1.033
Breaking	0.042	1.028

Figure 4.8: Calculated values for the observations determined with Equation (4.3)

4.2.3. Influence of the slope

An expected result for a milder slope is a reduction of the overtopping discharge. This is explained by an increase of wave dissipation on milder slopes and a decrease of $\xi_{m-1,0}$, which can be observed in Figure 4.1. The objective that remains is to show how the influence is accounted for in the expressions proposed by literature and developed in the previous two sub-sections.

Figure 4.9 shows for each expression the calculations of the measurements. Figure 4.9a shows how the measurements corresponding to a mild slope are overestimated, with the clear observation that a steeper waves are further underestimated. As there are no changes concerning the slope applied for the modified version of the expression, the same can be observed from Figure 4.9b. However, the expression developed by Irias Mata & van Gent (2023) seems to be more applicable for the measurements obtained from the data set in this report, but still shows a clear distinction between the steep slope and the mild slope. Finally, Figure 4.9d provides an accurate calculation corresponding to the results obtained in this research, and is therefore the more suitable expression for this research.

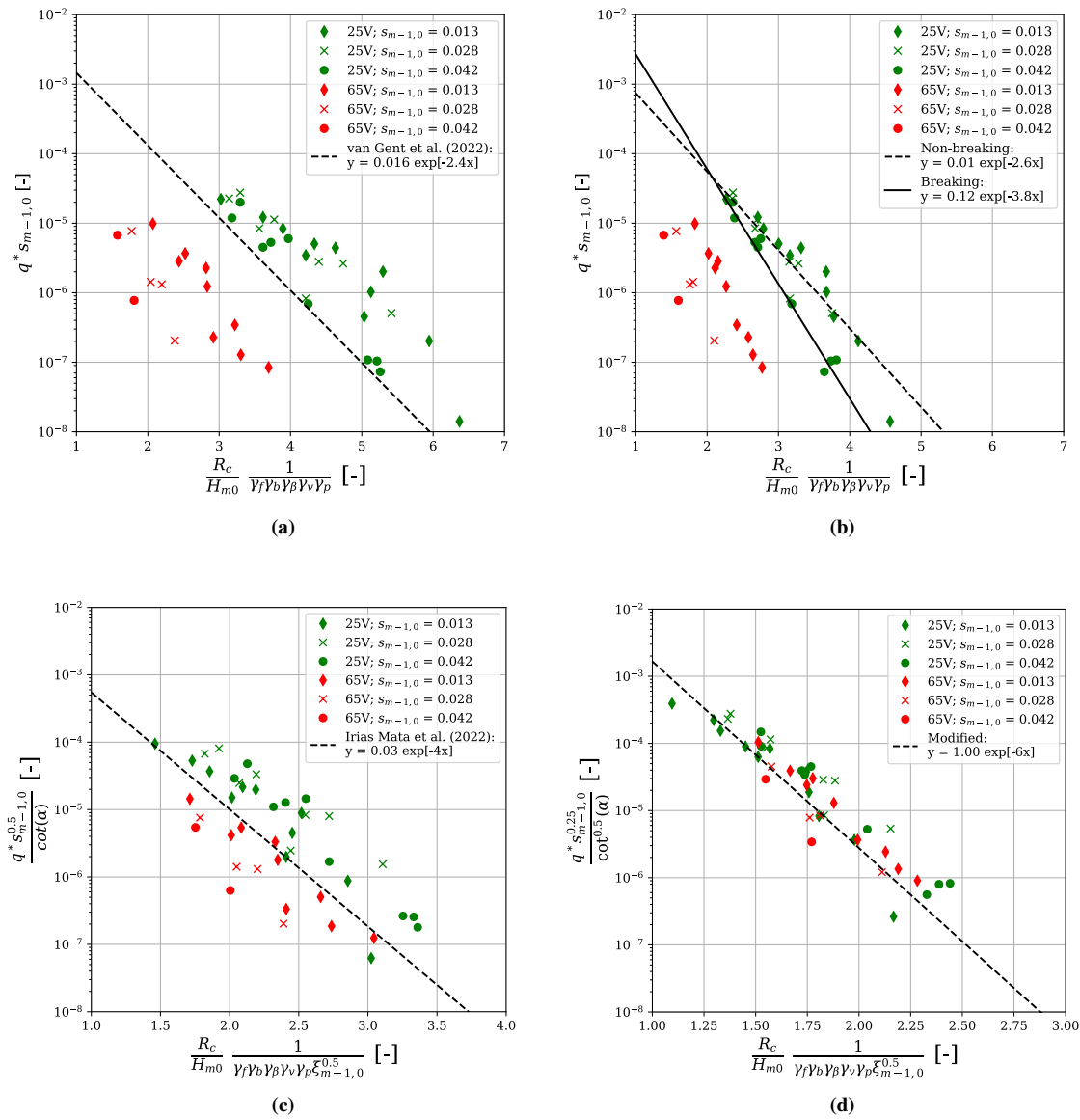


Figure 4.9: Measurements with varying slope angles compared with various expressions; (a) Measurements calculated using Equation (2.4) (Van Gent et al., 2022); (b) Measurements calculated using Equation (4.2); (c) Measurements calculated using Equation (2.5) (Irias Mata & van Gent, 2023); (d) Measurements calculated using Equation (4.3).

4.2.4. Influence of a crest wall with an increased height

In this subsection it is investigated how the height of a crest wall influences the mean overtopping discharge. This is done by evaluating the influence factors that have been developed for a crest wall. If the expression does not correspond to the obtained measurements, it should be modified or a new expression required.

When the influence factor of the crest wall height is not taken into account ($\gamma_v = 1$), the overtopping discharge is likely to be underestimated. As shown in Figure 4.10, this expectation is confirmed. It can also be seen that the wave steepness has a larger influence for the mild slope than for the steep slope, which might be a result of the presence of the crest wall.

Furthermore, the taller crest wall has an increased underestimation of the value on the y-axis than the shorter crest wall, which implies that increasing the height of a crest wall leads to a breakwater design that is less effective in resisting overtopping discharges, which is explained from literature treated in Chapter 2, where the ratio of the crest wall over the height of the breakwater increases, meaning that the relative portion where waves are dissipated on the slope decreases, and the relative portion where the waves collide into the vertical wall increase. This influence will be significant for future adaptation designs resulting from sea level rise. It is also seen that the wave steepness has an increased influence for the milder slope, which again implies that the slope and the surf similarity parameter contribute to the outcome of the result.

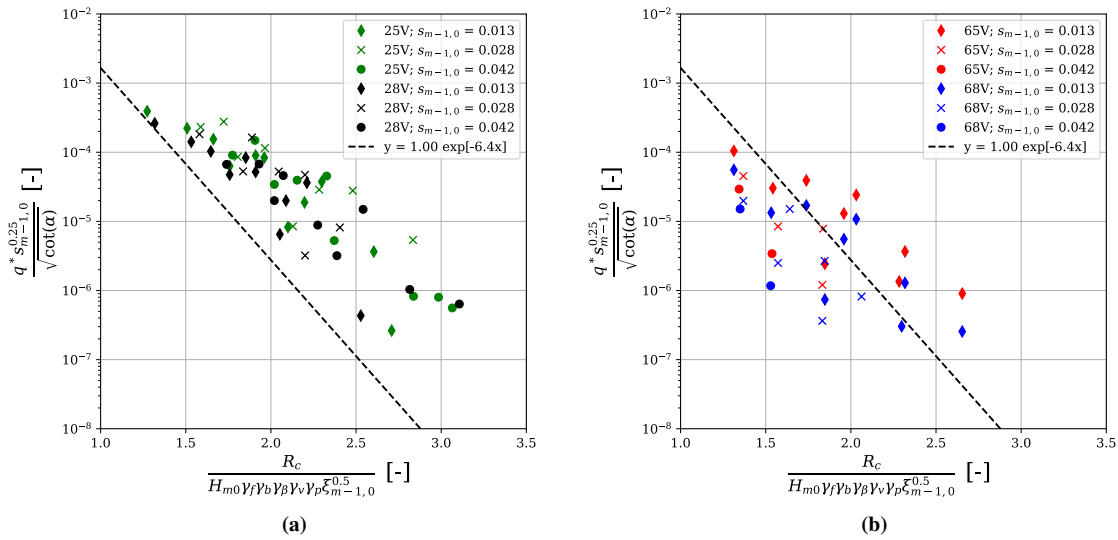


Figure 4.10: Measurements without the influence of the crest wall height ($\gamma_v = 1$); (a) measurements obtained from the configurations with a 1:2 slope; (b) measurements obtained from the configurations with a 1:6 slope.

Figure 4.10 shows the measurements in comparison with Equation (4.3). The parameters within the exponent are depicted on the x-axis, and the parameters in front of the exponent describe the y-axis. Each color corresponds to a different configuration and each marker type corresponds to a value for the wave steepness. In Figure 4.10 it is observed that the effect of the crest wall can not be neglected (i.e. $\gamma_v = 1$) as the implementation of the Equation (2.15) leads to a more concentrated result around function y . However, the data points from the tallest crest wall still do not fully correspond to the data points from the smallest crest wall. As mentioned earlier, the contribution of the slope angle is also required. This is explained by the fact that a distinction can be observed between the different wave steepness values for both slopes.

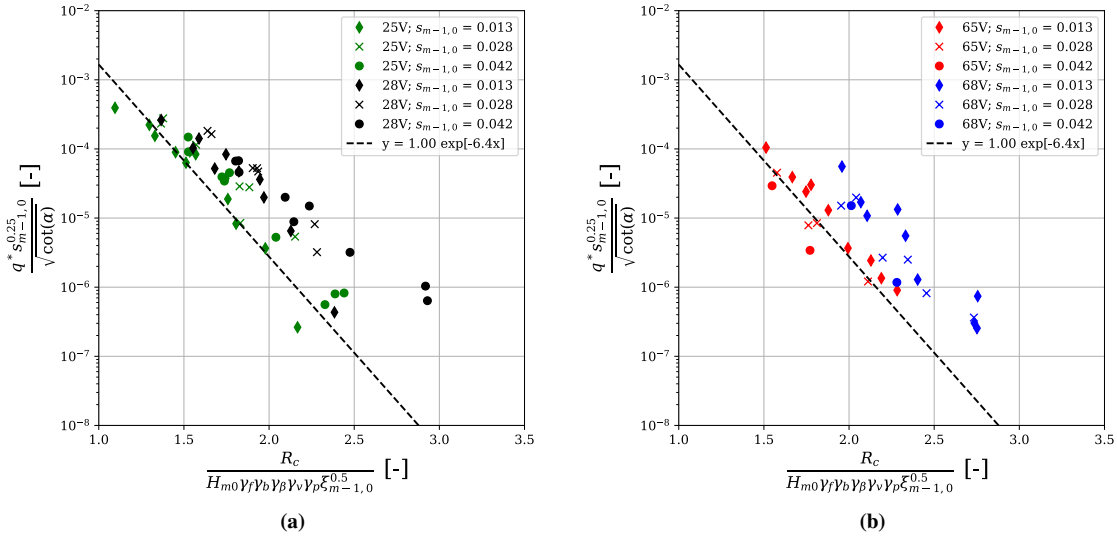


Figure 4.11: Influence of the crest wall according to Equation (2.15); (a) measurements obtained from the configurations with a 1:2 slope; (b) measurements obtained from the configurations with a 1:2 slope.

For these reasons, it is recommended to develop a new expression for the influence of the crest wall height that incorporates the breaker parameter and the breakwater slope. After an iteration process it could be concluded that the wave height also influences the ratio of the crest wall height over the crest freeboard. Therefore, the spectral wave height is included in the denominator of the expression. This leads to the ratio of the crest wall height over spectral wave height raised to the power 1.7, as seen in Equation (4.4)

$$\gamma_v = \frac{1 + \left(\frac{R_c - A_c}{H_{m0}} \right)^{1.7}}{1.55 - R_c/A_c} \quad (4.4)$$

When Equation (4.4) is included, the results provide a more accurate value in correspondence to the reference models (see Figure 4.12a for Configuration 1 (25V), and see Figure 4.12b Configuration 3 (65V)). However, the lower values on the y-axis still seem to consist of a relatively wide spread, which is assumed to be caused by scaling errors. Nonetheless, this observation does not appear to be present for the 1:6 slope.

While considering the wave steepness, there still appears to be a dependency which also has an opposite effect for the mild and steep slopes. The results of mildest waves for the 1:2 slope are overestimated, while the results for the 1:6 slopes are underestimated. For the steeper waves this effect occurs vice versa. Therefore, it can be confirmed that the wave steepness has an influence on the overtopping discharge.

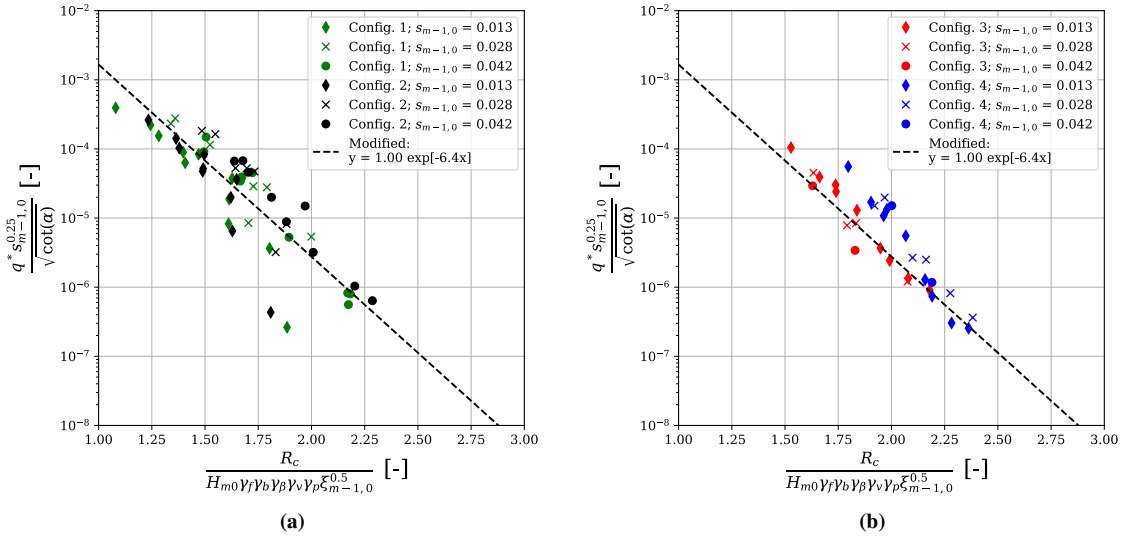


Figure 4.12: Influence of the crest wall according to Equation (4.4); (a) Results obtained for the 1:2 slope; (b) Results obtained for the 1:6 slope

4.2.5. Influence of a recurved parapet

It is observed in Figure 4.13, where the influence factor of the parapet is interpreted as $\gamma_p = 1$, that the presence of a parapet reduces the overtopping discharge (especially for the model with a 1:6 slope). This observation corresponds to the expectations based on prior studies from the literature. As treated in the background theory, several expressions that describe the influence of a parapet have been proposed in the past. The results of the first expression (composed by Van Doorslaer et al., 2015, Equation (2.17)) are depicted in Figure 4.13b from which can be concluded that the method is not applicable for the configurations considered during this research. The second method (developed by Oh et al., 2018, Equation (2.16)) is depicted in Figure 4.13c. This solution provides a better calculation of the results than the alternative, but requires some alterations of the for the concerned configurations as the reductioning effect of the recurved parapet is still overestimated.

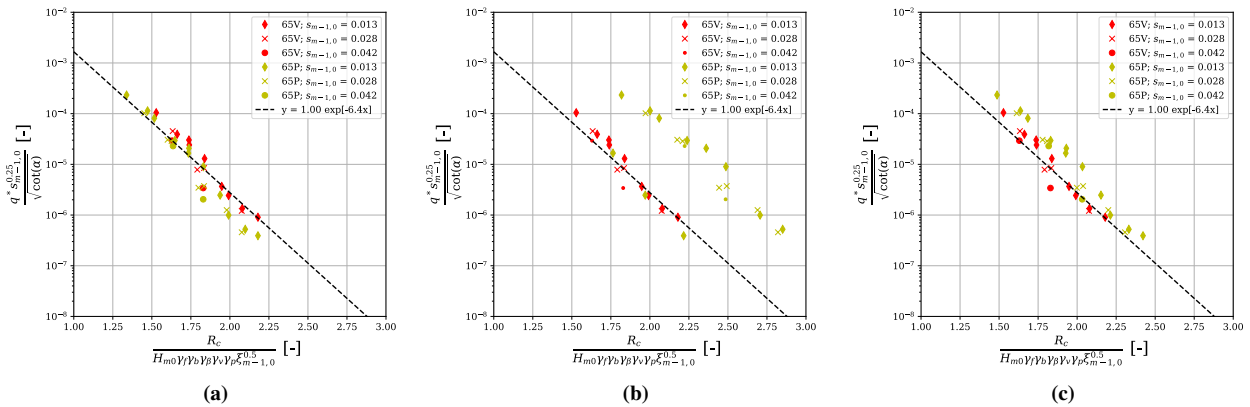


Figure 4.13: Measured overtopping discharges for configurations with a 1:6 slope and a 5 cm crest wall with and without a parapet ; (a) No influence of the parapet taken into account ($\gamma_p = 1$); (b) Influence of the parapet using Equation (2.17) (Van Doorslaer et al., 2015); (c) Influence of the crest wall using Equation (2.16) (Oh et al., 2018).

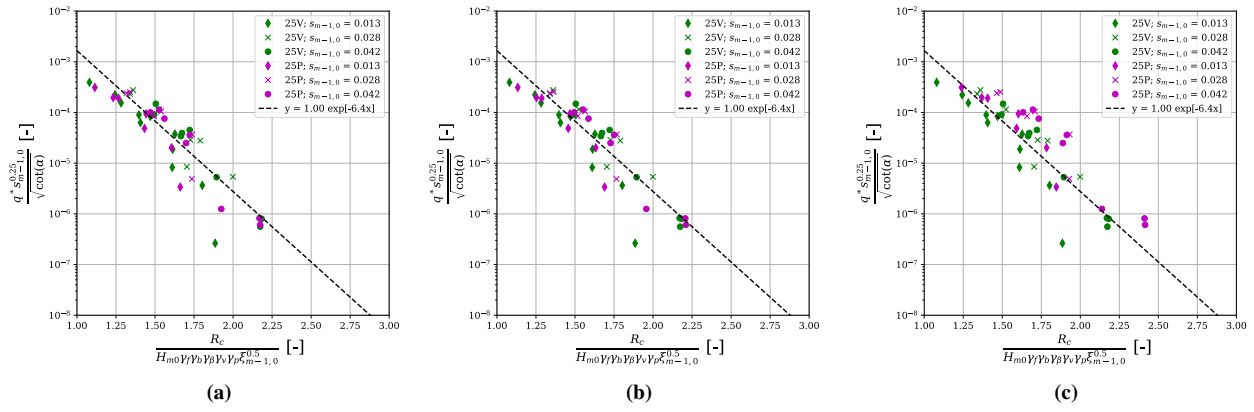


Figure 4.14: Measured overtopping discharges for configurations with a 1:2 slope and a 5 cm crest wall with and without a parapet ; (a) No influence of the parapet taken into account ($\gamma_p = 1$); (b) Influence of the parapet using Equation (2.16); (c) Influence of the crest wall using Equation (2.17).

Although the presence of a parapet led to small overtopping discharge differences (especially for the 1:2 slope), a new expression is still proposed to better understand its effect. It is observed that the influence of wave steepness and the slope play a crucial factor, which implies that the breaker parameter needs to be implemented into the expression. Equation (4.5) depicts the proposed equation incorporating the expression provided by Oh et al. (2018) including the effect of the breaker parameter. In addition, the expression is raised to the power factor of 1.1, which is obtained after iteratively optimizing the expression to arrive at a favourable RMSLE.

$$\gamma_p = 1 - \left(\frac{B_r}{h_r \xi_{m-1,0}} \right)^{1.1} \quad (4.5)$$

As depicted in Figure 4.15, it can be observed that the negative correlation consists of a narrower shape in comparison with the alternative expressions that describe the influence of a parapet. Meaning, by incorporating the surf similarity parameter into the expression, the influence of the wave steepness has been reduced. It is evident that the influence of the slope is also properly included, as the scatter plots of the 1:2 and 1:6 slope are positioned in the same range. As was observed in Figure 4.14a, a parapet has limited to no influence on the steep slope ($\cot \alpha = 2$), of which the effect is included in equation Figure 4.15a, being very similar to Figure 4.14a.

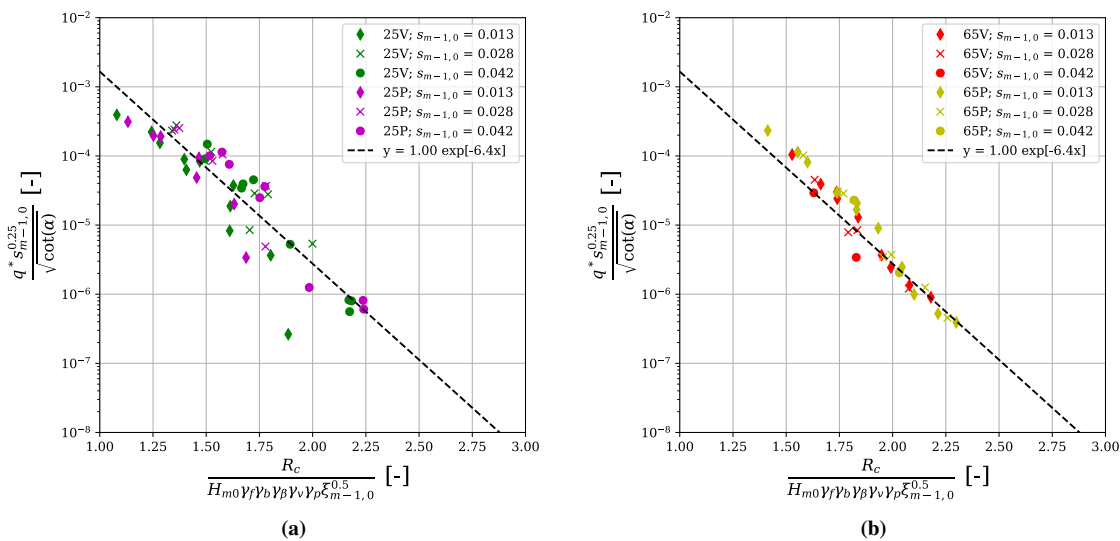


Figure 4.15: Influence of the parapet according to Equation (4.5); (a) measurements obtained from the configurations with a 1:2 slope; (b) measurements obtained from the configurations with a 1:6 slope.

4.2.6. Recap

Eventually, a modified version of the expression by [Irias Mata & van Gent \(2023\)](#) is proposed, including the influence factors that are validated for this specific test programme. This equation corresponds to all measurement points and provides an accurate calculation of the mean overtopping discharges measured, which is further confirmed by the RMSLE values given in [Table 4.3](#).

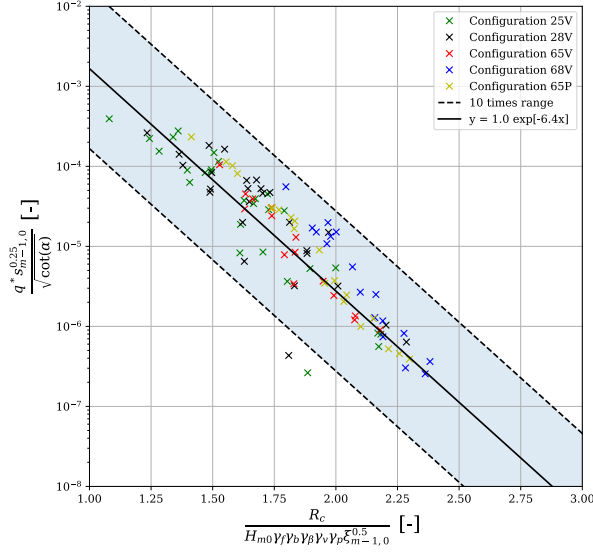


Figure 4.16: Calculations for the bulk of the data containing each separate configuration, including the factor 10 confidence area above and below function y .

According to the newly developed expression:

$$\frac{q}{\sqrt{gH_{m0}^3}} = \sqrt{\cot(\alpha)} s_{m-1,0}^{-0.25} \exp \left[-\frac{6.4R_c}{\gamma_f \gamma_b \gamma_\beta \gamma_v \gamma_p \xi_{m-1,0}^{0.5} H_{m0}} \right]$$

Which is validated for:

- Equation (2.9): $\gamma_f = 1 - 0.7 \left(\frac{d_{n50}}{H_{m0}} \right)^{0.1}$
- Equation (4.4): $\gamma_v = \frac{1 + (h_{wall}/H_{m0})^{1.7}}{1.55 - A_c/R_c}$
- Equation (4.5): $\gamma_p = 1 - \left(\frac{B_r}{h_r \xi_{m-1,0}} \right)^{1.1}$
- $\gamma_b = 1$
- $\gamma_\beta = 1$

Table 4.3: Root mean squared log errors between calculations with Equation (4.3) and the measurements without the maximum wind effect.

Bulk	cot α		S $_{m-1,0}$			Configuration				
	2	6	0.013	0.028	0.042	25V	28V	65V	68V	65P
0.686	0.772	0.562	0.885	0.776	0.836	0.728	0.952	0.194	1.089	0.391

The bulk data analysis depicted in [Figure 4.16](#) shows that the newly developed expression is sufficiently accurate for all wave steepness values. Especially for a lower value on the y -axis and a larger value on the x -axis less accurate calculation values are found. Nonetheless, it provides a sufficient calculation for the observations obtained in this experimental programme. In [Table 4.3](#) the error values (RMSLE) can be observed, highlighting different relevant elements such as the hydraulic conditions and dimensions of the breakwater.

4.3. Maximum influence of wind

The maximum effect of wind on wave overtopping has so far always been expressed by the ratio $\gamma_w = q_w/q$ (identical to $\gamma_w = q_w^*/q^*$), which is the ratio of the mean overtopping discharge including the maximum wind effect q_w over the mean overtopping discharge without this effect q . As demonstrated in [Section 4.2](#), numerous design parameters and wave characteristics were found to have an influence on the mean overtopping discharge without wind. Therefore, in correspondence with these findings and the results from previous research, it can be suggested that the maximum wind effect differs for various breakwater configurations and wave characteristics ([Wolters & van Gent, 2007](#)). This section covers the maximum influence of wind on wave overtopping by analysing the results quantitatively. A relation that is commonly applied to validate the observed maximum effect of wind follows from the following observation from literature: for a decreasing overtopping discharge q^* it is expected to have an increasing maximum effect of wind γ_w ([de Waal et al., 1996](#); [Wolters & van Gent, 2007](#); [Van der Bijl, 2022](#); [Van Gent et al., 2023](#); [Dijkstra, 2023](#)).

4.3.1. First look at the influence of wind

In Figure 4.17, an overview of the maximum wind effect of each configuration with the influence of the relative crest board is depicted. It can already be observed that a larger relative crest freeboard R_c/H_{m0} leads to an increase of the maximum wind effect γ_w . It is also observed that the influence of wind mainly leads to an increase of 1-3 times the mean overtopping discharge without wind, with some points exceeding this range. Additionally, it has to be emphasized that the influence of onshore wind conforms to the criterion $\gamma_w \geq 1.0$, which is also shown in the figure. Another observation is the clear distinction between different wave steepness values. Generally, a steeper wave leads to a large wind effect. This is in line with the expectations, as steeper waves lead to less wave overtopping, resulting in a larger effect of wind.

While some differences can be seen for the various configurations, a more detailed analysis is carried out in a later stage of this chapter. However, this section will first treat the influence of the water level and the wave characteristics.

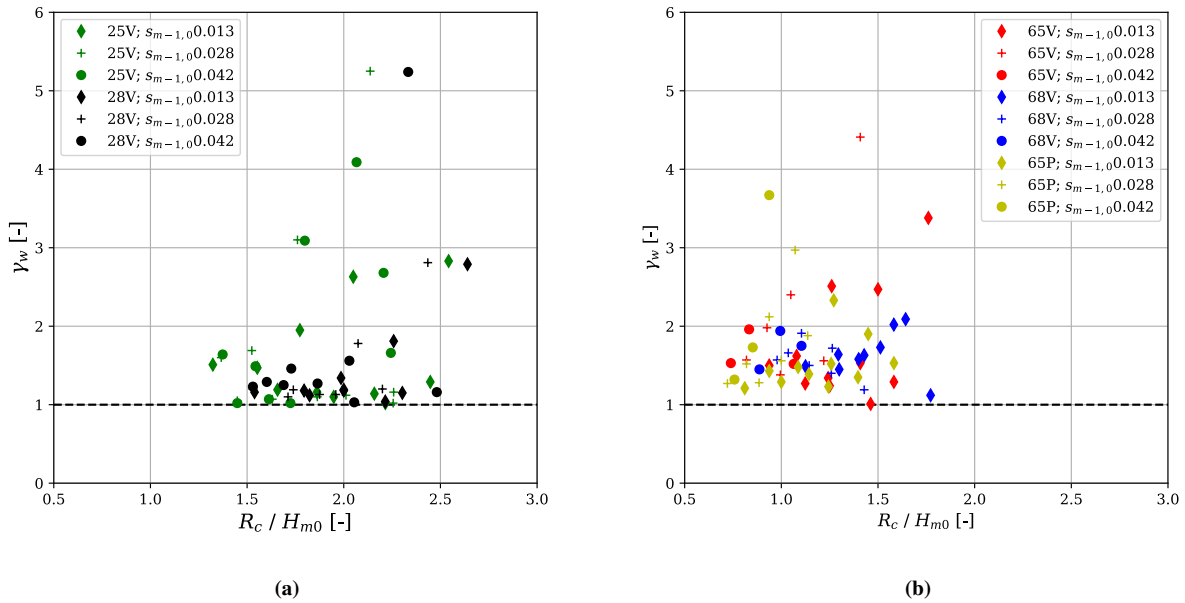


Figure 4.17: The influence of the relative crest freeboard on the maximum wind effect; (a) influence for the 1:2 slope; (b) influence for the 1:6 slope.

4.3.2. Influence of the wave characteristics

In Table 4.4 the various ranges of the maximum wind effect for the different wave characteristics are depicted. This Table provides a quick interpretation of the results. One can see for instance that the influence of the wave steepness appears to increase for the 1:2 slope, while one could interpret the opposite for the 1:6 slope. The results from the 1:6 slope appear to contradict with the assumption that the maximum wind effect increases when the overtopping discharge decreases. This can be reasoned by observations during the experiments, where different types of wave breaking could be seen. One could argue that the type of breaking also influences the effect of wind, which would imply that the maximum wind effect is larger for plunging breakers than for spilling breakers. Or mathematically: the maximum wind effect increases from towards $\xi_0 \approx 1.5$ and then decreases for an increasing ξ_0 .

Subsequently, while looking at the influence of the γ_w ranges for varying spectral wave heights, it can also be observed that the maximum wind effect decreases with an increasing wave height. This is in line with the findings from earlier research carried out by Van Gent et al. (2023) and Dijkstra (2023), and is substantiated by the relation between the maximum wind effect and amount of wave overtopping: as lower waves result in lower wave overtopping discharges, the maximum wind effect is likely to increase.

Table 4.4: Influence ranges of the maximum wind effect γ_w for each configuration with various wave characteristics including the wave steepness and the spectral wave height.

Config.	Wave steepness $s_{m-1,0}$			Spectral wave height H_{m0}						
	0.013	0.028	0.042	0.10	0.12	0.14	0.16	0.18	0.20	0.22
25V	1.02-2.83	1.02-5.25	1.02-4.09	-	2.63-5.25	1.02-3.10	1.02-1.69	1.07-1.64	1.02-1.05	-
28V	1.04-2.79	1.10-2.81	1.03-5.24	-	1.81-5.24	1.04-1.78	1.15-1.46	1.12-1.27	1.03-1.29	-
65V	1.01-3.38	1.38-4.41	1.52-7.38	2.48	1.56-2.51	1.52-4.41	1.29-7.38	1.01-1.96	1.24-1.53	-
65P	1.02-6.69	1.04-6.67	1.02-2.23	-	2.33	1.48-10.33	1.43-3.67	1.21-1.88	1.23-1.56	1.28
68V	1.29-6.29	1.19-2.08	1.45-1.94	-	1.73-6.29	2.09	1.12-2.08	1.45-2.02	1.45-1.5	1.64

In Figure 4.18 the influence of the wave steepness is depicted. With this more detailed representation of the results, it can be seen how the mean tends to increase for an increasing value which could not be observed in the Table. For both slopes the median and the mean of the wind maximum wind effect increases. In Appendix E.1 a more detailed overview of the influence of the wave steepness is provided from which can be concluded, that when the water level is varied, the maximum wind effect still increases for an increasing wave steepness. This still corresponds to the theory of an increasing wind effect for a decreasing overtopping discharge, which occurs for an increasing wave steepness value.

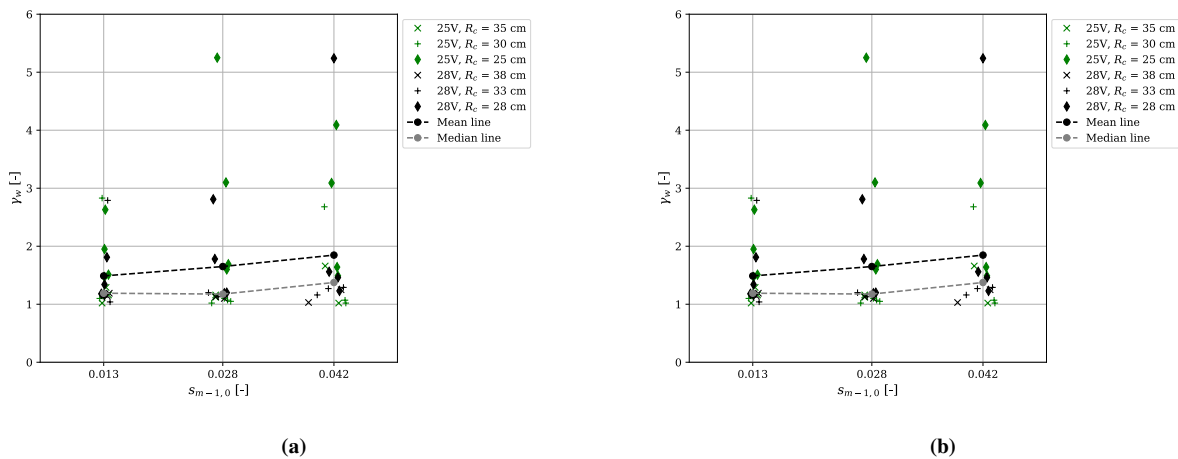


Figure 4.18: Maximum influence of wind for the wave steepness including the median and mean line of all configurations; (a) Data points for the configurations with a 1:2 slope; (b) Data points for the configurations with a 1:6 slope

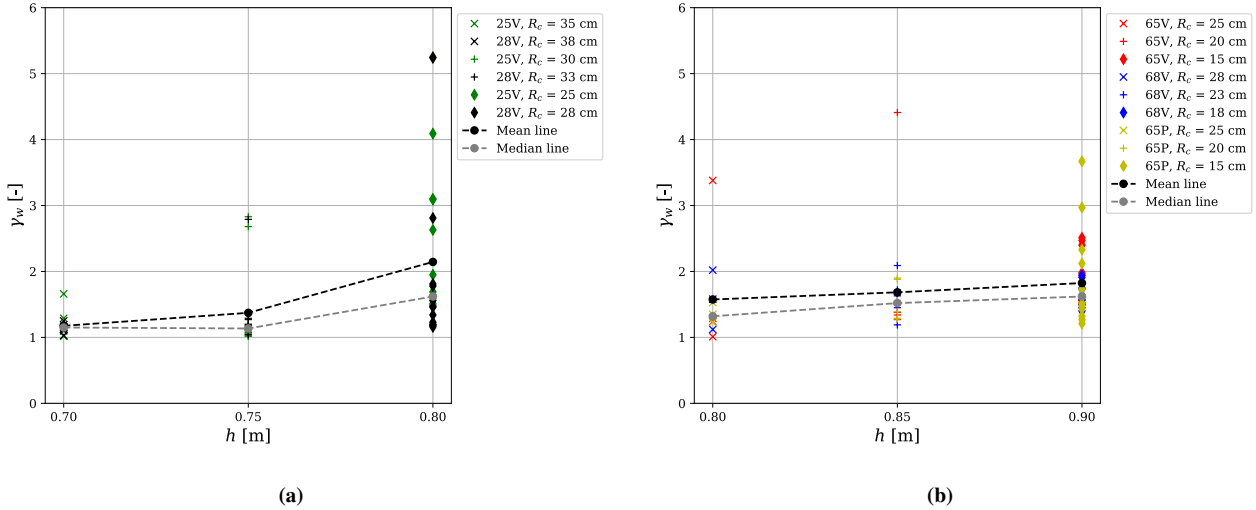
4.3.3. Influence of the water level

To investigate the dependency of the maximum wind effect on different water levels, Table 4.5 is constructed to obtain a quick overview in order to interpret the results. It can be observed how the data tend to increase for an increasing water level, which slightly contradicts with the assumption that the effect of wind decreases for an increasing overtopping discharge. This is explained as one would expect an increased overtopping discharge at higher water level, and thus leading to a decrease of the maximum wind effect.

Therefore, the data is plotted in Figure 4.19 to obtain a more detailed representation of the results. On the x-axis and the y-axis the water level and the maximum wind effect are respectively depicted. Here it can be seen that the mean and median values still tend to increase when the water level is increased, which corresponds to the conclusion that could be drawn from Table 4.5. This observation still contradicts with the statement that an increase of the overtopping discharge leads to a decrease of the maximum wind effect, while an increasing water level generally leads to an increasing overtopping discharge. It is also noted that other explanations could be valid here that correspond to the structural elements of the structure. A reasonable argument for this increase is the more dominant presence of the crest wall when the relative crest board decreases.

Table 4.5: Influence ranges of the maximum wind effect γ_w for each configuration with various water levels.

Configuration	Water level h				
	70	75	80	85	90
25V	1.02-1.66	1.02-2.83	1.47-5.25	-	-
28V	1.03-1.25	1.04-2.79	1.16-5.24	-	-
65V	-	-	1.01-1.24	1.27-4.41	1.50-7.38
65P	-	-	1.23-1.53	1.28-1.90	1.21-3.67
68V	-	-	1.12-2.02	1.45-2.09	1.40-2.08

**Figure 4.19:** Maximum influence of wind within the water level ranges for: (a) 1:2 slope; (b) 1:6 slope

4.3.4. Influence of the crest wall

In Figure 4.20 it is observed how the median and the mean differ over an increasing water level. It has already been demonstrated that the influence of wind increases for an increasing water level. However, the influence of the 8 cm crest wall appears to be slightly constant for an increasing water level, indicating that other factors start to intervene. This is argued by the highest water level and the highest crest wall, where the crest wall represents 44.4% of the crest freeboard (see Table 4.6 showing the relative presence of each crest wall and water level). For both the 1:6 slope and the 1:2 slope the median of the maximum wind effect reaches its maximum when the h_{wall}/R_c ratio amounts to approximately 0.3. In other words, when the crest wall height to freeboard height ratio reaches approximately a value of 0.3, the highest maximum wind effect is observed. However, it stands out that the highest water level in Figure 4.20a the maximum wind influence is obtained from the 5 cm crest wall. This indicates that the slope also influences the behaviour of a crest wall, substantiated by a theory from Dijkstra (2023), who argues that overshooting of water at a crest wall is more dominant for low crest walls than for high crest walls.

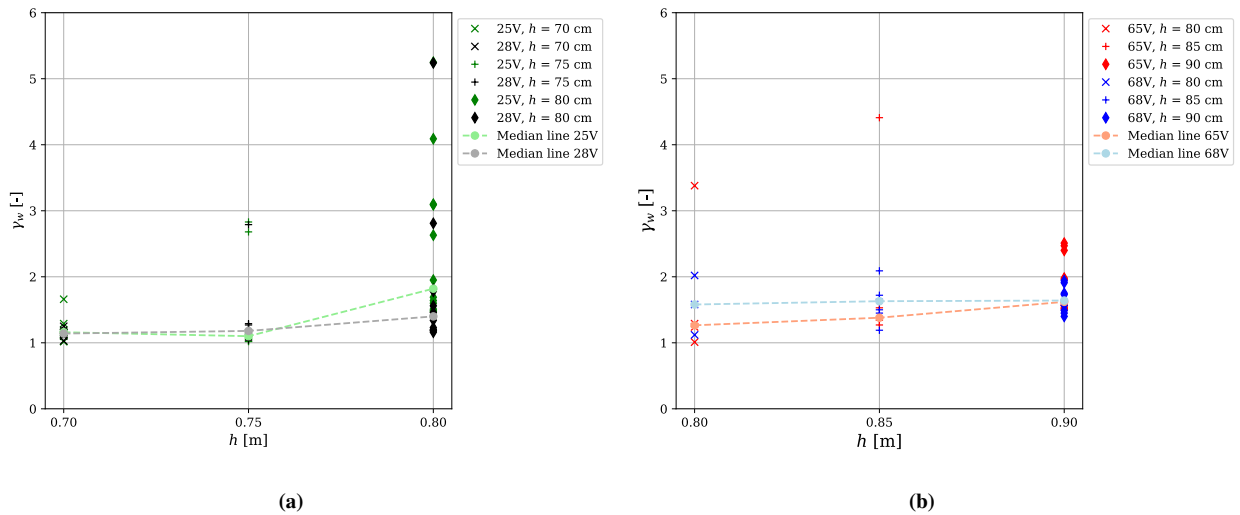


Figure 4.20: Influence of the crest wall for each water level; (a) 5 cm vs 8 cm crest wall at a breakwater with a 1:2 slope; (b) 5 cm vs 8 cm crest wall at a breakwater with a 1:6 slope.

Table 4.6: The R_c/h_{crest} ratios with the corresponding values for the crest height h_{crest} and water levels h .

Crest wall height [cm]	Water level [cm]				
	70	75	80	85	90
5	0.14	0.17	0.20	0.25	0.33
8	0.21	0.24	0.29	0.35	0.44

4.3.5. Influence of the slope

In order to compare the different slope angles, the tests with identical hydraulic conditions are analysed. This occurs at a water level of 80 cm for waves with a wave steepness of $s_{m-1,0} = 0.013$. These results are observed in Figure 4.21 where two graphs are presented. The x-axis of the left figure is defined by the influence of the dimensional parameter R_c/H_{m0} (see Figure 4.21). The x-axis on the right figure is defined by the non-dimensional discharge q^* (see Section 4.3.5). First of all, it is observed that the γ_w values follow a clearer pattern for the 1:2 slope than for the 1:6 slope. A reasonable argument for this occurrence is the lower overtopping discharges that were measured for the 1:6 slope. Additionally, one can observe that the 1:6 slope tends to have a larger maximum wind effect for the same relative crest freeboard. However, when one looks at the right figure, it seems evident that the trends indicate a higher influence of wind for a 1:2 slope. Once again, this can be explained by the stream lines on a mild slope being more horizontally directed and requiring a larger force to redirect the water in the vertical direction. Water that is elevated for a longer period of time is more likely to be subjected to the effect of wind. This is also in line with the observations acquired by Dijkstra (2023), resulting in a shorter period of time for the water to be subjected to the effect of wind.

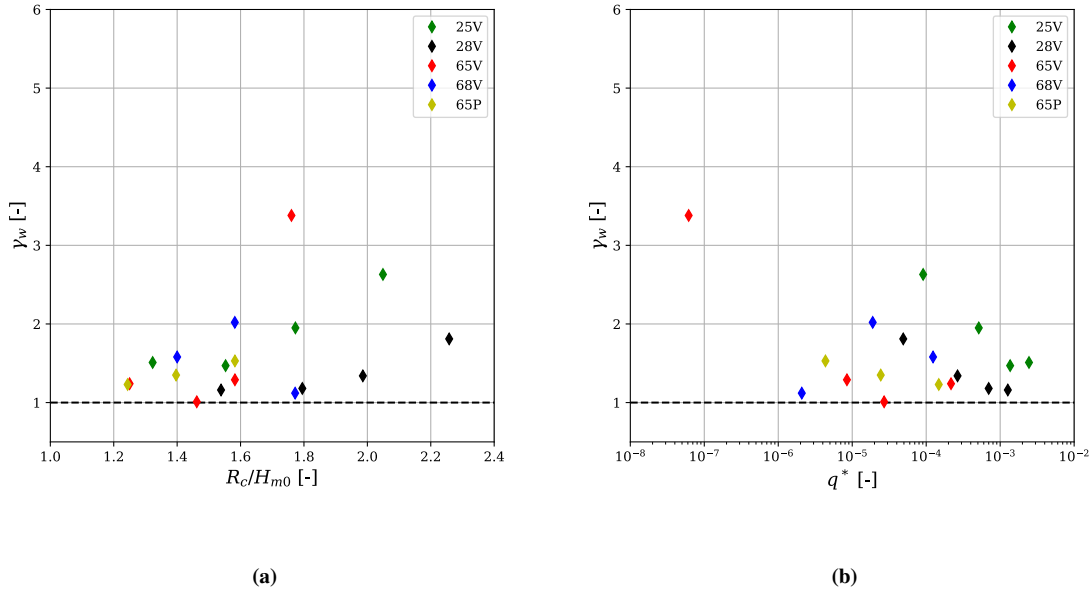


Figure 4.21: Comparison of each configuration for the maximum wind effect for water level $h = 0.80$ m and $s_{m-1,0} = 0.013$ with; (a) The effect of the non-dimensional freeboard; (b) The effect of the non dimensional overtopping discharge.

4.3.6. Constructing the influence factor

As explained in the background theory (Chapter 2), this section aims to provide an expression that best describes the influence of wind with the parameter γ_w . The parameter will be implemented in Equation (4.3), which is now represented by Equation (4.6). However, it is noted that the determination of the expression for the maximum influence of wind is tested for different configurations and hydraulic conditions. Consequently, in the following pages various factors are proposed that correspond to individual characteristics.

$$\frac{q}{\sqrt{gH_{m0}^3}} = \sqrt{\cot(\alpha)}s_{m-1,0}^{-0.25}\gamma_w \exp\left[-\frac{6.4R_c}{\gamma_f\gamma_b\gamma_\beta\gamma_v\gamma_p\varepsilon_{m-1,0}^{0.5}H_{m0}}\right] \quad (4.6)$$

First, a generalized factor is constructed and defined in Equation (4.7) with the 90% confidence interval, which is based on the root mean squared log error between the predicted values and the measured values. The confidence band is defined by Equation (A.7) with the Z-score corresponding to 1.645 for a 90% confidence interval (see Appendix A for more information). This expression includes the influences of all configurations with the aim to develop a general formula that upscales the predicted values to account for the influence of wind. Nonetheless, the equation exclusively depends on the mean overtopping discharge parameter q^* , and is written as a function described with the Power Law (Appendix A). The constant C , which is often defined as a constant uncertainty, is in this function set to 1 as the mechanics of the paddle wheel can only increase the overtopping discharge, stating that the influence factor can not fall below 1.

$$\gamma_w = 0.025q^{*-0.31} + 1 \quad (4.7)$$

The fitted curve is depicted in Figure 4.22 on a linear and logarithmic scale. One can immediately observe that this function is in line with the findings from earlier research, where each time an increased wind effect occurred for a lower overtopping discharge. Furthermore, it is depicted how, especially for the lower overtopping values, large outliers start to become more prevalent. Consequently, they have an increased potential of negatively influencing the accuracy of the developed expression.

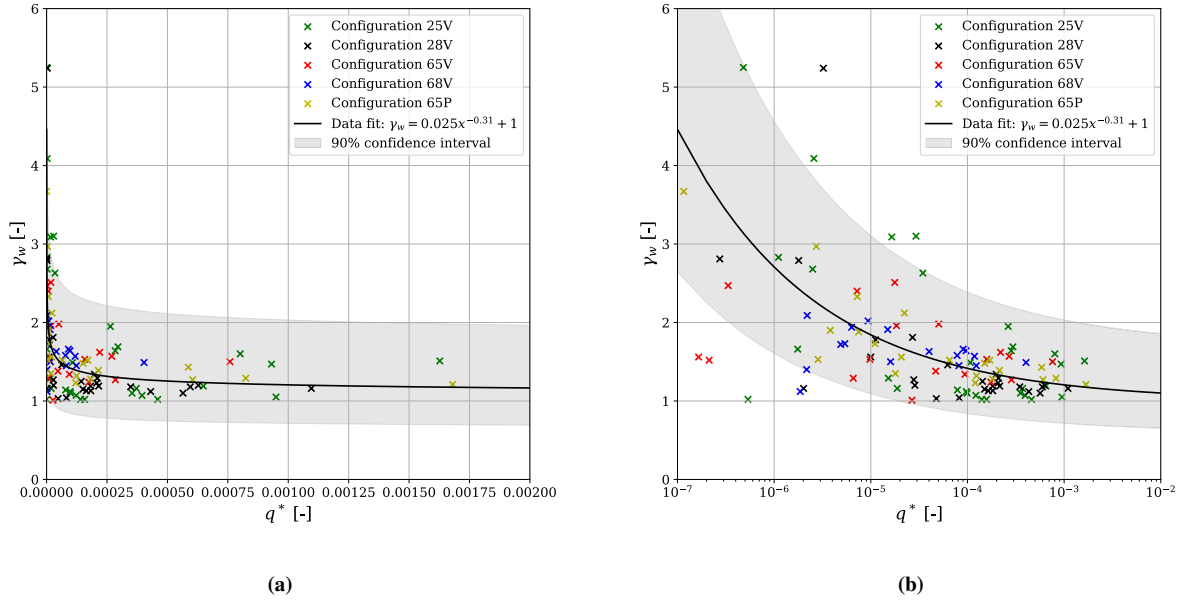


Figure 4.22: Generalized fit describing the maximum wind effect, including all measurement points; (a) Maximum wind effect on a linear scale; (b) Maximum wind effect on a logarithmic scale.

Subsequently, the generalized fit for the wind parameter is decomposed into two expressions corresponding to the 1:2 and 1:6 slopes. The methods describing the wind parameter are included in Equation (4.8). As depicted in Figure 4.23, it is seen how the influence of the mild slope is less pronounced in comparison with the steep slope. It stands out that the 1:6 slope possesses more outliers at the bottom side of the 90% confidence interval, while the opposite is observed for the 1:2 slope. This could partially explain the differences shown with the curves.

$$\gamma_{wind} = \begin{cases} 0.012q^{*-0.37} + 1 & \text{if } \cot(\alpha) = 2 \\ 0.046q^{*-0.25} + 1 & \text{if } \cot(\alpha) = 6 \end{cases} \quad (4.8)$$

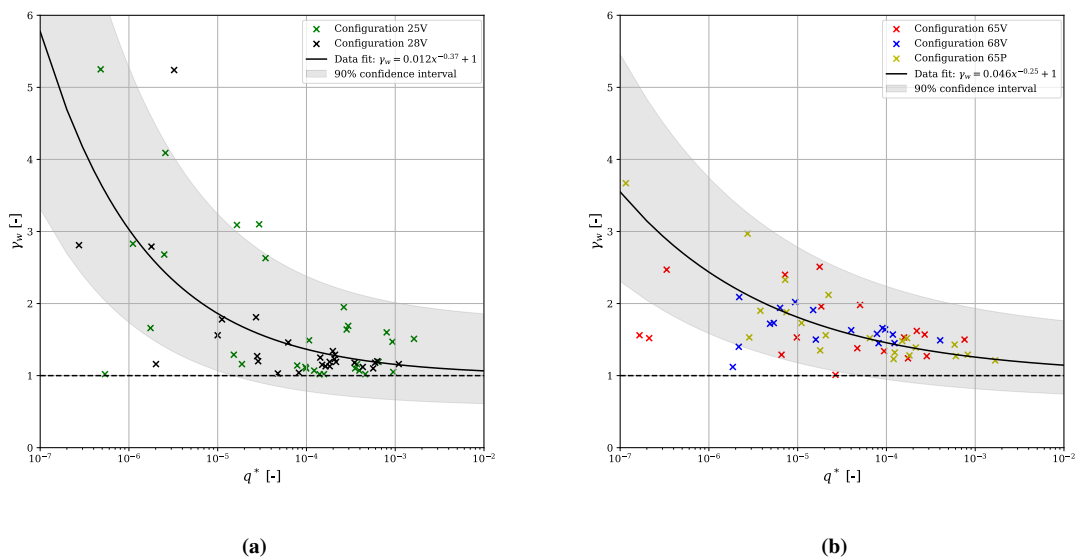


Figure 4.23: Fitted curves describing the maximum wind effect that distinguish between the influence of the 1:2 slope and the 1:6; (a) Fitted curve for the 1:2 slope; (b) Fitted curve for the 1:6 curve.

In the next step, the influence factor that distinguishes the ranges of the relative crest wall height is investigated. This factor found to be of significant influence by Dijkstra (2023). Equation (4.9) consists of two expressions that are each applied within the range given for the non-dimensional crest wall height ($h_{wall}^* = h_{wall}/H_{m0}$). While Dijkstra (2023) observed a decrease of the relative wind influence for a lower non-dimensional crest wall, Figure 4.24 shows very limited variations between the two influence factors for the relative crest wall ranges. Therefore, it can be assumed that the influence of the non-dimensional crest wall is negligible.

$$\gamma_{wind} = \begin{cases} 0.021q^{*-0.32} + 1 & \text{if } 0.20 \leq (R_c - A_c)/H_{m0} \leq 0.40 \\ 0.037q^{*-0.28} + 1 & \text{if } 0.40 \leq (R_c - A_c)/H_{m0} \leq 0.80 \end{cases} \quad (4.9)$$

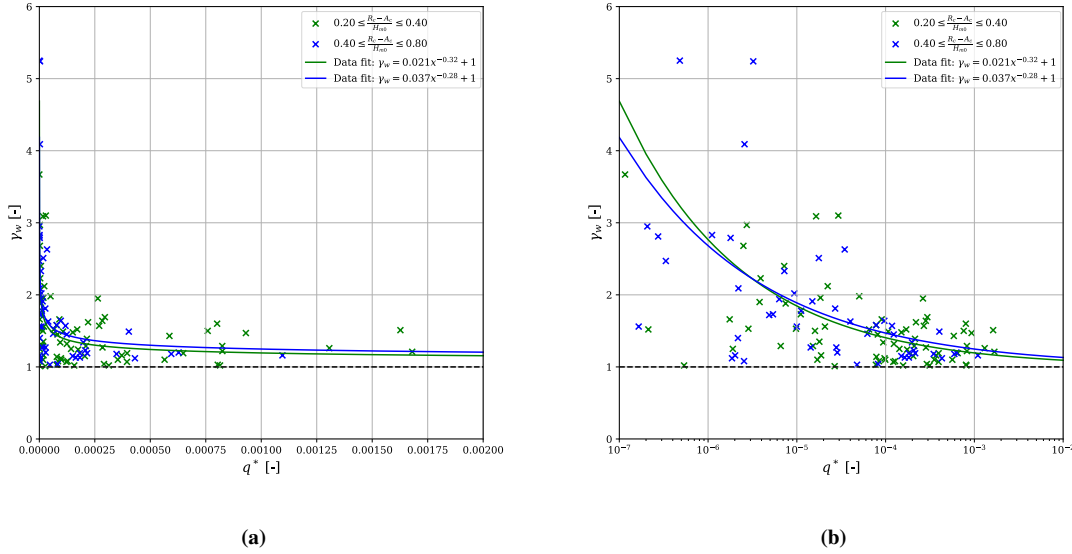


Figure 4.24: Fitted curves describing the maximum wind effect that makes a distinction of the non-dimensional crest height; (a) Fitted curve on linear scale; (b) Fitted curve on logarithmic scale.

Finally, the data is further decomposed into each separate configuration to individually highlight the influences obtained from the experiments for each slope and crest wall combination. Consequently, Equation (4.10) consists of five expressions that correspond to each configuration. Figure 4.25 shows how for every configuration the influence appears to be similar except for the 1:6 slope with 8 cm crest wall (68V) configuration. Although this observation can be reasonably substantiated, it is also observed that three outliers are located below the confidence interval for defining the lowest overtopping discharges. While it is argued how this might occur, it should also taken into consideration these results originate from scaling effects or errors in the experimental setup.

$$\gamma_{wind} = \begin{cases} 0.045q^{*-0.27} + 1 & \text{if } \cot(\alpha) = 2 \text{ and } 5 \text{ cm crest wall;} \\ 0.023q^{*-0.31} + 1 & \text{if } \cot(\alpha) = 2 \text{ and } 8 \text{ cm crest wall;} \\ 0.060q^{*-0.23} + 1 & \text{if } \cot(\alpha) = 6 \text{ and } 5 \text{ cm crest wall;} \\ 0.407q^{*-0.04} + 1 & \text{if } \cot(\alpha) = 6 \text{ and } 8 \text{ cm crest wall;} \\ 0.043q^{*-0.26} + 1 & \text{if } \cot(\alpha) = 6 \text{ and } 5 \text{ cm recurved crest wall;} \end{cases} \quad (4.10)$$

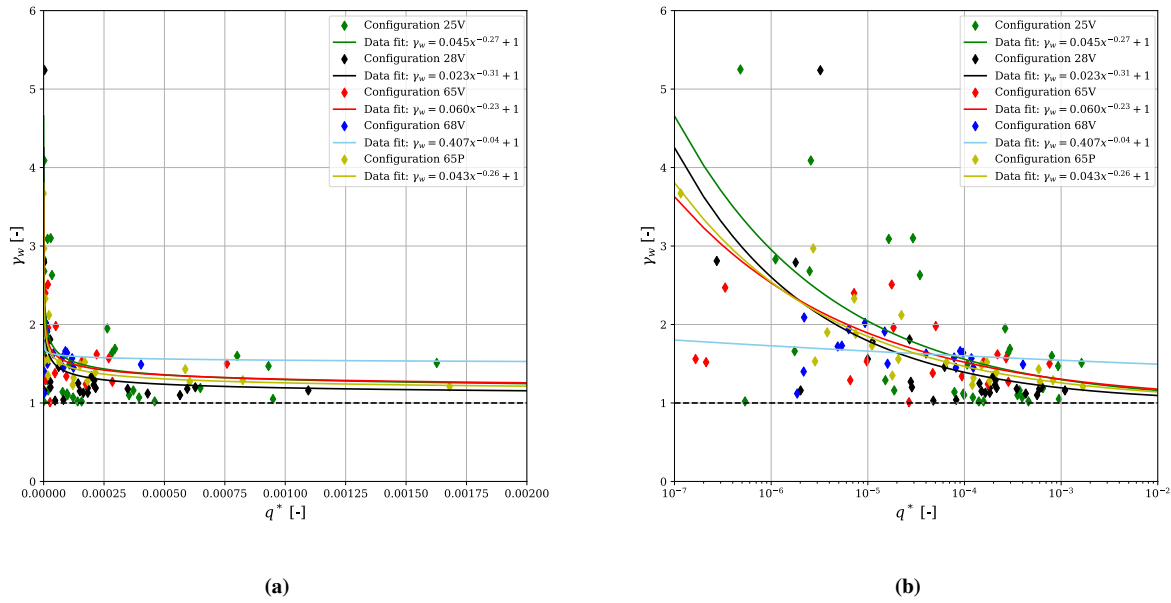


Figure 4.25: Fitted curves describing the maximum wind effect that distinguishes each configuration; (a) Fitted curve on linear scale; (b) Fitted curve on logarithmic scale.

4.4. Implementing the influence factors

In this section the factors found in literature and the constructed equations in this research are implemented in Equation (4.6). The predicted results including the maximum effect of wind will be compared with the calculations where no wind factor is applied to the expression (i.e. $\gamma_w = 1$). Figure 4.26 shows how the majority of the calculations underestimate the overtopping discharges from the observed values.

To enhance this analysis, the RMSLE errors are calculated for each relevant element of the breakwater for which the wind factors haven been constructed. The first error values corresponding to Figure 4.26 are presented in Table 4.7. On the x -axis one can find the measured overtopping values obtained from the tests defined as $q_{measured}^*$, and on the y -axis the predicted overtopping discharge values $q_{calculated}^*$ depicted. It is shown that the average error of the expression deviates roughly with a factor e from the observed value, which means that the expression underestimates or overestimates the actual values by a factor of approximately 2.72. Although this already provides quite an acceptable calculation method, it is tested whether the implementation of the factor for wind can further enhance the accuracy of the expression.

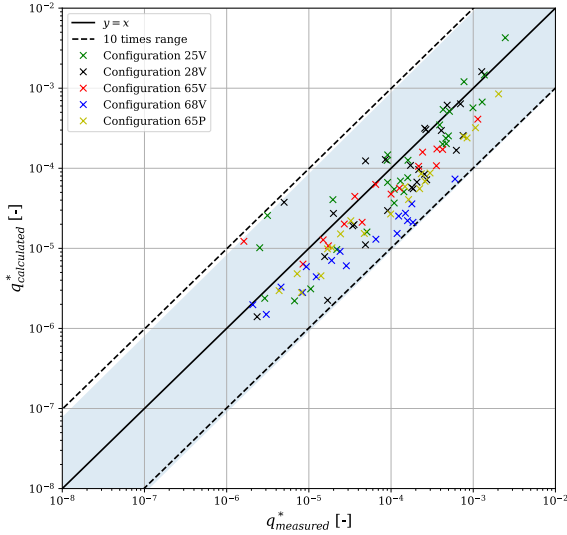


Figure 4.26: Measurements obtained from the experiments with wind predicted with Equation (4.6) where $\gamma_w = 1$.

Subsequently, the factors developed by [Van Gent et al. \(2023\)](#) and [Dijkstra \(2023\)](#) are incorporated into Equation (4.6). In Figure 4.27 their effects are depicted in similar plots, with the error values provided in Table 4.7. It can clearly be seen that for the lower overtopping discharges, the impact of the wind factor is dominant. This effect is slightly more pronounced for the wind factor constructed by [Van Gent et al. \(2023\)](#) in comparison with the factor developed by [Dijkstra \(2023\)](#). It can also be concluded that the distinction of the maximum wind influence between the slope angles is small, as the factor by van Gent was originally developed for a 1:3 sloped dike, the expression has remarkably reduced the error value by a factor of 2, validating its application for a wider range of slope angles.

Table 4.7: Root mean squared log error values.

Type	Description	RMSLE
Generalized	all data	0.989
Slope	$\cot \alpha = 2$	0.805
	$\cot \alpha = 6$	1.259
h_{wall}^*	0.20 - 0.40	0.778
	0.40 - 0.80	1.416
Config.	25V	0.666
	28V	0.969
	65V	0.676
	68V	2.067
	65P	1.038

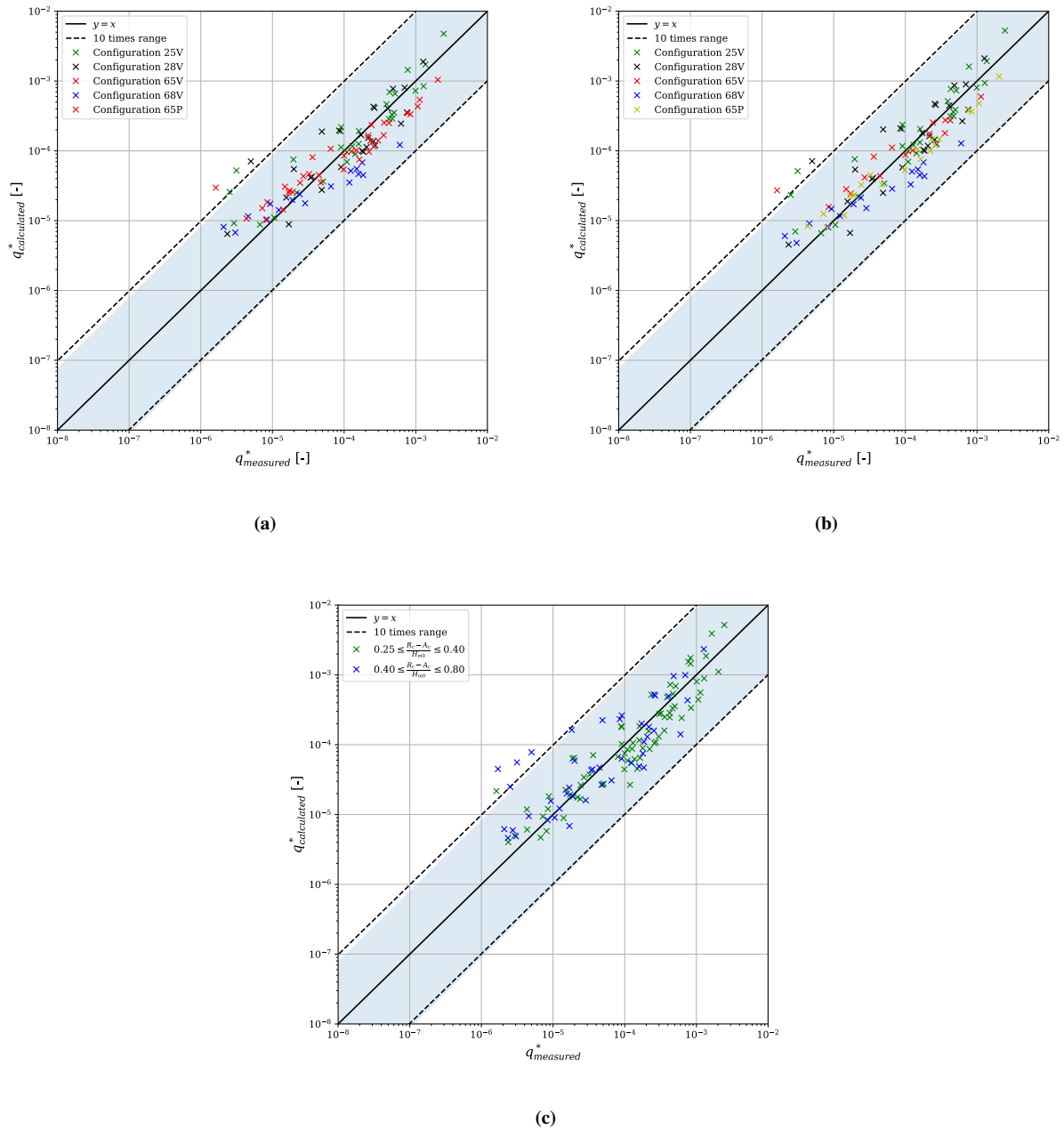


Figure 4.27: Predicted data with the influence of wind determined by parameters obtained from prior research; **(a)** General equation for the influence of wind constructed by Van Gent et al. (2023); **(b)** General equation for the influence of wind constructed by Dijkstra (2023); **(c)** General equation for the influence of wind with a dependency on the relative crest wall constructed by Dijkstra (2023).

Dijkstra (2023) proposes two expressions of which one relates to the influence of the crest wall, and one relates to the generalized maximum wind effect that averages all contributing elements. In general, both expressions slightly improve the calculations in comparison with the calculated discharges obtained with the factor presented by Van Gent et al. (2023). However, when the two expressions by Dijkstra are compared with each other, an improvement of the predictive value obtained with Equation (2.21) tends to be very limited considering the observations of this research. Especially when the influences of the non-dimensional crest wall are considered, for which the upper range even seems to contribute less to achieving an improved accuracy.

Additionally, it stands out that the RMSLE is significantly improved for the configurations with a deviating crest wall improving the RMSLE with roughly 70%. Especially the configuration with the 1:6 slope and a recurved crest wall. Conclusively, from this analysis it can be deduced that the wind factor from Equation (2.20) is definitely applicable for a rubble mound breakwater with a crest element and a varying slope angle, and is the favourable method obtained from prior research.

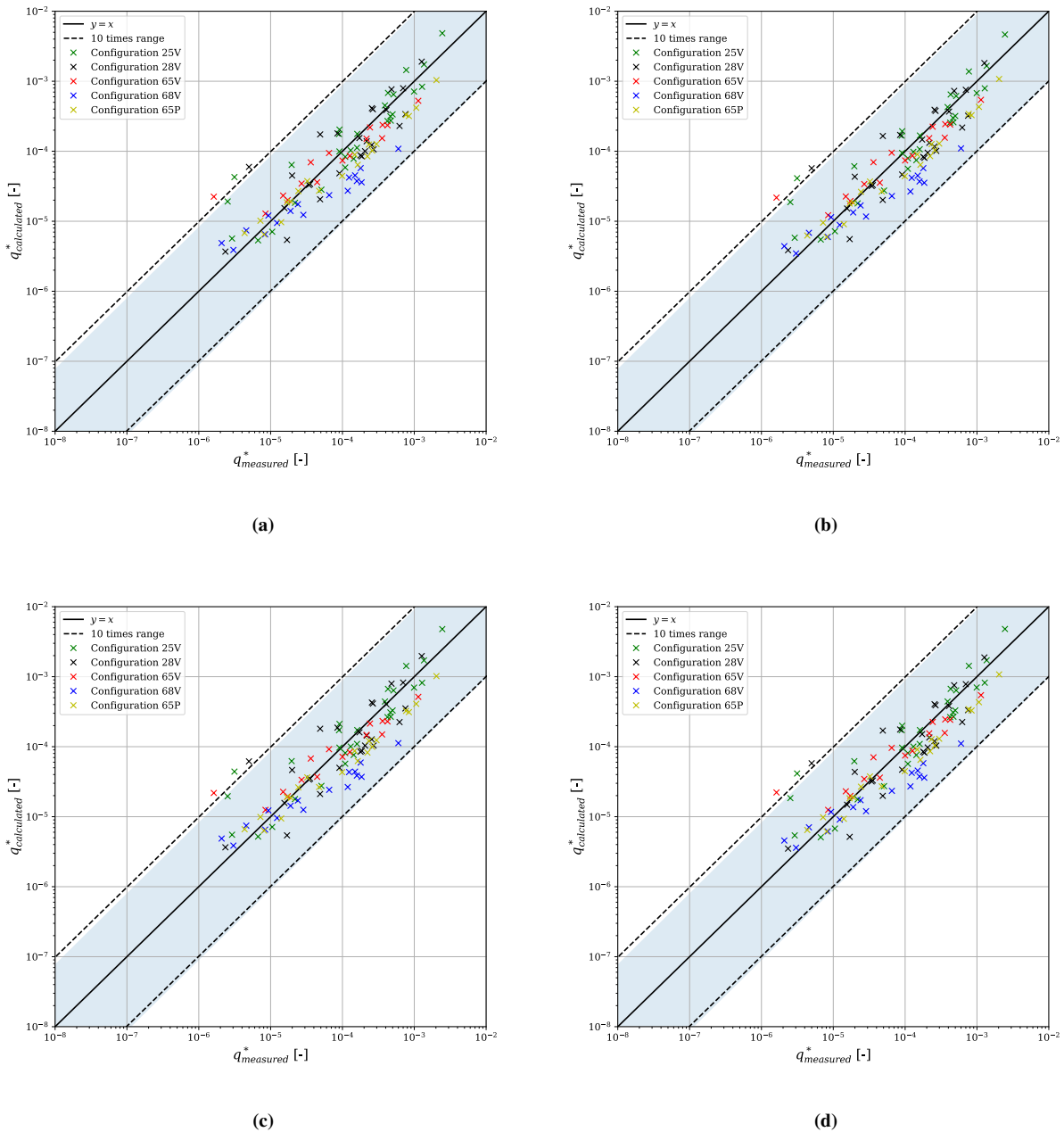


Figure 4.28: Predicted data with the influence of wind determined by parameters obtained from prior research; (a) General equation for the influence of wind constructed by [Van Gent et al. \(2023\)](#); (b) General equation for the influence of wind constructed by [Dijkstra \(2023\)](#); (c) General equation for the influence of wind with a dependency on the relative crest wall constructed by [Dijkstra \(2023\)](#).

Finally, the expressions constructed throughout Chapter 4 are also analysed. The plots in Figure 4.28 show the wind influences corresponding to each element, and the additional RMSLE of the expressions are found in Table 4.8. The overall predicting value of each expression is somewhat similar, providing a sufficient method to predict the measurements. However, it does stand out that the value for the configuration with 1:6 slope and 8 cm crest wall is further off from the predicted values calculated with the wind factors from literature.

While the most comprehensive expression (given in Equation (4.10)) provides the most accurate result, its applicability range is limited to the setups from this research. As the differences between the structure types are small, and the accuracy of the measurements is already sufficient, it is a reasonable to test the validity of the generalized expression developed in this research for other structures as well.

Table 4.8: Summary of the RMSLE for all relevant configurations and conditions

		$\gamma_w = 1$	eq. (2.19)	eq. (2.20)	eq. (2.21)	eq. (4.7)	eq. (4.8)	eq. (4.9)	eq. (4.10)
Generalized	All points	0.989	0.765	0.717	0.734	0.707	0.700	0.714	0.696
Slope	2	0.805	0.83	0.804	0.831	0.732	0.726	0.743	0.724
	6	1.259	0.669	0.590	0.591	0.672	0.662	0.672	0.655
h_{wall}	0.25 - 0.40	0.778	0.502	0.455	0.453	0.499	0.494	0.503	0.468
	0.40 - 0.80	1.416	1.256	1.209	1.256	0.152	1.133	1.158	1.134
Configuration	25V	0.666	0.715	0.691	0.717	0.613	0.606	0.626	0.605
	28V	0.969	0.666	0.670	0.738	0.667	0.670	0.678	0.673
	65V	0.676	0.786	0.706	0.601	0.637	0.613	0.631	0.620
	68V	2.067	0.871	0.801	0.804	0.993	1.002	0.972	0.982
	65P	1.038	0.403	0.318	0.402	0.427	0.412	0.449	0.405

III

Discussion, Conclusion and Recommendations

Discussion

This chapter covers the discussion of the research. First, the setup and methodology are discussed where different elements of the model are evaluated. This is supported by observations during the experiments and the results from the analysis. Subsequently, the applicability and the limitations are presented. This part incorporates the discussion on the overtopping formula developed in this report and discusses the theories behind the influence of various elements on the maximum wind effect.

5.1. Discussion on the methodology

During the test programme it stood out that various components could lead to inaccuracies. In the following pages different segments of the setup are evaluated such as the flume, chute, pumps and data analysis.

- Potential inaccuracies originating from the flume:** While at present, most experiments are conducted in flumes with particular smooth walls, this flume was constructed with smooth concrete blocks. The increased surface roughness of these blocks possibly induces more wall friction, leading to a thicker turbulent layer along the edges of the flume. This turbulent layer potentially leads to small deviations resulting in lower overtopping discharges. It is believed that this will not result in significant errors. The measured overtopping discharge could be slightly less when the same experiments were conducted in a flume with walls made out of glass. However, as the width of the chute does not extend to the total width of the flume, this effect is likely to be very small.
- Potential inaccuracies caused by pumping events:** The larger overtopping discharges did not appear to represent numerous unexpected values. Nonetheless, inaccuracies can still arise due to the occurrence of pumping events. During a pumping event the setup was unable to register incoming overtopping volumes. The amount of pumping events could be limited by implementing a smaller transportation chute. However, [Van Gent et al. \(2023\)](#) applied this technique and observed additional errors linked to this measure. It was observed that wave run-up is not evenly distributed over the width of the slope. This potentially results in inconsistencies of the measured overtopping discharges. Consequently, this inaccuracy was assumed to be of insignificant influence. This is explained with the observation that the measurement points in prior research were also located within the 90 percent confidence area. Moreover, the research focuses on the lower overtopping regime where pumping events scarcely occur.
- Potential inaccuracies caused by the chute:** For very low overtopping discharges, water flowed with very low velocities through the chute. This can lead to minor deviations in the lowest overtopping regime. When an overtopping wave occurs near the end of an experiment its water volume is not transported into the overtopping box in time, it is not included in the measurements. This could be fixed by increasing the slope of the chute. However, it was accepted that such inaccuracies start to compromise the validity of the data for non-dimensional overtopping discharges falling below $E-7$, which further motivates the exclusion of measurement results below this value.
- Outliers occurring in the data set:** As mentioned in the methodology chapter, the test accuracy was deemed sufficient. However, the complete data set still contained some outlying data points. It stands out that the majority of these data points are located within the lower overtopping regime, where larger deviations start to occur when the non-dimensional overtopping discharge drops below $q^* < 4 \cdot 10^{-5}$.

This quantity is characterized by a limited amount of overtopping waves, which means that small deviations of incoming wave characteristics will have more impact on the total outcome. These deviations might arise due to wave reflection, differences in wave run up or currents within the flume that might be different for each experiment.

Bottom outliers in the lowest overtopping regime can also be explained by the functioning of the paddle wheel. For waves that induce peculiar low overtopping volumes, the upwards splashing water is likely in the position to be transported for a very short time period. It might occur that the water drops already left the transportation area of the paddle wheel before being transported. This argument also works vice versa, as there likely is an optimum where the maximum water volume is transported at the most convenient timing, which would then lead to an outlier at the upper side of the spectrum.

5.2. Applicability and limitations

As is common practice in experimental research concerning wave overtopping, this study includes various new expressions to estimate the overtopping discharges and to find the maximum influence of wind. However, the developed expressions are validated for specific circumstances and are therefore subjected to certain limitations. For this reason, in the following section it is discussed what the associated limitations are and for what circumstances the formulae are deemed applicable.

5.2.1. Overtopping discharge (without wind)

As indicated, a new expression has been developed to calculate the overtopping discharge for a rubble mound breakwater with a crest element. Note that this does not imply that the expressions developed in previous studies are incorrect, but are merely not applicable for the measurements from this data set. As an example, this deviation might be due to various aspects involving the setup and analysis that are also treated in the discussion. However, first the development of Equation (4.6) is reviewed.

The expression that describes wave overtopping is of the form presented in Equation (2.1), which is no exception compared to previous studies. Although the expressions provided by Van Gent et al. (2022) and Irias Mata & van Gent (2023) provide a precise shape, they are not accurate for this specific measurement programme (as shown in Figure 4.9). The first step in adapting the expression to the results is by iteratively changing the constants a and b (in Equation (2.1)). Equation (4.3) was developed by applying changes to Equation (2.5) (Irias Mata & van Gent, 2023) as follows:

$$a: 0.03s_{m-1,0}^{-0.5} \cot \alpha \longrightarrow s_{m-1,0}^{-0.25} \sqrt{c \cot \alpha} \quad \text{and} \quad b: \frac{4}{\xi_{m-1,0}^{0.5}} \longrightarrow \frac{6.4}{\xi_{m-1,0}^{0.5}}$$

The modification of coefficients a and b , including the observed effect of the crest element and the crest freeboard, led to the plot shown in Figure 4.8. Although Equation (2.5) calculates the measurements obtained in this study accurately enough to construct a factor for the maximum effect of wind, additional elements were also assessed.

First, the effect of an increased crest wall height represented by γ_v was investigated. As Equation (2.15) was validated for the original formula Equation (2.5), it was also tested for this study. However, a clear distinction was found between the different crest wall heights, making the expression for γ_v invalid for this research. When one compares Figure 4.10 with Figure 4.11 it can be concluded that the influence of the expression by Van Gent et al. (2022) is too dominant, resulting in an increased underestimation. This is in contrast with the underestimation that is obtained when the influence of the crest wall height is taken as $\gamma_v = 1$.

Consequently, a new expression needed to be developed. This results of this expression are found in Figure 4.12, which instead of dividing the crest wall height by the crest freeboard, divides h_{wall} by the spectral wave height H_{m0} . This ratio is often called the non-dimensional crest wall height h_{wall}^* . Including its effect evidently improved the calculation incorporating the different crest element heights (see Figure 4.12 for a visualization of the expression).

Second, the effect of a recurved parapet was assessed. Although the differences that result from the presence of a parapet are limited (see Figure 4.13a), it can still have value to find an expression that calculates the

overtopping discharge including a parapet. The available expressions that were investigated were obtained from Equation (2.16) and Equation (2.17), and both returned less accurate results for the 1:6 slope, while Van Doorslaer et al. (2015) appeared to improve the calculation for the 1:2 slope. This can be explained by the fact that the equation by Van Doorslaer et al. (2015) was assessed and validated for non-breaking waves and on steep slopes (including 1:2).

Moreover, the setup tested in this research has some significant differences that might affect the influence of the parapet in comparison with the model used by Oh et al. (2018). First, different stone types were used (tetrapods), leading to a different roughness factor. Second, a slightly steeper slope is applied which has influence on the breaking-type of waves (ξ). And finally, the parapet used in this study is relatively small to that of Oh et al. (2018). The accumulation of these differences might have led to a fundamentally varying expression.

However, with limited availability of expressions concerning the influence of a parapet, the decision is made to modify Equation (2.16) (Oh et al., 2018). This is explained by the fact that it is expected for the dimensions of the parapet to influence the overtopping discharge, but also depends on the influence of wave breaking. Therefore Equation (4.5) is developed, implying a larger reduction of the overtopping discharge for a decreasing breaker parameter. Conclusively, this expression is only validated for the specific dimensions of the parapet used in this model.

5.2.2. Influence of the elements on the maximum wind effect

One of the key findings appears to be the influence of the crest freeboard, which is of significant influence to the maximum wind effect. Generally, a decrease of R_c is likely to increase the amount of wave overtopping. In agreement with the current state of knowledge, this would evidently lead to a decrease of the maximum effect of wind. However, the observations obtained during the test programme occasionally conflict with this statement. Therefore, assuming this applies for all circumstances may not be valid for rubble mound breakwaters with a crest wall. A reasonable explanation is the theory that for a decreasing A_c/R_c ratio, the structure increasingly adopts the properties of a vertical seawall, while the properties of a rubble mound breakwater are reduced. This effect can only be considered when a crest element is constructed on top of the breakwater. This theory is supported by the fact that de Waal et al. (1996) found larger wind influences for a vertical sea wall than Van Gent et al. (2023) and Dijkstra (2023) for a dike.

Conclusively, it should be carefully considered when to increase the height of a crest wall as an adaptation method. It is important which factor is governing when one looks into the water level influence considering the maximum wind effect as the proportions of the dimensional parameters are changed and the behaviour of the hydraulic characteristics will be altered. Therefore, there likely exists a transitional range where the overtopping expression of a vertical seawall should be applied to determine the overtopping discharge, including the maximum wind effect.

Furthermore, a milder slope tends to lead to a lower overtopping discharge. This is explained with the phenomenon that an increased amount of wave energy gets dissipated over the length of the slope. However, the objective that remains is to understand to what extent a milder slope affects the maximum wind effect. While Figure 4.25b shows a difference between the influence of the slope, this is likely caused by the increased crest height. From the figure can be concluded that when the configuration of the 1:6 slope 8 cm crest wall is excluded, the variation between the slopes will be diminished.

Another reasonable explanation for a higher influence of a slope is given in Figure 5.1, showing how a schematized flow pattern needs to follow a longer trajectory to reach the height of the crest wall from the nod of the slope to the x -location of the crest wall. When the trajectory is schematized as a straight line, a droplet emerging from the steep slope under a steep angle travels a shorter distance to reach the height of active area of the paddle wheel (where it is transported into the overtopping box). When considering the mild slope, the droplets follow a longer trajectory, providing more time for gravity to pull the droplets down.

Conclusions & Recommendations

First, this chapter presents the conclusion of this research. This is done by answering the main research question regarding the determination of the overtopping discharge, and the influence of wind. Subsequently, the sub-questions are answered, addressing specific aspects of the broader main research question. The second part of this chapter covers the recommendations, providing ideas and challenges for future studies to engage in.

6.1. Conclusion

The primary objective of this research was to investigate the maximum influence of onshore wind on wave overtopping at rubble mound breakwaters, while including the influence of a slope and crest wall design. The main research question is repeated below:

“What is the maximum effect of onshore wind on the mean overtopping discharge at rubble mound breakwaters with a crest element?”

Physical model tests were carried out to find an answer for this objective. The influence of the maximum wind effect was found to be within the range of $1.03 \leq \gamma_w \leq 5.25$ when applying the limits obtained from the 90% confidence interval. This range is similar to the experimental findings for the maximum wind influence at a dike, and corresponds to the observations obtained by [Wolters & van Gent \(2007\)](#), who found a wind factor range of 1.3 to 6.3 for smooth slopes and 1.2-4.7 for rough slopes.

Eventually, the answer to the main research question is presented in the form of an expression (Equation (4.7)). Similar to previous literature, this expression is a function of the non-dimensional overtopping discharge, which is defined by the various hydraulic conditions and physical elements of a breakwater structure. In addition to the expression below, additional formulae were developed with the aim to better calculate the measurement outcomes. These expressions incorporate various elements, such as the slope angle, crest wall height, or both. However, it was found that these expressions returned a similar wind factor, while simultaneously decreasing the applicability of the expression. Consequently, the research question is addressed with the following generalized equation:

$$\gamma_w = 0.025q^{*-0.31} + 1 \quad (4.6)$$

Furthermore, the maximum wind influence factor includes the non-dimensional overtopping discharge q^* . Consequently, the prediction method calculating the overtopping discharge without wind requires to be thoroughly understood as well. For this reason, each answer of the sub-question starts with examining each influential component excluding the effect of wind. The expression of this method is restated below:

$$\frac{q}{\sqrt{gH_{m0}^3}} = \sqrt{\cot(\alpha)} s_{m-1,0}^{-0.25} \exp \left[-\frac{6.4R_c}{\gamma_f \gamma_b \gamma_\beta \gamma_v \gamma_p \xi_{m-1,0}^{0.5} H_{m0}} \right] \quad (4.3)$$

6.1.1. Influence of the water level, wave period, and wave height on wave overtopping and the maximum wind effect

First, the question mentions the influence of the water level, which is incorporated in the physical parameter R_c/H_{m0} and the new factor $(1.55 - A_c/R_c)$. The results from the experiments showed that the water level led to an increased overtopping volume and an underestimation of the observed values. Consequently, a factor is added to increase the accuracy of the prediction when the water level rises without wind. The influence of A_c/R_c is mainly due to by the changing characteristics of the structure when the water level rises, described by an increasing wall to slope ratio. With the aim to find this influence, an iterative process led the development of the factor $(1.55 - A_c/R_c)$. This factor was included in γ_v , as the parameter A_c is originally included in the influence factor for the crest wall height.

It was found that the water level had an observable influence on the maximum wind effect, leading to an increase for an increasing water level. Additionally, increasing maximum wind influence factors were found for the same non-dimensional overtopping discharges. It is unclear whether this occurs for all types of structures, or that the A_c/R_c ratio mainly contributes to this effect.

The research also examined the influence of the wave height, which appeared to be sufficiently accounted for, as different wave heights did not lead to significant deviations within the patterns observed from the data analysis. However, the influence of the wave steepness did not seem to be properly accounted for, as the calculations led to an underestimation for an increasing wave steepness. Therefore the exponent of $s_{m-1,0}$ was iteratively adjusted, leading to an improvement of the calculation method.

It was also found that an increasing wave steepness led to an increasing maximum wind effect. This was mainly argued by the observation that the steeper waves result in lower overtopping volumes, which were found to lead to increasing maximum wind effects.

6.1.2. Influence of the height and shape of a crest wall on wave overtopping and the maximum wind effect

First, the effect of the crest wall height appeared to be influenced by the non-dimensional crest wall height h_{wall}^* , being a function of the dimensional crest height divided by the wave height. It was found that an increasing non-dimensional crest wall height lead to decreasing wave overtopping volumes. After iteratively optimizing the expression, the influence of the crest wall height was determined with the expression below:

$$\gamma_v = \frac{1 - \left(\frac{R_c - A_c}{H_{m0}} \right)^{1.7}}{1.55 - A_c/R_c} \quad (4.4)$$

It was reasoned that an increasing crest wall generally leads to a higher maximum wind effect as the overtopping discharge decreases. However, it was also observed that the increased crest wall of the 1:6 slope had lower wind influence factors for similar overtopping discharges. A possible explanation was found in the higher water levels used for the 1:6 slope which increases the relative presence of the crest wall significantly. As a consequence, this leads to less wave dissipation on the slope resulting in higher energy waves reaching the crest wall. Moreover, deviations were also explained with the effect of outliers. For this configuration mainly outliers at the bottom of the confidence interval were found within the lower overtopping regime. These outliers significantly influence the fitted curve through the data, potentially underestimating its magnitude.

The influence of a parapet appeared to slightly reduce the wave overtopping discharge. The expression developed by [Oh et al. \(2018\)](#) and [Van Doorslaer et al. \(2015\)](#) proved insufficient for this study. However, it was decided to adapt the equation from [Oh et al.](#) with the aim to preserve the dimensional parameters of the parapet in the expression. Eventually, an updated influence factor that represents the parapet was developed in Equation (4.5) which is repeated below:

$$\gamma_p = 1 - \left(\frac{B_r}{h_r \xi_{m-1,0}} \right)^{1.1} \quad (4.5)$$

It was observed during the experiments, that the manner in which the waves approach the recurved crest wall influences the effect of a parapet. This is described by the breaker parameter. A larger breaker parameter value would in this case lead to a larger reduction of the wave overtopping discharge. Although previous

research suggested that a parapet merely reduced overtopping discharges in the lowest regime, this study found a profound effect of a parapet when subjected to breaking waves including the higher overtopping regime.

As the presence of the parapet was observed to slightly decrease the wave overtopping discharge, so did the influence of wind. However, no significant differences were found between maximum wind effect for a vertical and recurved crest wall.

6.1.3. Influence of the slope angle on the mean overtopping discharge and the maximum wind effect

The components of the seaward slope that were examined throughout this research incorporate the slope angle and the roughness of the slope. Another factor often taken into consideration is a berm, which was excluded from this research programme.

First the influence of the roughness of the slope was considered. The expression calculates a lower overtopping discharge for a rougher slope. The decision was made to apply the variable expression, identical to the one used by [Van Gent et al. \(2022\)](#) and [Irias Mata & van Gent \(2023\)](#). However, no modified expression could be developed for this research, as no experiments were carried out that aimed at comparing different stone sizes (rocks) or shapes (concrete blocks).

Although the results from this study show a slight increase of the wind effect in comparison with the findings from [Van Gent et al. \(2023\)](#) and [Dijkstra \(2023\)](#), no additional wind effect originating from the roughness could be concluded from this experimental programme.

Subsequently, the influence of the slope angle was investigated, which is also incorporated in the breaker parameter $\xi_{m-1,0}$. It was observed that a milder slope led to a decreased overtopping discharge. As the prediction method developed by [Irias Mata & van Gent \(2023\)](#) already included these parameters, the expression still had to be modified to properly correspond to the measurements obtained from the experiments.

As the wave overtopping discharge decreased for a milder slope, the wind influence increased. The analysis showed that the maximum wind effect appeared lower for similar dimensionless discharge values for the milder slope. However, when each element was analysed separately, it was concluded that the tests on the higher crest wall for the 1:6 slope corresponded to a factor deviating from the other elements. The explanation given for this observations followed a similar rhetoric provided for the water level, which resolved around the A_c/R_c ratio.

6.1.4. Final remarks

This research has contributed to a deeper understanding of the influence of wind on wave overtopping for rubble mound breakwaters, considering varying slopes and crest wall designs. The developed wind factor expressions have enhanced our understanding on calculating its effect, offering broader applicability across different structure types. While the non-dimensional wave overtopping discharge quantity has been determined, the amplification factors developed in this research have proven applicable for various structure types, improving the observations obtained during this study.

6.2. Recommendations

Although a vast amount of new knowledge is obtained since the studies carried out by [de Waal et al. \(1996\)](#), there are still some issues untreated that were not within the scope of this research. Additionally, new questions have emerged from findings in this research. Consequently, the following recommendations have been proposed with the potential to state the course for future research:

- **Recurved parapet γ_p :** While Equation (4.5) accurately describes the reducing effect of a parapet for both slope angles of the models tested in this research, no variations of the dimensions of the parapet were tested. It could be that an increasing size of the bull nose eventually leads to an observable influence on the maximum wind effect. Therefore, it is recommended to validate Equation (4.5) for different shapes and is further optimized when necessary.
- **Slope angle α :** This study proposes an expression for the maximum wind factor that solely includes the non-dimensional overtopping discharge. Both slope angles treated in this research were provided with an individual expression. While the influence could not directly be related to the influence of the slope,

it can be further investigated how including the parameter for the slope angle within the expression of the wind factor γ_w might affect the solution. Therefore, for future research it is recommended to incorporate additional factors inside the expression that calculates the maximum effect of wind. Further understanding can be achieved by including tests on intermediate slopes.

- **Freeboard R_c :** Similarly to the slope angle, the influence of the crest free board was also found to have a unique influence on the maximum effect of wind. Therefore, it is also recommended for this parameter to investigate the wind factor expression when it is included, especially when a crest wall is present in the model.
- **Presence of a berm γ_b :** A berm or an extension of the width in front of the crest wall G_c still remains to be investigated. Additionally, the consideration of a berm is also necessary to investigate the influence factor corresponding to Equation (4.6). Can the equations obtained from [Irias Mata & van Gent \(2023\)](#) be applied, or to what extent do they need to be modified to become valid for the new expression.

For the same reason, the influence of obliqueness can be considered. It can be reasonable for obliquely incident waves to have a reduced effect of wind as the waves will not be redirected along the vertical direction, but also along the width of the structure. Consequently, leading to a decreased elevated time span, while at the same time the overtopping discharge is likely to decrease.

- **Obliqueness of waves γ_β :** As indicated throughout this study, the influence of obliqueness has not been investigated, nor included in the overtopping formula. As wave obliqueness has been studied in the past various expressions have been developed to include its influence. Therefore it is recommended to validate these expressions and develop a new expression that corresponds to the expression developed in this study.
- **Wave forcing:** Waves that cause larger forces on the structure, have the potential to transport more water into the vertical column, while not directly overtopping the wall. Therefore, it can be interesting to find a relationship between the forcing of waves and the maximum influence of wind. This could also bring light to the influence of a vertical sea wall and if the findings from this research can be validated. Additionally, the influence of the location of wave breaking can be tested. One can imagine that for a wave that plunges against a wall a significantly large amount of water is forced vertically, waiting to be transported by the effects of wind.
- **Individual waves:** Instead of investigating exclusively the mean overtopping discharge over a storm event, investigating the overtopping discharge of an individual wave would provide valuable information for a more detailed understanding of the wave characteristics. Although data was obtained for individual waves with the methodology of this study, due to the limitations of time this could not be properly investigated. Therefore, considering the availability of proper data, it is recommended as a followup study to investigate the influence of individual waves on the maximum wind effect.

References

- Battjes, J. A. (1974). *Computation of set-up, longshore currents, run-up and overtopping due to wind-generated waves*. Doctoral Thesis, TU Delft. <http://resolver.tudelft.nl/uuid:e126e043-a858-4e58-b4c7-8a7bc5be1a44>
- Besley, P. (1998). Wave overtopping of seawalls, design and assessment manual. *R&D technical report W178*. <https://repository.tudelft.nl/islandora/object/uuid%3A0cd1c50d-0957-4599-aa37-e6328da73988>
- Bruce, T., van der Meer, J., Franco, L., & Pearson, J. (2009). Overtopping performance of different armour units for rubble mound breakwaters. *Coastal Engineering*, 56(2), 166–179. <https://doi.org/https://doi.org/10.1016/j.coastaleng.2008.03.015>
- Burcharth, H. F. (1994). Reliability evaluation of structure at sea. *Wave Barriers in Deepwaters*, 470–517. <http://resolver.tudelft.nl/uuid:22243a72-a728-4649-97c1-bd1013d7f876>. Publisher: Port and Harbour Research Institute
- CETMEF (2007). The rock manual : the use of rock in hydraulic engineering. 1268. <https://www.kennisbank-waterbouw.nl/DesignCodes/rockmanual/>
- Chowdhury, S. D., Zhou, J. G., Khait, A., Pullen, T., Causon, D., Qian, L., & Mingham, C. (2020). Wind effects on wave overtopping at a vertical sea defense. *Journal of Waterway, Port, Coastal, and Ocean Engineering*, 149(4), 04023010. <https://doi.org/10.1061/JWPED5.WWENG-1960>
- de Waal, J. P., Tönjes, P., & van der Meer, J. W. (1996). Wave overtopping of vertical structures including wind effect. *Coastal Engineering 1996*, 2216–2229. <https://doi.org/10.1061/9780784402429.172>
- Dijkstra, S. (2023). The maximum influence of wind on wave overtopping at mildly sloping dikes with a crest element. *MSc. Thesis, TU Delft*. <https://repository.tudelft.nl/islandora/object/uuid%3A07ffde04-ab60-4b71-81a5-b3c3631e944d>
- EurOtop (2018). *Manual on wave overtopping of sea defences and related structures*. Van der Meer, J.W. and Allsop, N.W.H. and Bruce, T. and de Rouck, J. and Kortenhaus, A. and Pullen, T. and Schüttrumpf, H. and Troch, P. and Zanuttigh, B. <http://www.overtopping-manual.com/assets/downloads>
- Franco, L., de Gerloni, M., & Van der Meer, J. (1994). Wave overtopping on vertical and composite breakwaters. *Coastal Engineering Proceedings*, 1(24). <https://doi.org/10.1061/9780784400890.076>
- Goda, Y. (1971). Expected rate of irregular wave overtopping of seawalls. *Coastal Engineering in Japan*, 14(1), 43–51. <https://doi.org/10.1080/05785634.1971.11924125>
- Hasselmann, K., Barnett, T., Bouws, E., Carlson, H., Cartwright, D., Enke, K., Ewing, J., Gienapp, H., Hasselmann, D., Kruseman, P., Meerburg, A., Muller, P., Olbers, D., Richter, K., Sell, W., & Walden, H. (1973). Measurements of wind-wave growth and swell decay during the joint north sea wave project (jonswap). *Deut. Hydrogr. Z.*, 8, 1–95.
- Hogeveen, K. (2021). Climate adaptation of rubble mound breakwaters. *MSc. Thesis, TU Delft*.
- Holthuijsen, L. H. (2007). *Waves in Oceanic and Coastal Waters*. Cambridge University Press. <https://doi.org/10.1017/CBO9780511618536>
- IPCC (2022). *Climate Change 2022: Mitigation of Climate Change. Contribution of Working Group III to the Sixth Assessment Report of the Intergovernmental Panel on Climate Change*. Cambridge University Press. <https://doi.org/10.1017/9781009157926>

- Irias Mata, M. & van Gent, M. R. (2023). Numerical modelling of wave overtopping discharges at rubble mound breakwaters using openfoam®. *Coastal Engineering*, 181, 104274. <https://doi.org/https://doi.org/10.1016/j.coastaleng.2022.104274>
- Koosheh, A., Etemad-Shahidi, A., Cartwright, N., Tomlinson, R., & van Gent, M. R. (2021). Individual wave overtopping at coastal structures: A critical review and the existing challenges. *Applied Ocean Research*, 106, 102476. <https://doi.org/https://doi.org/10.1016/j.apor.2020.102476>
- Koosheh, A., Etemad-Shahidi, A., Cartwright, N., Tomlinson, R., & van Gent, M. R. (2022). Experimental study of wave overtopping at rubble mound seawalls. *Coastal Engineering*, 172, 104062. <https://doi.org/https://doi.org/10.1016/j.coastaleng.2021.104062>
- Lioutas, A., Smith, G. M., & Verhagen, H. J. (2012). Spatial distribution of overtopping. *Coastal Engineering Proceedings*, 1(33), structures.63. <https://doi.org/10.9753/icce.v33.structures.63>
- Marsman, E., Hoogland, K., & Van der Zijp, N. (2007). Stormverslag petten.
- Mayo, T. L. & Lin, N. (2022). Climate change impacts to the coastal flood hazard in the northeastern united states. *Weather and Climate Extremes*, 36, 100453. <https://doi.org/https://doi.org/10.1016/j.wace.2022.100453>
- Molines, J., Bayon, A., Gómez-Martín, M. E., & Medina, J. R. (2019). Influence of Parapets on Wave Overtopping on Mound Breakwaters with Crown Walls. *Sustainability*, 11(24), 7109. <https://doi.org/10.3390/su11247109>
- Molines, J. & Medina, J. R. (2016). Explicit wave-overtopping formula for mound breakwaters with crown walls using clash neural network-derived data. *Journal of Waterway, Port, Coastal, and Ocean Engineering*, 142(3), 04015024. [https://doi.org/10.1061/\(ASCE\)WW.1943-5460.0000322](https://doi.org/10.1061/(ASCE)WW.1943-5460.0000322)
- NOS (2023). *Dode in Schotland door storm Babet, ook extreem weer verwacht in Scandinavië*. <https://nos.nl/artikel/2494722-dode-in-schotland-door-storm-babet-ook-extreem-weer-verwacht-in-scandinavie>
- Oh, S. H., Jang, S. C., & Lee, J. (2018). Wave overtopping and loading for the recurved parapets on the crest of rubble mound breakwater. *Coasts, Marine Structures and Breakwaters 2017*, 979–985. <https://doi.org/10.1680/cmsb.63174.0979>
- Owen, M. (1980). Design of seawalls allowing for wave overtopping.
- Pierson, J. & Moskowitz, L. (1963). A proposed spectral form for fully developed wind seas based on the similarity theory of s. a. kitaigorodskii. *Journal of Geophysical Research*, 69, 32. <https://doi.org/10.1029/JZ069i024p05181>
- Radfar, S., Shafieefar, M., Akbari, H., Galiatsatou, P. A., & Mazyak, A. R. (2021). Design of a rubble mound breakwater under the combined effect of wave heights and water levels, under present and future climate conditions. *Applied Ocean Research*, 112, 102711. <https://doi.org/https://doi.org/10.1016/j.apor.2021.102711>
- Schiereck, G. & Verhagen, H. (2019). *Introduction to bed, bank and shore protection: Revised edition*. Delft Academic Press.
- Takagi, H. & Esteban, M. (2013). Practical methods of estimating tilting failure of caisson breakwaters using a monte-carlo simulation. *Coastal Engineering Journal*, 55(3), 1350011–1–1350011–22. <https://doi.org/10.1142/S0578563413500113>
- TAW (2002). Technical report wave run-up and wave overtopping at dikes. *TAW report (incorporated in the EurOtop manual)*.
- Van der Bijl, R. (2022). The maximum wind effect on wave overtopping at dikes with crest elements. <https://doi.org/https://doi.org/10.1016/j.coastaleng.2015.02.004>

- Van Doorslaer, K., de Rouck, J., Audenaert, S., & Duquet, V. (2015). Crest modifications to reduce wave overtopping of non-breaking waves over a smooth dike slope. *Coastal Engineering*, 101, 69–88. <https://doi.org/https://doi.org/10.1016/j.coastaleng.2015.02.004>
- Van Gent, M. R. (2020). Influence of oblique wave attack on wave overtopping at smooth and rough dikes with a berm. *Coastal Engineering*, 160, 103734. <https://doi.org/https://doi.org/10.1016/j.coastaleng.2020.103734>
- Van Gent, M. R. (2021). Influence of oblique wave attack on wave overtopping at caisson breakwaters with sea and swell conditions. *Coastal Engineering*, 164, 103834. <https://doi.org/https://doi.org/10.1016/j.coastaleng.2020.103834>
- Van Gent, M. R. & van der Werf, I. M. (2019). Influence of oblique wave attack on wave overtopping and forces on rubble mound breakwater crest walls. *Coastal Engineering*, 151, 78–96. <https://doi.org/https://doi.org/10.1016/j.coastaleng.2019.04.001>
- Van Gent, M. R., Wolters, G., & Capel, A. (2022). Wave overtopping discharges at rubble mound breakwaters including effects of a crest wall and a berm. *Coastal Engineering*, 176, 104151. <https://doi.org/https://doi.org/10.1016/j.coastaleng.2022.104151>
- Van Gent, M. R. A. (1999). Physical model investigations on coastal structures with shallow foreshores: 2D model tests with single and double-peaked wave energy spectra. *H3608*. <https://repository.tudelft.nl/islandora/object/uuid%3A1b4729de-2e86-4b8a-98d5-48d8e07d5902>. Publisher: Deltares (WL)
- Van Gent, M. R. A. (2014). Oblique wave attack on rubble mound breakwaters. *Coastal Engineering*, 88, 43–54. <https://doi.org/https://doi.org/10.1016/j.coastaleng.2014.02.002>
- Van Gent, M. R. A. (2022). Wave overtopping at dikes and breakwaters under oblique wave attack. *Coastal Engineering Proceedings*, (37), 5–5. <https://doi.org/10.9753/icce.v37.papers.5>. Number: 37
- Van Gent, M. R. A., van der Bijl, R. J., Wolters, G., & Wüthrich, D. (2023). The maximum influence of wind on wave overtopping at seawalls with crest elements. Deltares, Dept. of Coastal Structures & Waves, Delft, NL; TU Delft, Dept. of Hydraulic Engineering, Delft, NL.
- Wolters, G. & van Gent, M. (2007). Maximum wind effect on wave overtopping of sloped coastal structures with crest elements. https://doi.org/10.1142/9789814282024_0111
- Zelt, J. A. & Skjelbreia, J. E. (1992). Estimating incident and reflected wave fields using an arbitrary number of wave gauges. *Coastal Engineering Proceedings*, (23). <https://doi.org/10.9753/icce.v23.%p>. Number: 23

IV

Appendices



Statistical Methods

Mean value (μ):

$$\mu = \frac{\sum_{i=1}^n (x_i)}{n_{test}} \quad (\text{A.1})$$

Standard deviation (σ):

$$\sigma = \sqrt{\frac{\sum_{i=1}^n (x_i - \mu)^2}{n_{tests} - 1}} \quad (\text{A.2})$$

Root Mean Squared Error (RMSE):

$$\text{RMSE} = \sqrt{\frac{\sum_{i=1}^{n_{test}} (Q_{measured} - Q_{calculated})^2}{n_{tests}}} \quad (\text{A.3})$$

Root Mean Squared Log Error (RMSLE):

$$\text{RMSLE} = \sqrt{\frac{\sum_{i=1}^{n_{test}} (\log(Q_{measured}) - \log(Q_{calculated}))^2}{n_{tests}}} \quad (\text{A.4})$$

Power Law:

$$\hat{y}_{pl} = Ax^B + C \quad (\text{A.5})$$

Exponential fit:

$$\hat{y}_{exp} = Ae^{Bx} + C \quad (\text{A.6})$$

Confidence interval on fit (logarithmic):

$$\text{CI}_{\log} = \hat{y} \times e^{\pm z \times \text{RMSLE}} \quad (\text{A.7})$$

B

Wave conditions

The hydraulic conditions that were generated during the tests are presented in this appendix. Table B.1 includes 56 different wave conditions that were generated during the experiments, including the relevant parameters to initialize the wave generators.

Table B.1: Hydrodynamic conditions as input variables for the various breakwater scale models.

Index	Depth (m)	Wave Steepness	Significant wave height (m)	Peak period (s)	Mean spectral wave period (s)	Duration of experiment (s)
1	0.70	0.013	16	3.088	2.808	2552
2	0.70	0.013	18	3.276	2.978	2707
3	0.70	0.013	20	3.453	3.139	2854
4	0.70	0.013	22	3.621	3.292	2993
5	0.70	0.028	16	2.104	1.913	1739
6	0.70	0.028	18	2.232	2.029	1845
7	0.70	0.028	20	2.353	2.139	1944
8	0.70	0.028	22	2.468	2.243	2039
9	0.70	0.042	16	1.718	1.562	1420
10	0.70	0.042	18	1.822	1.657	1506
11	0.70	0.042	20	1.921	1.746	1588
12	0.70	0.042	22	2.015	1.832	1665
13	0.75	0.013	14	2.675	2.626	2388
14	0.75	0.013	16	2.889	2.808	2552
15	0.75	0.013	18	3.088	2.978	2707
16	0.75	0.013	20	3.276	3.139	2854
17	0.75	0.028	14	1.968	1.790	1627
18	0.75	0.028	16	2.104	1.913	1739
19	0.75	0.028	18	2.232	2.029	1845
20	0.75	0.028	20	2.353	2.139	1944
21	0.75	0.042	14	1.607	1.461	1328
22	0.75	0.042	16	1.718	1.562	1420
23	0.75	0.042	18	1.822	1.657	1506
24	0.75	0.042	20	1.921	1.746	1588

Index	Depth (m)	Wave Steepness	Significant wave height (m)	Peak period (s)	Mean spectral wave period (s)	Duration of experiment (s)
25	0.80	0.013	12	2.675	2.432	2210
26	0.80	0.013	14	2.889	2.626	2388
27	0.80	0.013	16	3.088	2.808	2552
28	0.80	0.013	18	3.276	2.978	2707
29	0.80	0.013	20	3.453	3.139	2854
30	0.80	0.028	12	1.822	1.657	1506
31	0.80	0.028	14	1.968	1.790	1627
32	0.80	0.028	16	2.104	1.913	1739
33	0.80	0.028	18	2.232	2.029	1845
34	0.80	0.042	12	1.488	1.353	1230
35	0.80	0.042	14	1.607	1.461	1328
36	0.80	0.042	16	1.718	1.562	1420
37	0.80	0.042	18	1.822	1.657	1506
38	0.85	0.013	12	2.675	2.432	2210
39	0.85	0.013	14	2.889	2.626	2388
40	0.85	0.013	16	3.088	2.808	2552
41	0.85	0.013	18	3.276	2.978	2707
42	0.85	0.028	16	2.104	1.913	1739
43	0.85	0.028	18	2.232	2.029	1845
44	0.85	0.028	20	2.353	2.139	1944
45	0.85	0.028	22	2.468	2.243	2039
46	0.90	0.013	10	2.442	2.432	2018
47	0.90	0.013	12	2.675	2.626	2210
48	0.90	0.013	14	2.889	2.808	2388
49	0.90	0.013	16	3.088	2.978	2552
50	0.90	0.028	12	1.822	1.657	1506
51	0.90	0.028	14	1.968	1.790	1627
52	0.90	0.028	16	2.104	1.913	1739
53	0.90	0.028	18	2.232	2.029	1845
54	0.90	0.042	14	1.607	1.461	1328
55	0.90	0.042	16	1.718	1.562	1420
56	0.90	0.042	18	1.822	1.657	1506
57	0.90	0.042	20	1.921	1.746	1588

C

Technical Drawings

In this Appendix technical drawings are provided, enabling detailed insights into the setup. Figure C.1 the side-view and the back-view show the different components that were installed to catch and measure the overtopping volumes.

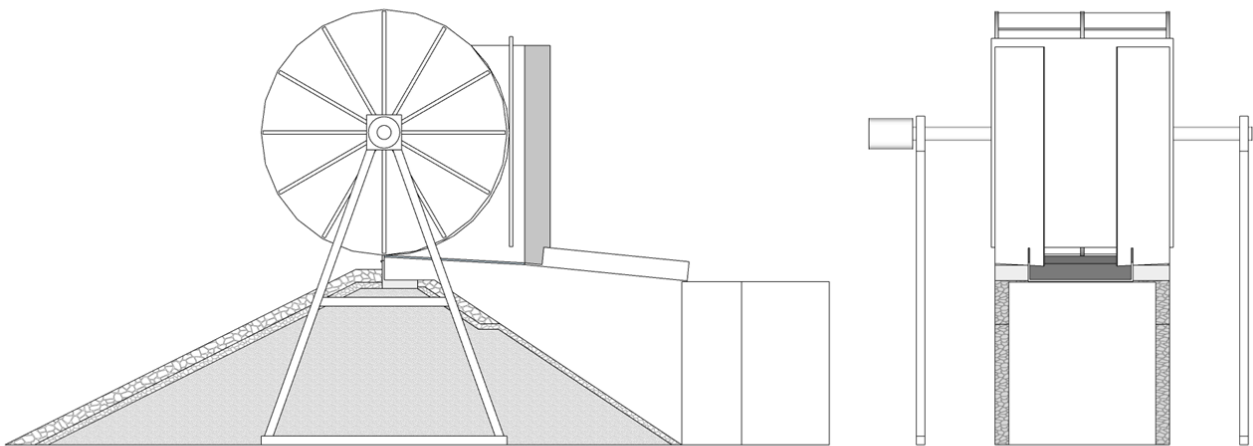


Figure C.1: Side view and front view of the installation, showing the breakwater, paddle wheel, splash board, transportation chute and overtopping box

Figure C.2 shows a detailed cross-section of the breakwater along with the measurements associated with the elements of each configuration. Detailed drawings of the various crest wall designs are also provided within the figure.

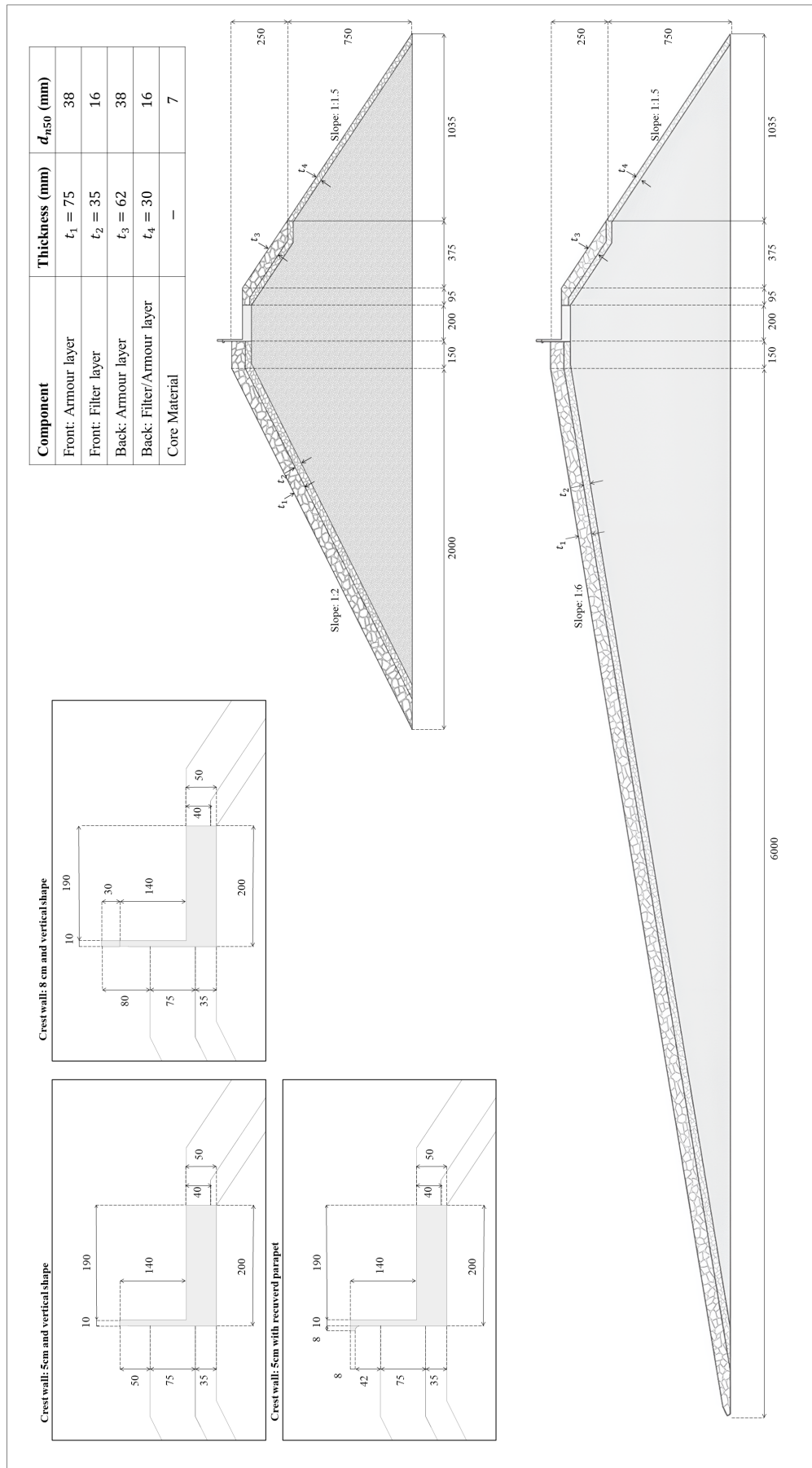


Figure C.2: Technical drawing including the cross-sections of the different breakwater models and crest walls

Grading curves

The grading curve of stone material in a rubble mound breakwater is a critical factor in determining the structural effectiveness of the coastal defense structure. One of the key properties commonly used to characterize this grading curve is the D_{n50} , which is also known as the median grain size, representing the particle size at which 50% of the material by weight is finer and 50% is coarser (W_{50}). When considering a rubble mound breakwater, a d_{n50} value is typically specified to ensure the proper functioning of the structure. This parameter is calculated with the expression in Eq. D.1.

$$d_{n50} = \sqrt[3]{\frac{W_{50}}{\rho_s}} \quad (\text{D.1})$$

Additionally, parameters such as d_{n15} and d_{n85} , which represent the particle sizes at which 15% and 85% of the material is finer, respectively, are also considered. These parameters collectively provide a comprehensive picture of the size distribution of the core material. Properly designed grading curves are crucial for the long-term success of rubble mound breakwaters.

D.1. Core Material

The core of a rubble mound breakwater takes the major fraction of the volume inside a breakwater and serves as the foundation of the structure, providing the breakwater with its essential mass and stability. The material is relatively small compared to the other elements. Its properties can be observed in Figure D.1.

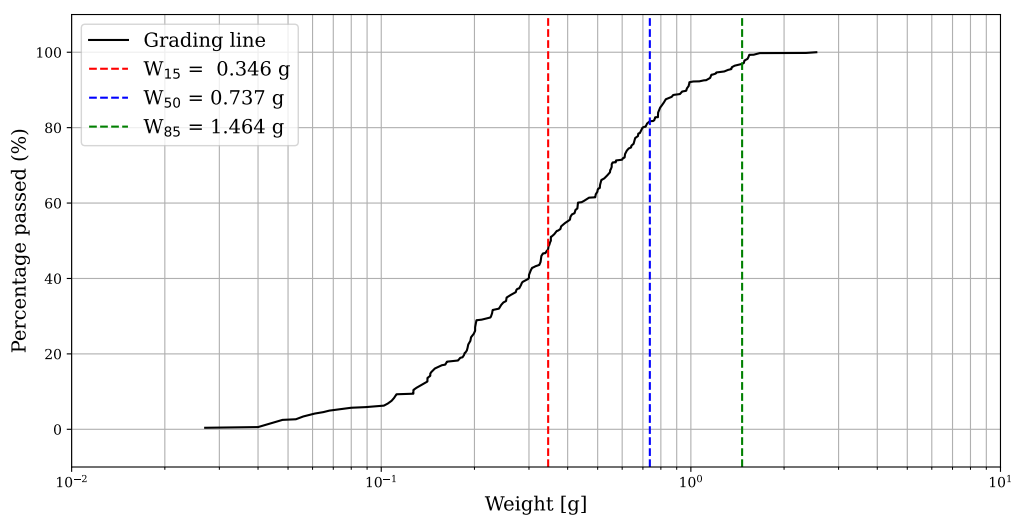


Figure D.1: Weight distribution of the core material ($d_{n15} = 0.5$ cm; $d_{n50} = 0.65$ cm; $d_{n85} = 0.82$ cm).

D.2. Filter Material

The filter layer is a vital component of the breakwater that lies between the core and the armour layer. Its weight distribution curve is presented in Figure D.2. The main function of the filter is to prevent transport gradients of sediment inside the structures. First, transport gradients of fine materials between the water body and the breakwater are not allowed as it compromises the permeability of the structure or leads to erosion of the core. Essentially, the function of the filter layer is to sufficiently improve the durability and constructional lifetime of the structure.

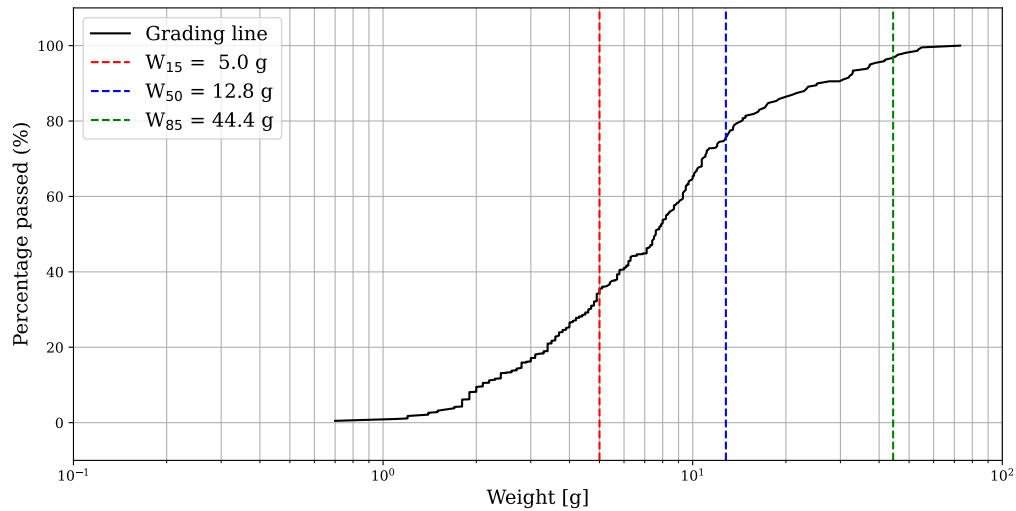


Figure D.2: Weight distribution of the core material ($d_{n15} = 1.23$ cm; $d_{n50} = 1.68$ cm; $d_{n85} = 2.54$ cm).

D.3. Armour Material

The armour layer of the rubble mound break water has the function to withstand the forces of the sea (i.e. currents, wave impact, etc.). This is realised by wave dissipation caused by the rough character of the slope, reducing erosion caused by friction and displacement. To guarantee this, the dimensions of the stones are largest in this component. The dimensions of the stones can be observed in Figure D.3.

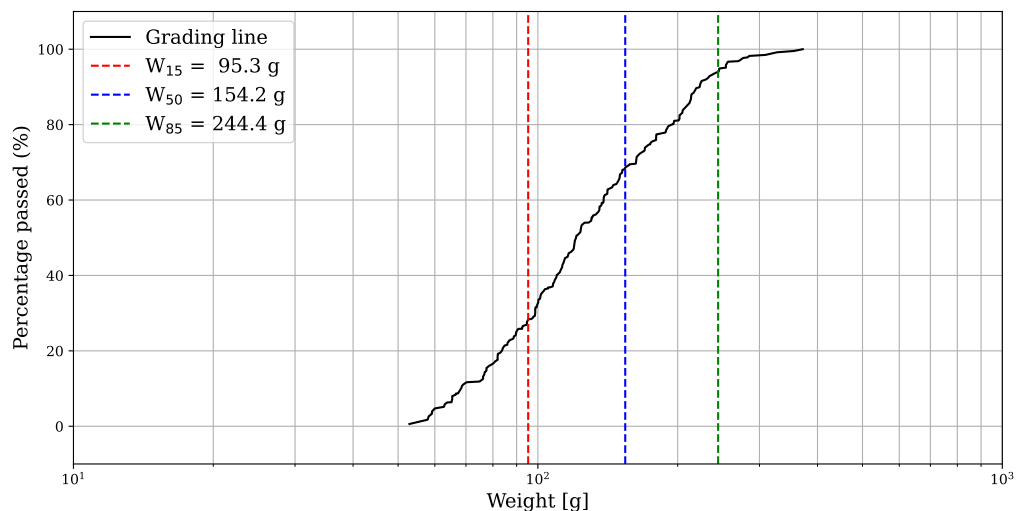


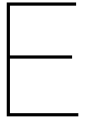
Figure D.3: Weight distribution of the core material ($d_{n15} = 3.28$ cm; $d_{n50} = 3.85$ cm; $d_{n85} = 4.49$ cm).

D.4. Summary

The main dimensions of each filter layer can be seen in Table D.1, where can be observed that for the armour layer a narrow grading is applied, and for the other elements a wide grading is implemented. This is explained by the desired properties of the armour layer using larger and more uniform stones, while the filter layer generally uses a broader range of particle sizes to facilitate filtration and stability. For the core are wider range is generally advised to ensure interlocking between the particles, reducing the likelihood of settlement and displacement due to wave action.

Table D.1: Gradings of the materials applied for the core, filter layer and armour layer.

Layer	W_{50} [g]	d_{n50} [cm]	W_{85}/W_{15} [-]	Grading type
Core	0.737	0.65	4.23	Wide
Filter	12.8	1.68	8.88	Wide
Armour	154.2	3.85	2.56	Narrow



Data Overview with wind

This appendix serves as an addition to the plots presented in the results chapter (Section 4.1). To avoid extensive repetition of the results within the report these are not included within the chapter itself, as similar patterns are shown and no additional information can be drawn that support the statements that were made. However, the figures do contribute to a better understanding on the influence of wind and are therefore included in the report.

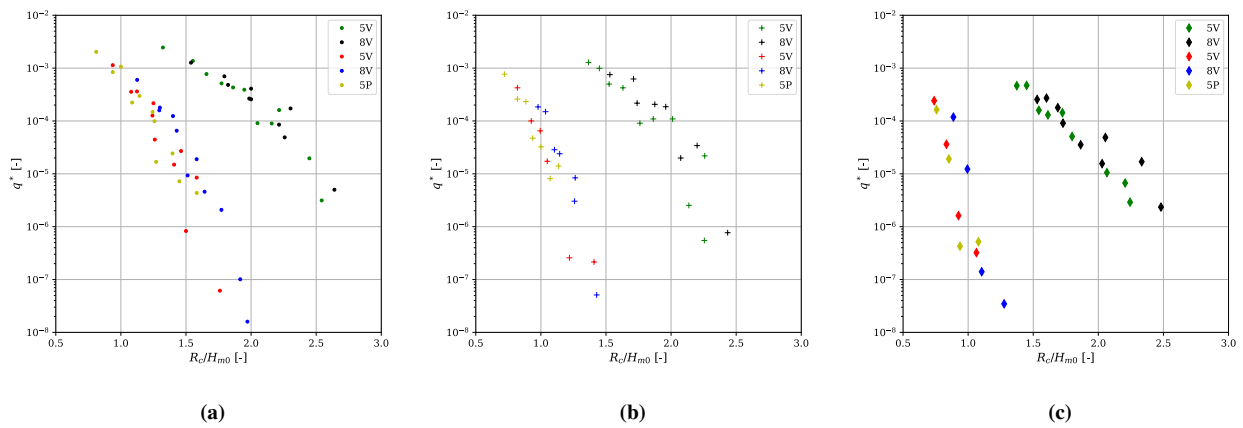


Figure E.1: Measured overtopping discharges for all configurations; (a) Measurements with the maximum wind effect; (b) Measurements with the maximum wind effect.

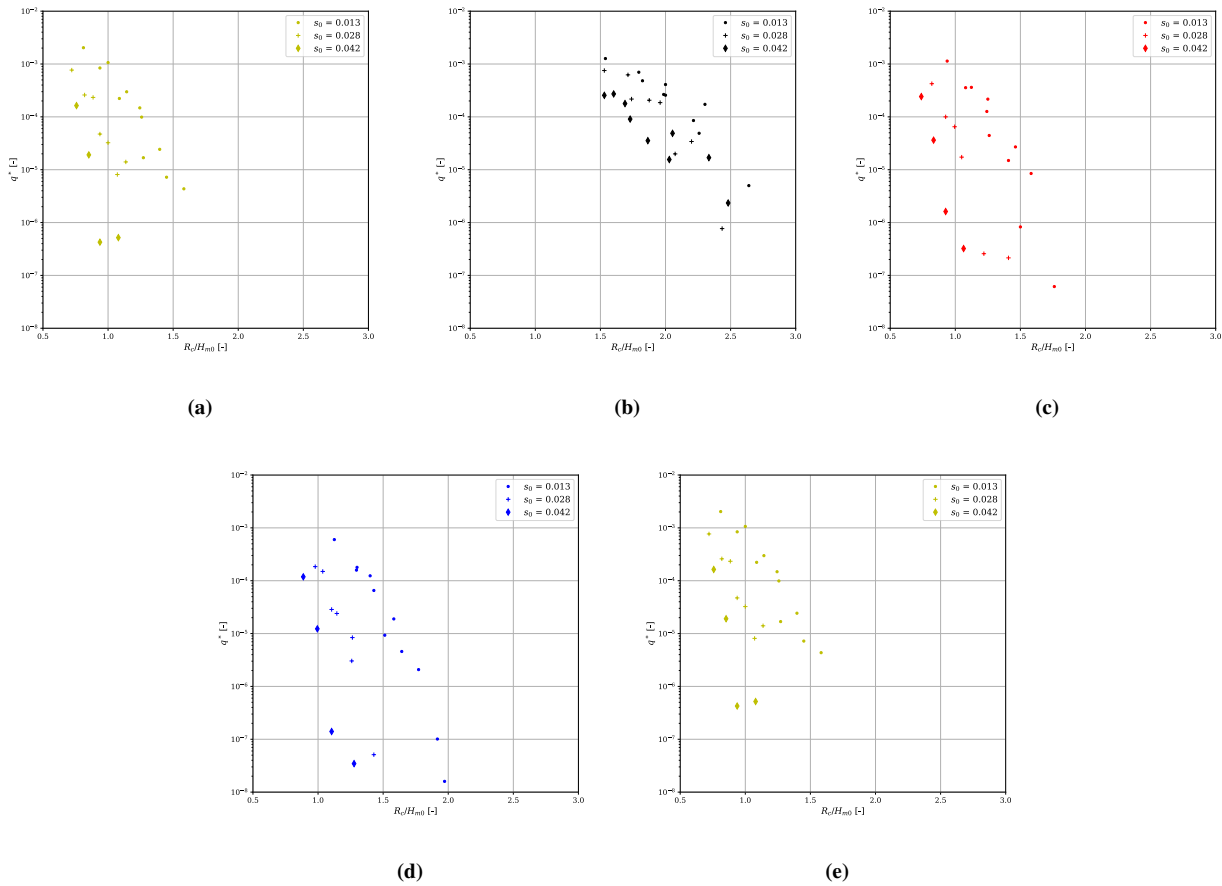


Figure E.2: Measured overtopping discharges for each configuration including the results with the maximum wind effect; **(a)** Observations from configuration 1 (25V); **(b)** Observations from configuration 2 (28V); **(c)** Observations from configuration 3 (65V); **(d)** Observations from configuration 4 (68V); **(e)** Observations from configuration 5 (65P);

E.1. Influence of wind - wave steepness

This section includes the rest of the data corresponding to the maximum wind effect on wave overtopping plotted against the wave steepness (See Section 4.3.2). Although not complete, patterns are visible that support the claim that the maximum wind effect increases when the wave steepness increases. The plots are shown in Figure E.3 on the next page.

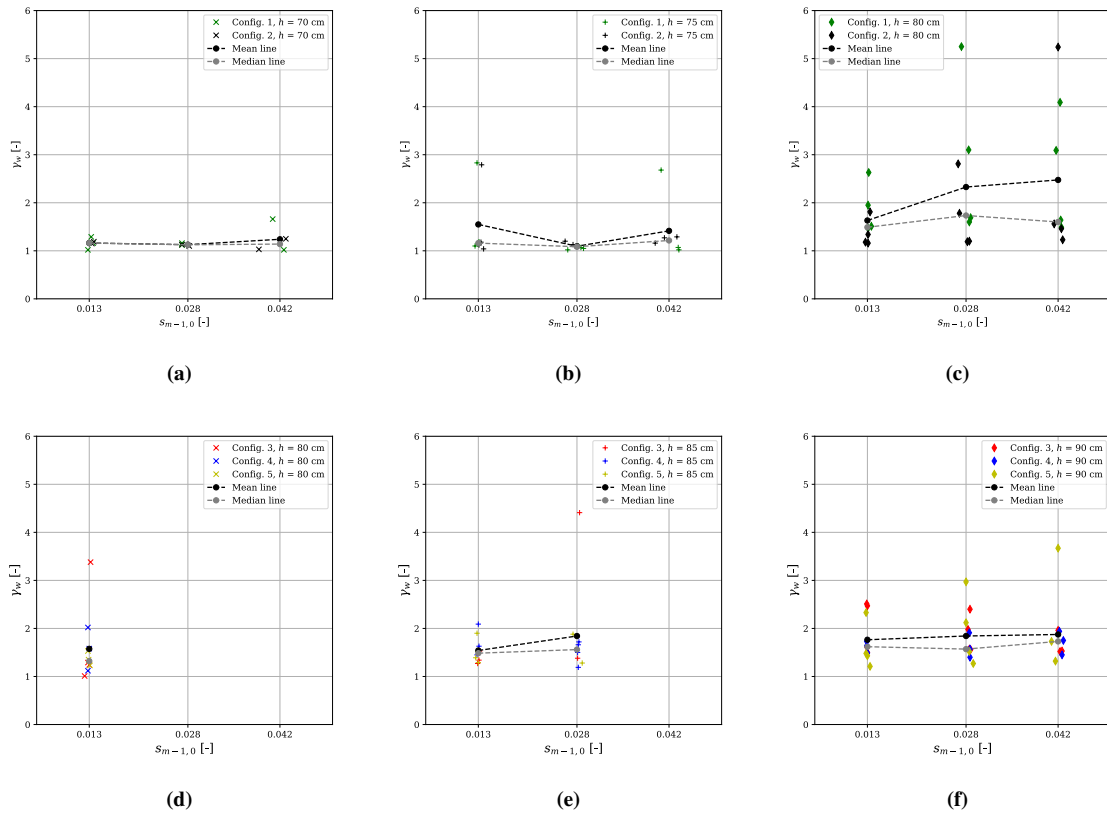


Figure E.3: Maximum influence of wind for the wave steepness including the median and mean line for different water levels; **(a)** Data points for the 1:2 slope with $A_c = 30$; **(b)** Data points for the 1:6 slope with $A_c = 25$; **(c)** Data points for the 1:2 slope with $A_c = 20$; **(d)** Data points for the 1:6 slope with $A_c = 20$; **(e)** Data points for the 1:2 slope with $A_c = 15$; **(f)** Data points for the 1:2 slope with $A_c = 10$.

F

Pictures of the Setup



Figure F.1: Side picture of the setup including the paddle wheel.

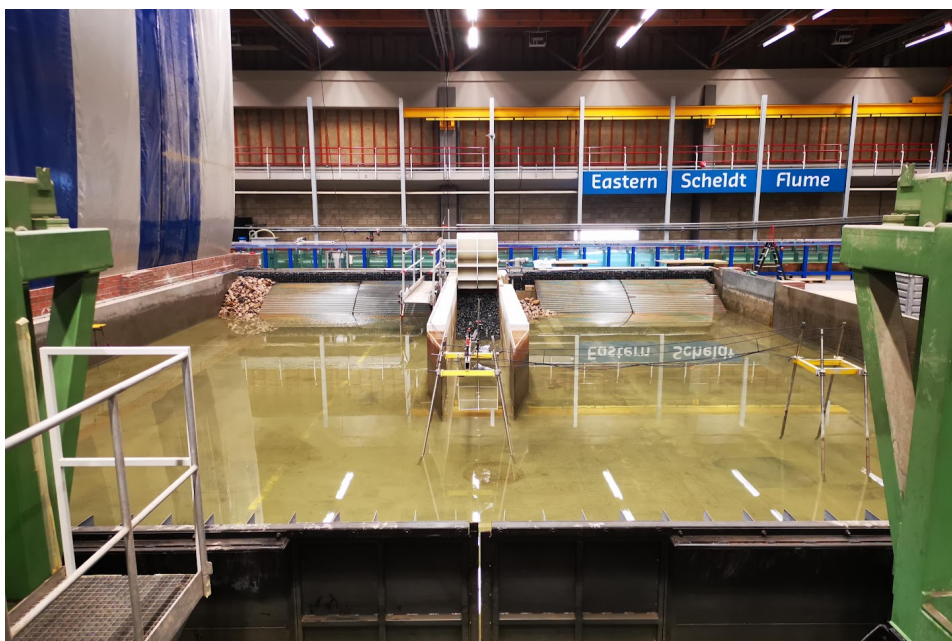


Figure F.2: Picture of the front of the setup, showing the measurement devices and the flume



Figure F.3: Picture of the back of the setup.



Figure F.4: Isometric view of the model.



Figure F.5: Picture of the chute and the overtopping box at the back of the model setup.



Figure F.6: Picture of wave overtopping at the crest wall.



Figure F.7: Picture of a breaking wave on the slope of the breakwater with $\cot \alpha = 6$



Figure F.8: Picture of the bull nose that was attached to the 5 cm crest wall